Jaakko Jussila

S-band transmitter for Aalto-1 nanosatellite

School of Electrical Engineering

Thesis submitted for examination for the degree of Master of Science in Technology.

Espoo

Thesis supervisor:

Prof. Ville Viikari

Thesis advisor:

D.Sc. (Tech.) Jari Holopainen

Aalto University
School of Electrical
Engineering

AALTO UNIVERSITY
SCHOOL OF ELECTRICAL ENGINEERING

ABSTRACT OF THE
MASTER'S THESIS

Author: Jaakko Jussila

Title: S-band transmitter for Aalto-1 nanosatellite

Date: Language: English Number of pages:8+67

Department of Radio Science and Engineering

Professorship: Radio Sciense and Engineering Code: S-26

Supervisor: Prof. Ville Viikari

Advisor: D.Sc. (Tech.) Jari Holopainen

Aalto-1 is a CubeSat type nanosatellite mission used for Earth-observation. The satellite requires a radio link with high data throughput. The satellite carries AaSI spectral imager which is able to produce tens of megabytes of scientific data during an orbit period. In this thesis the design and implementation of an S-band transmitter for the Aalto-1 nanosatellite are presented. Requirements for the transmitter are defined by data throughput simulation, the CubeSat power limitations and the space environment. Based on the derived requirements, commercially available off-the-shelf components are selected. The transmitter consists of Texas Instruments CC2500 transceiver, RF Micro Devices RF5602 power amplifier and Texas Instruments MSP430 microcontroller. The RF transmission lines are designed and implemented with microstrip elements by using RF circuit simulators. First prototype board of the transmitter is implemented, as well as, control software developed for the microcontroller. First tests of the prototype indicate that the chosen architecture is capable of fulfilling the design requirements. The test results with the RF transmission lines indicate that further optimization work is required in order to deliver the maximum RF power to the output of the transmitter.

Keywords: CubeSat, impedance matching, microcontroller, power amplifier, RF, S-band, transceiver, transmitter

AALTO-YLIOPISTO
SÄHKÖTEKNIIKAN KORKEAKOULU

DIPLOMITYÖN
TIIVISTELMÄ

Tekijä: Jaakko Jussila

Työn nimi: Aalto-1 nanosatelliitin S-kaistan lähetin

Päivämäärä: Kieli: Englanti Sivumäärä:8+67

Radiotieteen ja -tekniikan laitos

Professuuri: Radiotiede ja -tekniikka Koodi: S-26

Valvoja: Prof. Ville Viikari

Ohjaaja: TkT Jari Holopainen

Tässä työssä esitellään Aalto-1 satelliitin S-kaistan lähettävän radion suunnittelu. Aalto-1 on CubeSat-standardiin perustuva kaukokartoitussatelliitti, jossa on hyötykuormina kolme tieteellistä instrumenttia: korkearesoluutioinen AaSI sepktrikamera, säteilymittari ja plasmajarru. Spektrikamera tuottaa informaatiota jopa useita kymmeniä megatavuja yhden kuvauksen aikana, joten lähettimeltä vaaditaan suurta tiedonsiirtonopeutta. Työssä määritellään vaatimukset, jotka perustuvat CubeSat-satelliittien tehorajoituksiin, avaruusolosuhteiden haasteisiin sekä linkkibudjettisimulaatioihin. Lähetin rakennetaan kaupallisista komponteista, jotka on valittu edellä määritettyjen rajoitteiden perusteella. Lähettimen topologia perustuu Texas Instruments:n CC2500 lähetin-vastaanottimeen, RFMD:n RF5602 tehovahvistimeen ja Texas Instuments:n MSP430 mikro-ohjaimeen. RF-sovituspiirit suunnitellaan käyttäen RF-piirisimulaattoreita ja toteutetaan mikroliuskatekniikalla. Lähettimelle suunniteltiin ensimmäinen prototyyppilevy sekä kehitettiin mikro-ohjaimen ohjelmiston ensimmäinen versio. Prototyypin ensimmäiset funktionaaliset testit osoittavat, että suunniteltu lähettimen rakenne pystyy täyttämään sille asetetut vaatimukset. RF-sovituspiirien testit osoittavat, että sovituspiirien suunnitelmat vaativat jatkokehitystä, jotta lähetin pystyy tuottamaan lähetyksessä tarvittavan tehotason.

Avainsanat: CubeSat, impedanssisovitus, lähetin, lähetin-vastaanotin, mikro-ohjain, RF, S-kaista, tehovahvistin

Preface

I want to express my graditude for my thesis supervisor Professor Ville Viikari, instructor Jari Holopainen, Sami Ben Sheick, Jaan Praks and Aalto-1 team.

Otaniemi, 1.5.2013

Jaakko M. Jussila

Contents

Symbols and abbreviations

Symbols

c	speed of light in vacuum $\approx 3 \times 10^8$ [m/s]
λ	wave length [m]
k	Boltzmann's constant $\approx 1.38 \times 10^{-23}$ [J/K]
f	frequency [Hz]
F	noise factor
ω	angular frequency [rad/s]
ϵ_r	Relative permittivity
$Baud$	symbols per second
N_0	noise power spectral density [W/Hz]
C/N_0	carrier power to noise power spectral density ratio [1/Hz]
E_b/N_0	energy per bit to noise power spectral density ratio [J/Ws]
C	capacitance [F]
L	inductance [H]
R	distance [m]
T	temperature [K]
Z	impedance [Ω]
P	power [W]
L_x	attenuation
G	antenna gain
G/T	antenna gain to noise temperature ratio [1/K]

Opetators

$d/d\Omega$	Derivative with respect to Ω
$\int_a^b$	Defined integral from a to b
$\int\int_{4\pi} A(\theta, \Phi) d\phi$	Integral over space angle $d\phi$

Abbreviations

AaSI	spectral imager of Aalto-1
ADCS	attitude determination and control system
ADS	antenna deployment system
AFSK	amplitude frequency shift keying
ASK	amplitude shift keying
COM	communication system
COTS	commercial of the shelf
DQPSK	differential quadrature phase shift keying
EPS	electrical power system
FEC	forward error correction
FSK	frequency shift keying
GDIO	general digital input/output
IF	intermediate frequency
ISM	industrial, scientific and medical
I2C	two wire interface
LV	launch vehicle
LEO	low Earth orbit
LVDS	low voltage differential signaling
MSK	minimum shift keying
OBC	on board computer
PA	power amplifier
PB	plasma brake
PCB	printed circuit board
P-POD	poly-picosatellite orbital deployer
PSK	phase shift keying
QFN	quad-flat no-leads
QPSK	quadrature phase shift keying
RADMON	radiation monitor
RAM	random access memory
RF	radio frequency
RFIC	radio frequency integrated circuit
RISC	reduced instruction set computer
SPI	serial peripheral interface
SW	software
UART	universal asynchronous receiver transmitter
UHF	ultra high frequencies
VHF	very high frequencies

1 Introduction

The first artificial satellite, Sputnik 1, was launched to space by Soviet Union in 1957. Since then, many satellite missions have been launched to the Earth orbit. Most of the satellites, used for example by NASA during the past decades, have been physically large and economically expensive [1]. The Earth observation satellite Aqua, launched in 2002, had a mass of 2.9 tons [2]. Generally, the players in the space business have been either governmental institutions or large private companies specialized to space business. However, when the CubeSat standard was introduced by California Polytechnic State University and Stanford University's Space Systems Development Lab in the early 2000 [3], the trend has started to change. Many universities around the world have been building their own satellites completely by student forces. At the moment, tens of different CubeSat missions have been launched to space with budgets that are a fraction that of the traditional satellite missions. The reason for the CubeSat success during the recent years is simple: the CubeSat standard introduces a complete framework for pico- and nanosatellite design.

This thesis presents the design of an S-band transmitter for Aalto-1 nanosatellite [4]. Aalto-1 is a hyper-spectral Earth observation CubeSat mission, designed and built in Aalto University. The satellite has a novel, miniaturized adjustable spectral imager, developed by VTT Technical Research Center of Finland, as the main payload. The instrument produces large images of several megabytes. The large sized images have to be broadcasted to Aalto-1 ground station during the short over passes with maximum fly-over time of about 15 minutes. Thus, the mission requires a high data rate transmitter in order to broadcast one image with a reasonable number of over passes. CubeSat missions make usually heavy use of the low bandwidth VHF/UHF amateur radio bands in their communication systems. However, as known from the basic communication theory, the data rate of a communication link is a function of the bandwidth. Thus, the VHF/UHF frequency bands are not suitable for high data rate communication links. A suitable frequency band exists at S-band frequencies of 2.4 - 2.45 GHz: the frequency band is dedicated for amateur radio usage and the radio waves do not face too high attenuation.

The goal of this thesis is to design the first prototype for the Aalto-1 S-band transmitter that fulfills the requirements set by the mission. The transmitter architecture is based on a custom design, combining different commercial components. Such an approach provides most benefits on the education aspects, since one is encouraged to experience the whole design process of a satellite subsystem. The components are chosen based on the requirements derived from data throughput simulations, CubeSat power constraints and space environment challenges. The impedance matching between the RF components is designed and implemented with microstrip elements. First version of the transmitter control software is also developed. The prototype is characterized experimentally and by simulations.

This thesis is organized as follows: chapter 2 introduces the background research and chapter 3 the implementation of the design. Chapter 4 analyses the results achieved with the prototype and chapter 5 summarizes the achieved work.

2 Background research

This chapter introduces the CubeSat concept and typical CubeSat communication systems. Aalto-1 nanosatellite mission is described, including the subsystems of the satellite. Theory on the satellite transmitters is introduced, including the transmitter structure, radio wave propagation and space environment challenges. Based on the known theory and Aalto-1 mission constraints, requirements are defined for the transmitter.

2.1 CubeSat standard and CubeSat Kit

The development of CubeSat standard started in CalPoly and Standford in 1999. The objective of the initiative was to provide a standard for the design of pico- and nanosatellites in order to reduce the costs and development time [3]. The standard became rabidly popular and currently more than 100 educational institutes and private companies are developing CubeSat standard based satellites as an international collaboration. A CubeSat is a 10 cm cube with total mass of no more than 1.3 kg [5](see Fig. 1). Each CubeSat satellite consists of one or more standard cubes. The CubeSat standard defines also the standard launch pod for a CubeSat, P-POD (Poly-Picosatellite Orbital Deployer)(see Fig. 1). The CubeSat satellite will be placed inside the launch pod prior to the launch and it serves as the interface between the CubeSat and the launch vehicle (LV). The P-POD contains a spring, so after the rockect is in a desired orbit, the spring is released and pushes the CubeSat out of the P-POD and the rocket. The CubeSat standard defines also limits for the materials used and electrical, operational and testing requirements.

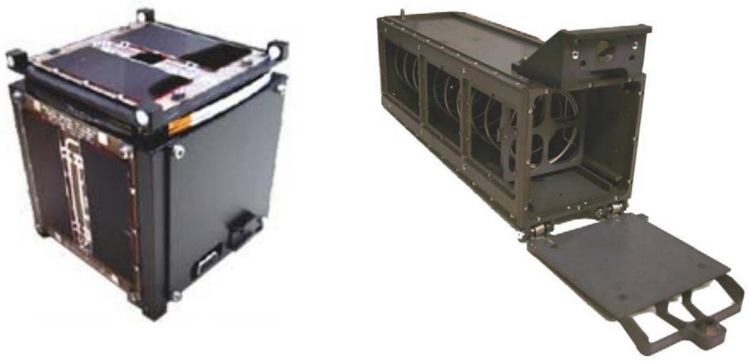

Figure 1: CP1, Cal Poly's first 1U CubeSat, left. The standard launch pod, P-POD, on the right [5].

CubeSat Kit was the first commercially available satellite building framework based on CubeSat standard, developed by Pumpkin [6]. The CubeSat Kit electronics

board is loosely based on widely used PC-104 standard and it has been gaining wide popularity among CubeSat developers. Nowadays CubeSat Kit PCB board is de facto industry standard and large variety of CubeSat Kit compatible subsystems are available from variety of manufacturers (see Fig. 2).

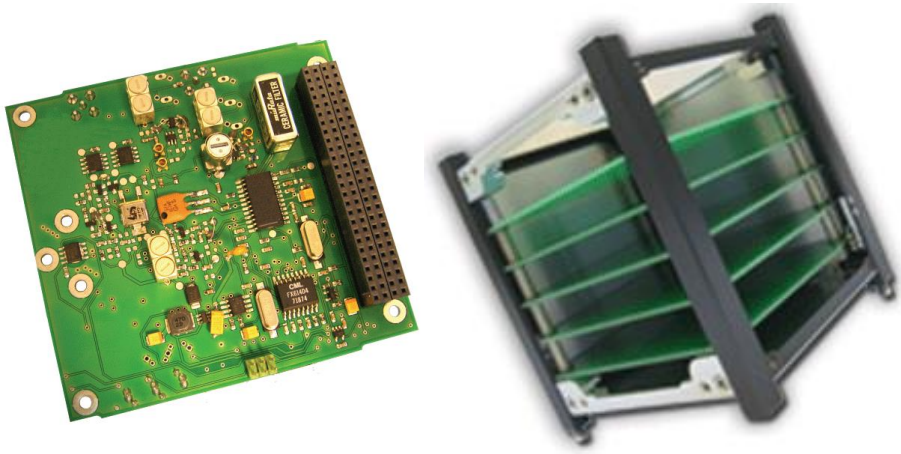

Figure 2: CubeSat Kit systems: a CubeSat communication module on left and a CubeSat cube with CubeSat Kit boards stacked on each other on right [7].

2.2 CubeSat communication systems

The CubeSat missions have taken heavy use of the amateur VHF/UHF (very high frequencies / ultra high frequencies) frequency bands due to the fact that designing of radio frequency (RF) systems is easier and the signal attenuation levels are lower as compared to higher frequencies. Typical data rate on these bands is 9600 bit/s with FSK (frequency shift keying) modulated signal [8]. Also, most of the CubeSat missions have not required high data throughput. Thus, VHF/UHF frequencies have been suitable for achieving the mission goals. A few CubeSat satellite communication (COM) systems including the transmitter module, frequencies and transmitted power levels are shown in Table 1 [9].

GeneSat-1 and Can-X2 missions, shown in Table 1, used the S-band frequencies for data transmission. The data throughput of Can-X2 was more than 22 CubeSat missions using UHF frequencies achieved together during 5 years. This highlights the fact of using higher frequencies when more data throughput is required. Moreover, since Can-X2 used RF transmit power of 500 mW, the use of S-band communication systems is feasible within the CubeSat power constraints.

Sometimes ready made integrated systems are used for the COM circuits. For example, Microhard MHX-2400, shown in Table 1, is a ready transmitter circuit. Such an approach is fast and most reliable due to the fact that the manufacturer

Table 1: CubeSat COM systems.

Satellite	**Transmitter circuit**	**Frequency**	**Power**
AAU1	Wood & Douglas SX450	UHF	500 mW
Cute-1 (C0-55)	Manki Denki (Beacon), Alinco DJ-C4 (Data)	UHF	100 mW (Beacon) 350 mW (Data)
QuakeSat-1	Tekk KS-960	UHF	2 W
UWE-1	PR430	UHF	1 W
GeneSat-1	Atmel ATA8402 (Beacon), Microhard MHX-2400 (Data)	UFH (Beacon), S-band (Data)	500 mW (Beacon) 1 W (Data)
CP4	TI CC1000	UHF	1 W
CAPE1	TI CC1020	UHF	1 W
CP3	TI CC1000	UHF	1 W
CanX-2	Custom built	S-band	500 mW

has tested the transmitter operation. Wood & Douglas SX450, Alinco DJ-C4, Tekk KS-960 and PR430 (shown in Table 1) are ready transmitter circuits that need an additional control unit. Some of the missions have taken a custom built approach. Examples of such are the missions using TI CC1000 and TI CC1020, as shown in Table 1. These components are ready transceiver circuits but need also an additional power amplifier due to the low RF power produced by the circuits [10],[11]. Can-X2 mission used also a custom built solution. Such an approach contains more risks and design effort due to the fact that an integration process is required for the radio circuit. Anyhow, the approach has also more educational value on the RF circuit design process.

Beside the S-band transmitter MHX-2400 mentioned in Table 1, there exists also other commercial transceiver circuits such as STX [12] and HISPICO [13]. Clyde Space has designed the STX specifically for CubeSat missions for high data rate downlinks. STX has programmable data rates up to 2 Mbit/s. HISPICO is provided by IQ wireless and uses the other part of the S-band frequency band 2.2 - 2.3 GHz. It provides data rates up to 1 Mbit/s and output power levels up to +27 dBm.

2.3 Aalto-1 nanosatellite

2.3.1 Aalto-1 mission

Aalto-1 student nanosatellite project started in spring 2010 [4]. Aalto-1 is a three-unit CubeSat satellite, with total size of about 34 x 10 x 10 cm and mass of 4 kg.

The satellite is aimed to be launched to space in 2014 and to have a mission lifetime of 2 years. Main mission of the satellite is to demonstrate the operation of three different scientific payloads: a spectral imager, a radiation monitor and a plasma brake. Aalto-1 mission has been designed for a sun-synchronous polar orbit with height of 500 to 900 km from the surface of the Earth. The satellite is designed and built in Aalto university in a co-operation with VTT Technical Research Center of Finland, Finnish Meteorological Institute (FMI), Universities of Helsinki and Turku, Berlin Space Technologies (BST), Turku University of Applied Sciences and Clyde Space. Mission goals of Aalto-1 are the following:

- The spectral imager (AaSI) images Earth's surface. The images are then transmitted down to ground stations. Based on the images scientists can make conclusions about vegetation on forests, water quality and glaciers.
- Radiation monitor (RADMON) will measure the radiation environment (electrons and protons) on the orbit and the measured data will be transmitted to ground stations.
- At the end of the two years mission time, the plasma brake (BP) will be released. The brake should slow down the satellite speed and bring it down to a lower orbit so that it burns due to the friction caused by the more dense atmosphere [4].

2.3.2 Subsystems of Aalto-1 nanosatellite

Aalto-1 nanosatellite has a size of three CubeSat cubes that are stacked on each other. The electronic system inside the satellite is formed by two stacks of CubeSat Kit type subsystems, called long stack and short stack. The configuration is shown in Figs. 3 and 4. Aalto-1 satellite consists of several subsystems. On board computer (OBC) controls all the satellite's subsystems and payloads. Communication system (COM) consists of VHF/UHF transceiver providing the command link between the satellite and ground station. It provides also the radio beacon signal. S-band transmitter provides the high data throughput link between the satellite and ground station. Antenna deployment system (ADS) deploys the VHF/UHF antennas when the satellite is released from the rocket. GPS system is responsible of providing orbital coordinates and time for the satellite. Electronic power system (EPS) delivers the power produced by the solar panels to the satellite bus and charges the batteries located on the battery board. Attitude determination and control system (ADCS) controls the satellite's body orientation on the orbit. The payloads of the satellite form the last group of subsystems.

The long stack includes ADS, satellite's power board and batteries, VHF/UHF transceiver, S-band transmitter, GPS, OBC, ADCS and spectral imager. Plasma brake and radiation monitor are located in the short stack. The satellite is covered on each long side with solar panels which are the energy source for the satellite together with the batteries. Due to the small size of the satellite (the total area for solar cells is about 1000 cm^2 [14]), the power budget for all the subsystems is limited

as shown in Table 2 [14]. Therefore, all the subsystems of the satellite have to be designed as low power and efficient as possible. On the satellite, OBC, VHF/UHF transceiver, GPS, ADCS and electrical power system are online during the whole mission life time. Rest of the subsystems are online when initiated by OBC [14].

Table 2: Power budget for Aalto-1 nanosatellite.

System	**Standby power (W)**	**Peak power (W)**
ADS	0	7
VHF/UHF	0.2	1.55
S-band	0	5
GPS	0.045	0.13
OBC	0.1	2
ADCS	0.66	1.8
AaSI	0	4
RADMON	0	1.5
EPB	2.3	3
EPB completely off	0	0

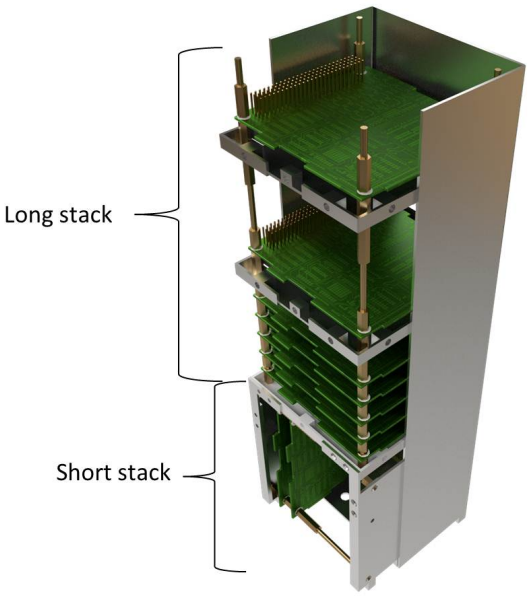

Figure 3: Aalto-1 nanosatellite frame structure (Copyright Pekka Laurila).

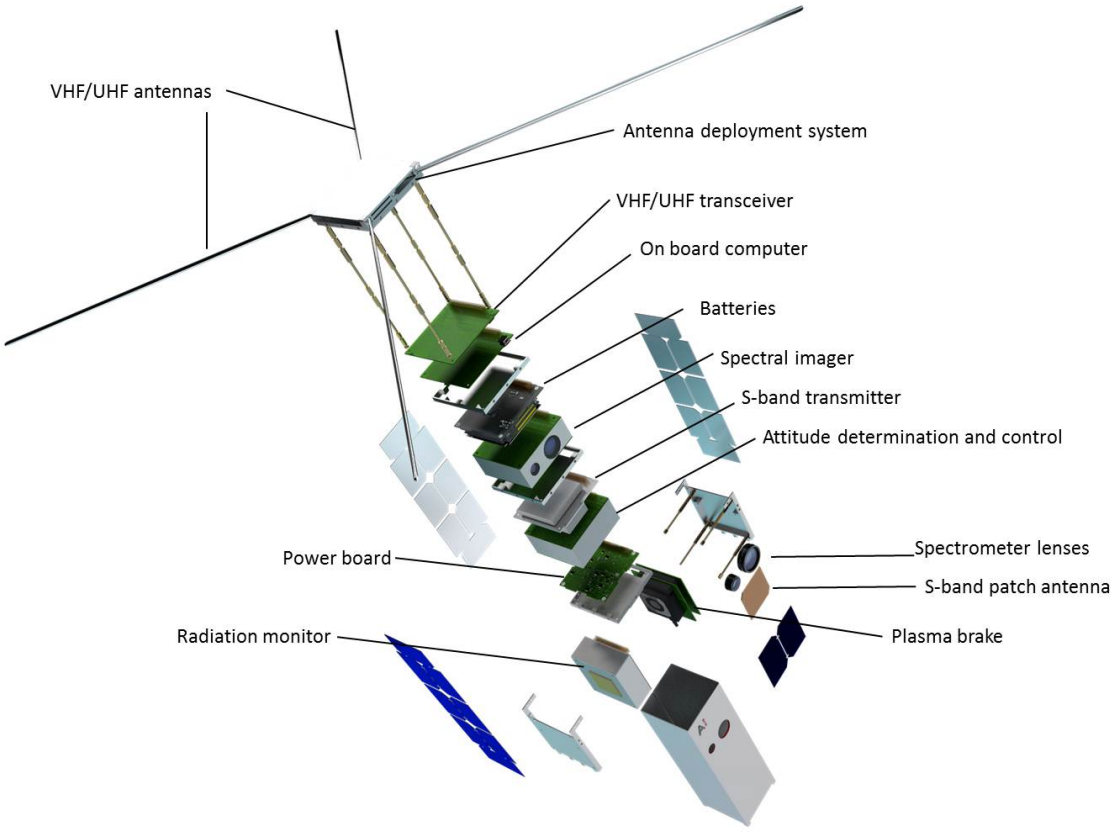

Figure 4: Aalto-1 nanosatellite inner stucture explosion (Copyright Pekka Laurila)[15][16].

2.3.3 Aalto-1 communication system

The COM system of Aalto-1 consists of two different radio systems that utilize three different frequency bands [14]: VHF, UHF and S-band. All of these frequency bands are allocated for amateur radio use and the S-band belongs also to the ISM (industrial, scientific and medical) band [17]. The VHF/UHF frequencies are 147 MHz and 437 MHz and the S-band is 2.4 - 2.45 GHz. The COM system of Aalto-1, including the ground segment, is illustrated in Fig. 5.

If the ADCS system fails, the satellite's body orientation cannot be determined. Therefore, omnidirectional antennas were required to be used with the radio system providing the command link. Due to the high levels of free-space loss in satellite communications, the lower VHF/UHF frequencies were chosen for the command link of Aalto-1. Since the VHF/UHF transceiver does not require high data throughput, the narrow bandwidth of the VHF/UHF frequency bands is not a problem. The mission of Aalto-1 requires also a high data throughput downlink. Due to the bandwidth requirements, higher frequencies had to be used. S-band frequencies at

2.4 -2.45 GHz were chosen, since they are suitable for CubeSat communications and there exists also good quality and low power ISM band RF electronics designed for these frequencies.

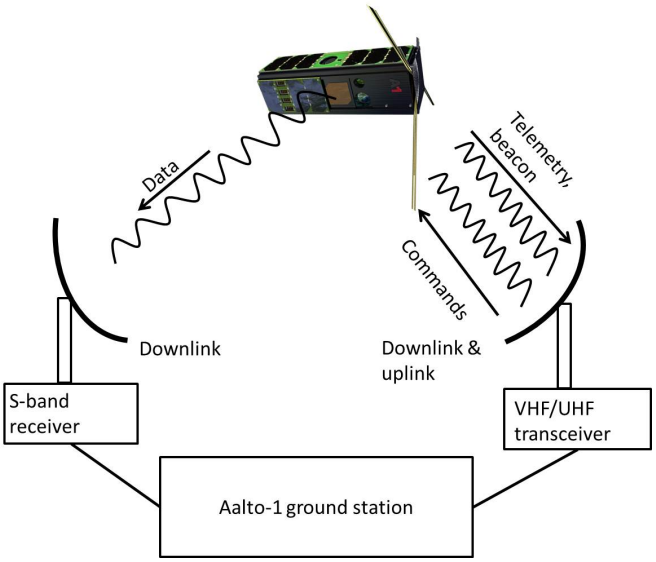

Figure 5: Aalto-1 communication system.

Every RF transmission is initialized by the ground station. Therefore, the commands will be transmitted via the VHF/UHF uplink. The uplink can also be used for software updates of the satellite's subsystems. The VHF/UHF downlink will be used for satellite's telemetry data transmission. The telemetry data includes information on the satellite's subsystems status. The VHF/UHF downlink is also used for the radio beacon. The beacon signal is a simple RF transmission, such as the Morse coding. The transmission will include identification of the satellite so that the radio amateurs operating around the world can listen and identify the satellite. Small sized payload data packages will be transmitted with the VHF/UHF downlink and it is also the backup system for the S-band transmitter. The VHF/UHF transceiver is controlled by the OBC but it can also be seen as standalone system. The transceiver is transmitting the beacon signal individually and it is listening constantly any transmissions by the ground station in order to receive possible commands.

The S-band is responsible for the high data throughput downlink, since the large sized spectral images will be transmitted by using the S-band. The S-band transmitter is controlled by the OBC and all the transmission are separately commanded by the ground station. Outside the transmission operation, the S-band transmitter has to be in power-off mode. The S-band system of Aalto-1 is illustrated in Fig. 6. The satellite segment consists of interface towards the OBC, S-band transmitter circuit and S-band patch antenna. Between the satellite and the ground station is the radio wave propagation medium that is an important factor in the design of radio links. The ground segment consists of ground station equipment, such as the receiving

antenna, the antenna rotating and control system, low noise amplifier located after the antenna, the receiver and the whole ground station control software.

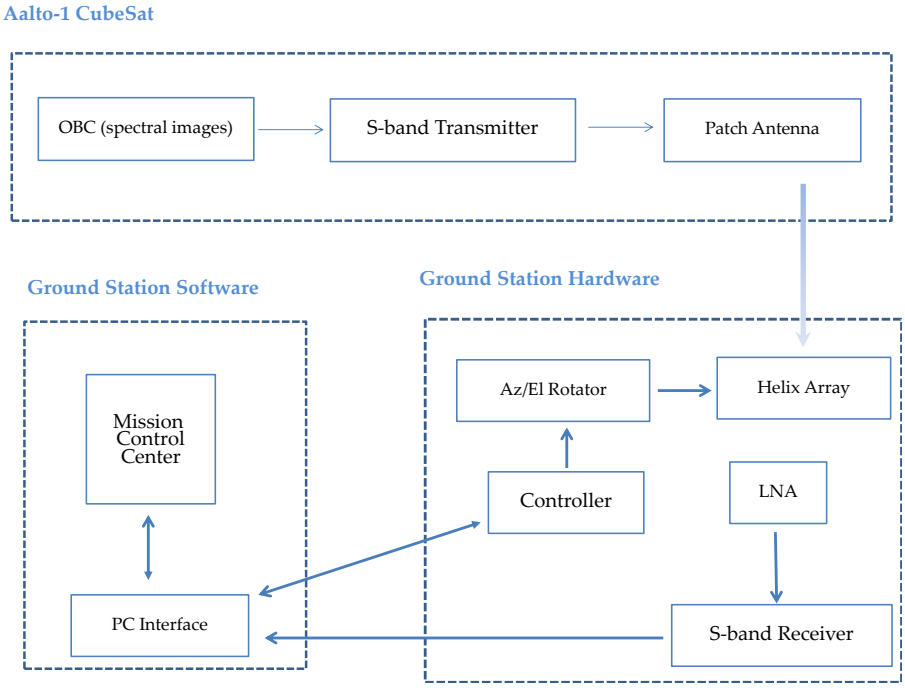

Figure 6: Aalto-1 S-band system.

2.4 Transmitters and receivers

In order to transmit information through a wireless channel, the information has to be transferred onto a carrier wave with modulation. The carrier wave is usually a high frequency signal due to the fact that the antennas are physically smaller and the allocation for frequency bands is easier at higher frequencies. In order to modulate the information onto the carrier wave, the transmitter consists of a modulator that transfers the data as symbols onto the carrier wave. The signal on which the symbols are transferred is called baseband. The local oscillator (LO) provides the higher frequencies with which the baseband symbol signals are mixed in order to produce the modulated carrier wave. After the baseband signals are mixed with the carrier wave, the modulated carrier wave has to be amplified with a power amplifier (PA). After the signal has been amplified, it is transferred trough a RF signal line to the transmitting antenna. In the transmitter, different filters are typically used to filter out unwanted frequencies caused by the nonlinearities of the RF components. Parts of a typical transmitter are shown in Fig. 7.

The information symbols can be expressed as amplitude changes on the carrier wave, which is called amplitude modulation. They can also be expressed as frequency changes or phase changes of the carrier wave which means frequency modulation or phase modulation, respectively. In satellite communications, the following digital modulation schemes are used: frequency shift keying (FSK), amplitude shift keying

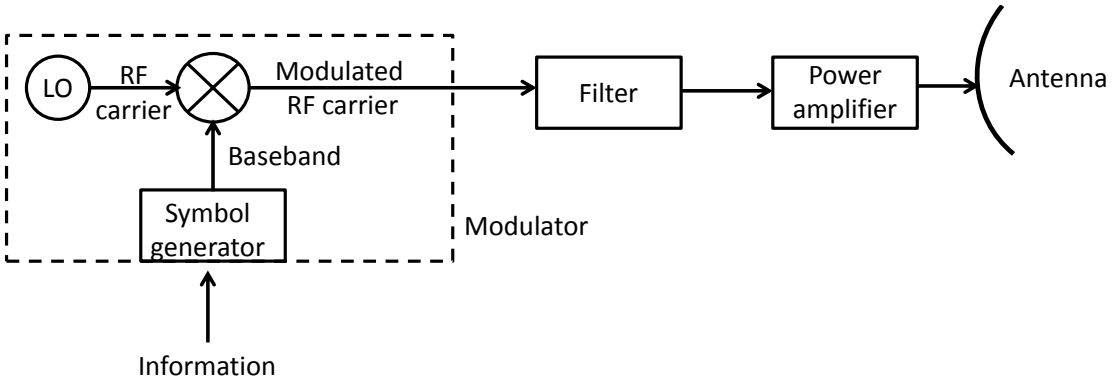

Figure 7: Parts of a typical transmitter.

(ASK) and phase shift keying (PSK) [18]. Since the RF transmissions with a constant envelope curve have less strict linearity requirements compared to non-constant envelope transmissions, the PSK and FSK modulation schemes are preferred instead of ASK.

When the transmitted signal arrives to the ground station receiving antenna, the signal has traveled through the atmosphere that attenuates the signal. The receiver system at the ground station operates conversely compared to the satellite's transmitter. A low noise amplifier amplifies the received signal that is on very low power level. Then, the signal is filtered and down-converted to a lower frequency and then demodulated in order to retrieve the original information at the baseband frequency. Such an architecture is called the superheterodyne receiver. There exist also receiver architectures where the baseband signal is directly de-modulated from the high frequency carrier wave. Such an architecture is called the zero-IF (zero intermediate frequency). As the signal has low power level at the ground station receiver, the information de-modulated by the receiver may contain errors due to the attenuation phenomena caused by the propagation channel. Therefore, usually some forward error correction (FEC) is added to the transmitted signal. FEC can be implemented by adding redundant bits to the data which are then used at the receiver to detect and correct errors. By using FEC, the quality of the transmission can be enhanced. Parts of a typical receiver and the principle of FEC are shown in Fig. 8.

2.5 Radiowave propagation

2.5.1 Attenuation

As the transmitted signal travels through the space and atmosphere, it is attenuated by different phenomena. When the RF signal is transmitted from the antenna, it is spread over the space depending on the directivity of the antenna. Therefore, not all transmitted power reaches the receiving antenna. The power density decreases as a

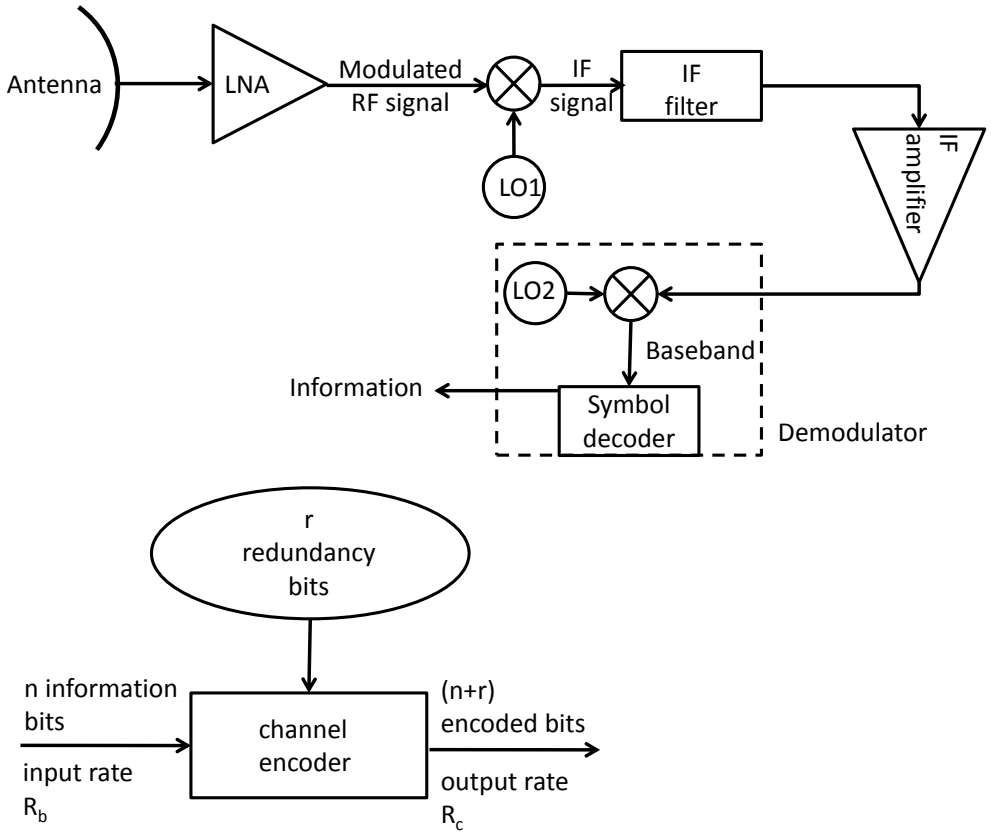

Figure 8: Typical superheterodyne receiver architecture on top and the principle of FEC on the bottom.

function of the distance. The received power level at the ground station receiver is:

$$P_r = \frac{P_t G_t G_r}{L_a} (\frac{\lambda}{4\pi R})^2, \tag{1}$$

where P_t is the transmitted power level, G_t is the transmitting antenna gain, G_r is the receiving antenna gain, L_a is the attenuation caused by the atmosphere and de-pointing of antennas, λ is the wavelength and R is the distance between the transmitting and receiving antennas. $(\frac{4\pi R}{\lambda})^2$ is the attenuation caused by the distance, known as the free-space loss.

The free space loss increases as the frequency increases. The frequency relates to the wavelength λ as $\lambda = c/f$. Therefore, the free space loss is greater with the S-band frequencies than with the VHF/UHF frequencies of Aalto-1. The free space loss as a function of the elevation angle of the ground station receiving antenna and frequency is shown in Fig. 9. In Fig. 9, the elevation angle of 90 degrees is perpendicular to the ground, i.e. the satellite is directly over the ground station. The height of the orbit is 900 km. As can be seen from Fig. 9, the free-space loss for the S-band frequencies of Aalto-1 is about 159 - 168 dB, depending on the elevation angle of the ground station receiving antenna.

When the transmitted signal travels towards the ground station receiver, it goes through layers causing additional attenuation to the signal. The radio wave interacts

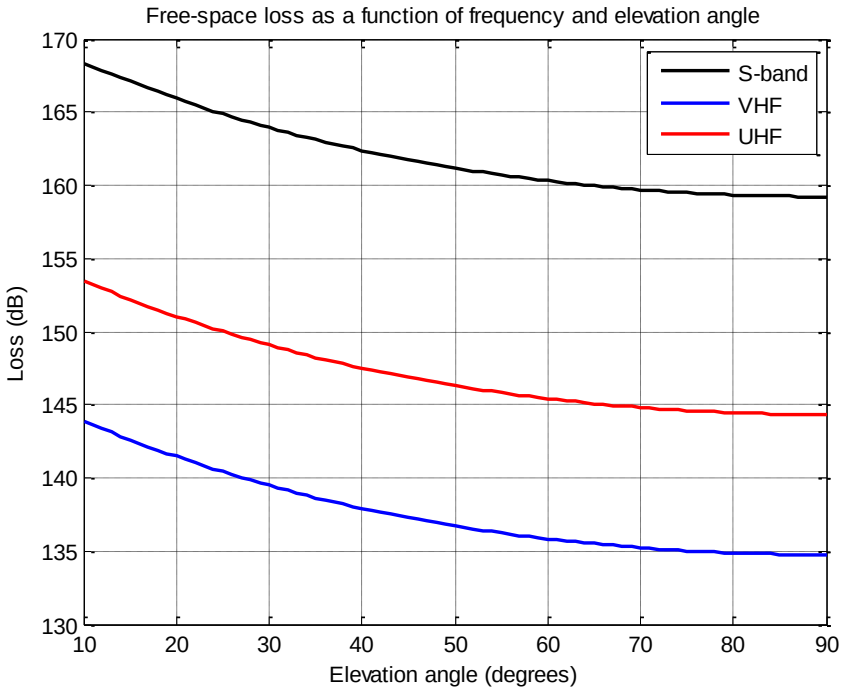

Figure 9: Free space loss as a function of frequency and elevation angle of the ground station antenna. The height of the orbit is 900 km.

with plasma in the ionosphere that can cause time delay, scintillation and disturb the wave polarization. Scintillations are signal amplitude fluctuations causing losses. As the signal travels through the troposphere, it faces absorption by the atmospheric gases, rain and clouds. Troposphere causes also scintillation which introduces additional attenuation. ITU-R P.618-9 recommends that at least the attenuation caused by atmospheric gases, rain, other precipitation and clouds, scintillation and multipath effects and sand and dust storms should be considered [19].

The recommendation states that ionosphere effects should also be considered, especially at frequencies below 1 GHz. At frequencies above 10 GHz the ionosphere effects can be neglected. At elevation angels above 10 degrees, only gaseous, rain and cloud attenuation and also the troposphere and ionosphere scintillation are significant compared to the other sources of attenuation. The atmospheric attenuation sources together with the free space loss are taken into account in the link budget calculations. The link budget is important for the design process of a transmitter: it gives the total attenuation of the signal. Based on the attenuation and on the quality of the ground station equipment one can have estimates on how much power the satellite's transmitter should be able to produce for the RF signal in order to have a reliable communication link.

The attenuation caused by the atmospheric gases can usually be neglected at frequencies below 10 GHz. ITU-R P676 [20] introduces a complex method for calculating the attenuation and SW code for Matlab is also available at the ITU-R software database [21]. The method gives attenuation levels of about 0.05 - 0.25 dB

for the ground station antenna elevation angles of 10 - 90 degrees for Aalto-1 S-band frequencies.

The attenuation caused by clouds and fog can be estimated with the methods given in ITU-R recommendation ITU-R P840 [22] and by the Matlab code on the ITU-R software database [23]. The methods give attenuation levels of about 0.006 - 0.035 dB exceeded at 1 % probability for the ground station antenna elevation angles of 10 - 90 degrees for Aalto-1 S-band frequencies.

The attenuation caused by rain can be estimated with methods presented in ITU-R recommendation P.838-3 [24]. The recommendation presents a specific attenuation model for rain that utilizes the rain height model available also on the software database of ITU-R [25]. The methods give attenuation levels of about 0.007 - 0.035 dB exceeded at 0.01 % probability for the ground station antenna elevation angles of 10 - 90 degrees for Aalto-1 S-band frequencies.

The attenuation caused by the tropospheric scintillations can be estimated with method specified in ITU-R P.618 and by using ready data for 50 % probability available from ITU-R software database [26]. The method can then be used to calculate the attenuation for different probabilities. The method gives attenuation levels of about 0.04 - 0.35 dB exceeded at 0.01 % probability with the ground station antenna elevation angles of 10- 90 degrees for Aalto-1 S-band frequencies.

Total tropospheric attenuation can be estimated as described in ITU-R recommendation P.618:

$$A_T(p) = A_G(p) + \sqrt{(A_R(p) + A_C(p))^2 + A_S^2(p)}, \tag{2}$$

where, A_R(p) is the attenuation caused by rain, A_C(p) by clouds, A_G(p) by atmospheric gases and A_S(p) by tropospheric scintillations, each at probability level of p exceeded during time. The probabilities for clouds and fog attenuation should be set as $A_C(p) = A_C(1\%)$ for $p < 1.0\%$ and for gases attenuation $A_G(p) = A_G(1\%)$ for $p < 1.0\%$. Total attenuation becomes then 0.09 - 0.6 dB exceeded at 0.01 % probability with the ground station antenna elevation angles of 10 - 90 degrees for Aalto-1 S-band frequencies. The tropospheric attenuation levels are summarized in Table 3.

Table 3: Tropospheric attenuation.

Source	**Level (dB)**
Gases	0.05 - 0.25
Clouds and fog	0.006 - 0.035
Rain	0.007 - 0.035
Scintillations	0.04 -0.35
Total	0.09 - 0.6

According to ITU-R recommendation P.531 [27], the scintillation should be taken into account when ionospheric attenuation is considered at frequencies of 0.1 - 12

GHz. The scintillation occurrence is the highest at the equatorial and polar regions. The mid-latitudes, such as the ground station for Aalto-1, do not face scintillation such frequently. The recommendation gives a rough estimate for the scintillation fade depth at 1.5 GHz, at solar maximum, at the altitudes of Aalto-1 ground station, to be about 1 dB. A simple ionospheric effects calculator is available in the IEEA web page [28] that is based on the GISM software of IEEA. GISM is recommended by the ITU-R recommendation P531. The calculator gives zero fade due to the ionospheric scintillations at Aalto-1 ground station latitudes for Aalto-1 S-band frequencies.

In case of a low Earth orbit (LEO) mission requiring one of the satellite's body axis to be aligned constantly with the tangent of a certain point on the Earth's surface, a constant attitude control of the satellite's body is needed. Such a case exists with Earth observation satellite missions which require the side containing for example the lenses of the imaging instruments to be pointed towards the imaging area. The antenna has to be pointed towards the ground station antenna in order to have maximally strong signal. The ground station receiving antenna has to be steered to point towards the satellite. If the two antennas are not pointed towards each other, there exists de-pointing losses, defined as [18]:

$$L_T = 12(\theta_T/\theta_{3dB})^2(\text{dB}) \ , \ L_R = 12(\theta_R/\theta_{3dB})^2(\text{dB}) \ , \tag{3}$$

where, θ_T and θ_R are the misalignment angles of the transmitting and receiving antennas orientation and θ_{3dB} is the 3 dB angular beam width of the antennas.

2.5.2 Noise in the communication link

Noise can cause errors to the RF transmissions if the noise level is high enough compared to signal level. If the received signal is too weak, it can be overcome totally by the noise that derives from the receiver and the sky. The noise is modeled as the noise temperature [29]. The sky noise, seen by the receiving antenna, can be derived from the different attenuation sources with the help of equation presented in ITU-R P.372 [30]:

$$t_b = t_e(1 - e^{-d}) + 2.7 \text{ K}, \tag{4}$$

where t_b is the sky noise temperature, t_e is the effective temperature (275 K), d is the total attenuation caused by the different attenuation sources as dB / 4.343 and 2.7 K is the cosmic background noise temperature. If the total attenuation caused by the different sources (see Table 3) is taken into account, the sky noise temperature is about 8 - 37 K for the ground station antenna elevation angles of 10 - 90 degrees for Aalto-1 S-band frequencies.

Another remarkable source of noise is the man made noise. If the antenna's main beam is directed close to the horizon level or the antenna has high side lobe levels, it can receive remarkable levels of interference noise from different sources. As the Aalto-1 S-band frequencies belong to the free ISM band, large amount of noise sources exists on the horizontal level, such as WLAN base stations, Bluetooth devices and microwave ovens [31]. Therefore, in order not to receive remarkably high noise levels as compared to the low signal levels, it is important to use high enough

elevation angles for the receiving ground station antenna and design the antenna so, that the side lobe levels are remarkably lower than the main lobe level. In the link budget calculations of Aalto-1 S-band system, the man-made noise was ignored; it was estimated that the elevation angle is above 10 degrees and the receiving antenna side lobe levels are low enough.

2.5.3 Effect of noise on digital communications

When the transmitter design process is considered, it is important to know the noise and signal power levels at the receiver. As stated before, the transmitted signal power level has to be high enough so that the noise level cannot overcome the signal level. The noise power spectral density is defined as:

$$N_0 = kT_s, \tag{5}$$

where k is the Boltzmann's constant and T_s is the receiving system noise temperature, consisting of the noise received by the antenna and the noise in the receiver system itself. In order to determine the relation between the noise and signal levels, one needs to determine the carrier power to noise power spectral density ratio C/N_0, defined as:

$$C/N_0 = \frac{P_s}{N_0}, \tag{6}$$

where P_s is the signal power. In satellite communications, there usually exists a certain lower limit for C/N_0 after which reliable communication link is not achievable. Therefore, it is important to derive the relationship between C/N_0 and the error probability for the transmissions. For digital communication systems utilizing digital modulation schemes, one of the most important factors is the bit error probability (BEP). BEP is directly related to the C/N_0, the modulation schemes and data rates used. In order to calculate BEP, one has to know the energy per bit to noise power spectral density ratio E_b/N_0 :

$$E_b/N_0 = (C/R_c)/N_0, \tag{7}$$

where R_c is the bit rate of the transmission. The value of BEP depends on the modulation scheme used. For coherent PSK modulation schemes the BEP is defined as:

$$BEP = (1/2)erfc\sqrt{E_b/N_0}. \tag{8}$$

For differential PSK modulation schemes the BEP is defined as:

$$BEP = (1/2)e^{-E_b/N_0}. \tag{9}$$

The $erfc$ function used in (8) and (9) is defined as:

$$erfc(x) = (\frac{2}{\sqrt{\pi}}) \int_x^{\infty} e^{-u^2}\, \mathrm{d}u. \tag{10}$$

A good approximation for $erfc\sqrt{E_b/N_0}$ at E_b/N_0 levels higher than 6 dB is given as:

$$erfc\sqrt{E_b/N_0} \approx (1/\sqrt{\pi})\frac{e^{-E_b/N_0}}{\sqrt{E_b/N_0}}. \tag{11}$$

The reliability of a satellite link can be enhanced by adding FEC to the transmitted signal. When FEC is added, the data rate of the transmission becomes:

$$R_b = \rho R_c, \tag{12}$$

where ρ is the code rate that is defined as:

$$\rho = n/(n+r), \tag{13}$$

where n is the number of data bits transfered and r is the number of error correction bits transfered.

In order to calculate the total noise at the receiver, one needs to know the receiver noise temperature which can be calculated from the receiver noise figure as:

$$T_R = (10^{F_R/10} - 1)T_0, \tag{14}$$

where F_R is the receiver noise figure in dB and $T_0 = 290$ K is the reference temperature. The noise factor of the receiver system can be calculated as:

$$F = F_a(F_c - 1) + F_c(F_t - 1) + L_c L_t(F_r - 1), \tag{15}$$

where F_a is the antenna noise factor, F_c is the noise factor associated with antenna circuit losses, F_t is the noise factor associated with transmission line losses, F_r is the receiver noise factor, L_c is the antenna circuit losses and L_t is the transmission line circuit losses. The noise factor associated with antenna circuit losses is defined as:

$$F_c = 1 + (L_c - 1)\frac{T_c}{T_0}. \tag{16}$$

The noise factor associated with transmission line losses is defined as:

$$F_t = 1 + (L_t - 1)\frac{T_t}{T_0}. \tag{17}$$

The total noise power spectral density at the receiver system is then defined as in (5). The transmitted signal power level at the receiver can be calculated as in (1).

For receivers, an important figure of merit is the relation between the antenna gain and noise, defined as:

$$G/T = \frac{G_r}{L_{total}T_{total}}, \tag{18}$$

where G_r is the receiving antenna gain. L_{total} is the total losses related to receiving system, including de-pointing loss of the receiving antenna and antenna feeding network and cable losses. T_{total} is the total noise temperature of the receiving system including antenna noise and receiver noise.

2.6 Space environment

The space environment causes its own challenges to the electronic circuit board design [32]. The solar wind is plasma, consisting mainly of protons and electrons and traveling at speeds of 200-2000 km/s. At 1 AU distance from Sun, the particle density is about 6 per cm^3. Especially remarkable the solar wind effects are during the so called coronal mass ejections. Energy of the protons and electrons varies from 100 MeV to GeVs. The solar wind causes the so called radiation belts inside the Earth's magnetosphere. The highly energetic particles in these radiation belts are potential danger for spacecrafts. The highly charged particles are able to ionize the electronic parts inside the satellite: they can cause electric charging and so called single event phenomena that degrade the electronic components. The cosmic background radiation causes gamma and X-rays that can also ionize the electronics. The degradation caused by the ionization can be divided into three categories. First, a single event upset can cause a temporal change in logical state (i.e. 1 to 0). Second, a single event latch-up can cause a static charge in a circuit that can only be recovered by a reset. Third, a single event burnout can cause a destruction of an integrated circuit.

Traditionally, the problems related to the ionizing radiation have been minimized by using radiation hardened components in the most sensitive parts of the space craft electronics, especially by NASA [33]. Radiation hardened electronics is expensive compared to the COTS (commercial of the shelf) products and therefore small satellite projects, such as CubeSat satellites, rarely have funding for such electronics. For example, the preceding model of RAD750, RAD6000, costs about 200 000 US dollars [34]. The model RAD750 was used in the Mars rover Curiosity mission [35] and the RAD6000 in Mars rovers Spirit and Opportunity [36].

In order to shield the electronics against radiation, one can also use aluminum shielding on the satellite, as is done with the Aalto-1 satellite. All the sides of the satellite are covered with aluminum plates. The thickness of the aluminum shield affects how much radiation is absorbed by the shield but there exists a certain limit after which the effect is saturated [37]. The risks can be evaluated also by testing the sensitive electronics already on Earth for radiation. The risks of the radiation can also be minimized by using radiation hardened software [38]. The use of error corrected memory (ECC) will also reduce the risk of corrupted memory blocks. Another good way of reducing the risks is to choose components that have been used in space applications before. Thus, it is important to make a survey on CubeSat missions and see, what components have been used for example in communications systems.

Vacuum in space can cause outgassing of certain materials. The outgassed material is very harmful because it can for example cover the lenses of scientific instruments. Therefore, ESA has lists of materials that they recommend that should or should not be used in space applications [39]. Also when the soldering of electronic components is considered, airbubles left inside the solder will be outgassed and therefore can cause a loss off electrical connections due to the damaged soldering. Therefore, specific methods in the soldering of the flight components have to

be taken into consideration [40].

When the satellite is on the orbit, it faces large temperature changes. They are caused by the fact that the satellite is facing both the shadow of the Earth and the sun light. Since the thermal expansion coefficient is not uniform inside the satellite, large temperature changes introduce stress to the subsystems. Therefore, when selecting the components and materials for the subsystems, these temperature changes have to be taken into account.

Meteoroids are formed by collisions between larger asteroids. After a collision has occurred, some of the parts head towards the Earth with an average speed of 17 km/s. Space debris consists of upper stages of rockets, old satellites and payloads, parts released during the missions, slag and dust. The sizes of space debris particles varies from micrometers to several meters. Relative speed of space debris particles can be as high of 16 km/s. Smaller sized meteoroids and space debris particles can cause degradation to solar panels and therefore lower the amount of power produced by the panels. Larger particles can damage the satellite severely due to the very high speeds of collision.

2.7 Requirements for Aalto-1 S-band transmitter

Before the transmitter design started, there existed also a commercial option for the Aalto-1 S-band transmitter. HISPICO from IQ wireless had been investigated to fulfill the mission requirements. The specifications of the radio module are listed in Table 4. The radio offers D-QPSK (differential quadrature phase shift keying) modulated transmissions with +27 dBm output power and 1 Mbit/s data rate. The power consumption is about 5 W, which is inside the Aalto-1 power budget. Forward error correction is also supported with TURBO codes, that is FEC with interleaving [41].

Table 4: HISPICO radio specifications.

Parameter	**Value**
RF power	+27 dBm
RF interface	50 Ω coaxial connector
Current consumption	1.5 A @ +27 dBm output power
Operation voltage	3.3 V
Modulation	D-QPSK
Data rate	1.06 Mbit/s
FEC	TURBO code, rate 0.489

In order to see, whether a transmitter is suitable for the mission, one has to determine the data throughput the transmitter offers. The data throughput can be evaluated with the help of a satellite orbit simulator tool, such as Satellite Toolkit from Agi. The simulator offers atmospheric attenuation models that take into account the phenomena described in Chapter 2.5.

The ground station receiver model requires information on the figure of merit of the receiver, G/T, defined in (18). Since there existed no receiving equipment for Aalto-1 S-band system during the design work introduced in this thesis, the specifications of the possible ground station equipment were estimated based on receivers offered by Quasonix [42] combined with a good quality LNA. Such a combination could be used within the Aalto-1 S-band ground station. The antenna feeding network and cable losses were both estimated to be about 1 dB. The receiving antenna gain was estimated to be about 30 dBi and elevation angle minimum of 10 degrees. The de-pointing angle of the receiving antenna was estimated to be about 1 degree. The receiving antenna was estimated not to receive any interference noise. Based on the noise figure of 3 dB and sky noise temperature of 8 - 37 K calculated in Chapter 2.5.2, one can calculate the noise temperature with (16) and (17). The average noise temperature becomes about 634 K. The figure of merit becomes then about 4.2 dB/K.

The data throughput depends on the error levels of the transmission. Therefore, one has to determine a certain threshold for the error levels after which the transmissions are not reliable enough. The bit error probability depends on the energy per bit to noise power spectral density ratio E_b/N_0 as in (10) and (11) for PSK modulation schemes. The BEP as a function of E_b/N_0 is shown in Fig. 10. A transmission can be considered reliable when the BEP is below 10^{-5} since there exists only one bit error within 100 000 transmitted bits. Therefore, the E_b/N_0 threshold was determined to be about 10.4 dB, as shown in Fig. 10. The receiver specifications used in the simulations are summarized in Table 5.

Table 5: Estimations Aalto-1 ground station receiver characteristics.

Parameter	**Value**
Antenna gain	30 dBi
Elevation angle minimum	10 degrees
Antenna feeding network losses	1 dB
Cable losses	1 dB
Receiver noise figure	3 dB
Sky noise	13 K
Receiver noise temperature	634 K
G/T	4.2 dB/K
E_b/N_0 threshold	10.4 dB

A sun-synchronous orbit was simulated with the orbit height of 900 km and by using the specifications of the commercial radio and the estimated ground station equipment. The transmitting antenna gain was estimated to be about 9 dBi, a typical value for a patch antenna. Based on the E_b/N_0 threshold, the simulations indicate that the average duration of a reliable transmission is about 3 min 40 s during one flyover of the satellite for the data rate of 1 Mbit/s. The achievable data throughput can be calculated from the access time by multiplying the access

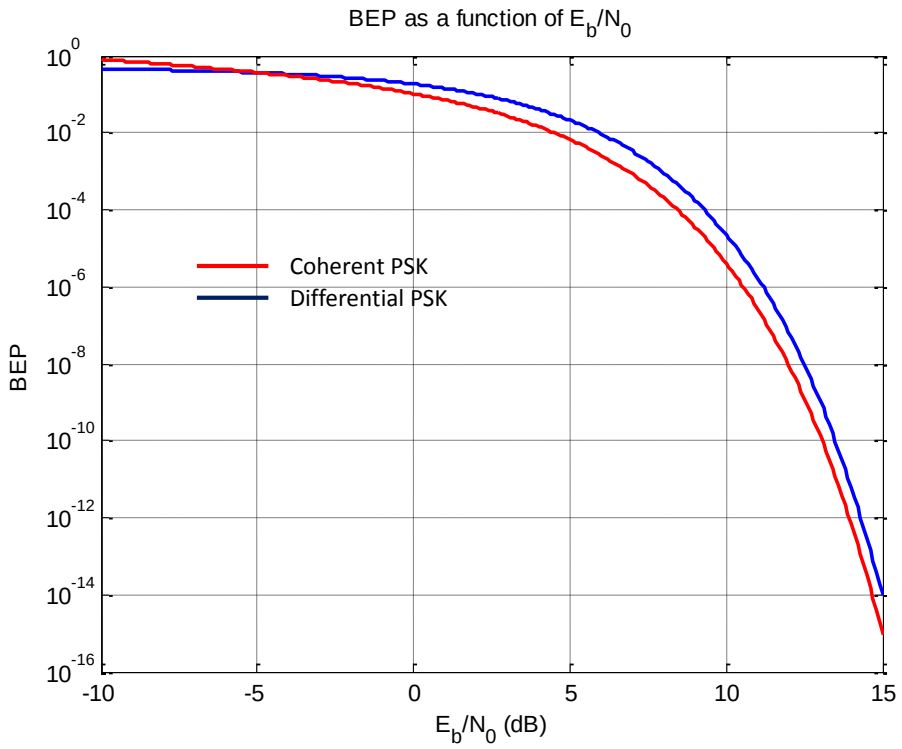

Figure 10: BEP as a function of E_b/N_0 for PSK modulation schemes.

time with the bit rate, resulting as the total number of transmitted bits. Then, the number of transmitted bits is divided by 8 in order to calculate the amount of transmitted bytes. Thus, the data throughput is about 26.3 MB per one fly over of the satellite. If the TURBO FEC of rate about 0.5 was used, the actual data rate of the transmissions becomes 0.5 Mbit/s, as defined in (12). With such a data rate, the simulations indicate that the average duration of a reliable transmission is about 4 min 38 s during one fly over. Thus, the data throughput during one flyover is about 16.6 MB. The data throughput of 26.3 MB achieved with the commercial radio was taken as the requirement for the S-band transmitter design: there is no reason to design a transmitter with lower data throughput since the mission of Aalto-1 would then be degraded. The data throughput simulation results are summarized in Table 6.

Table 6: Data throughput simulation results with the commercial radio.

Parameter	**No FEC**	**FEC**
Average access time	3 min 40 s	4 min 38 s
Data throughput	26.3 MB	16.6 MB

Based on the data throughput simulation results shown in Table 6 and on the interface constraints set by the Aalto-1 satellite bus, and as the space environment

challenges are taken into account, the S band transmitter has the requirements as shown in Table 7.

Table 7: Requirements for the S-band transmitter of Aalto-1.

Parameter	**Requirement**
Data throughput during one flyover	26.3 MB
Max power consumption	5 W
Circuit board size	CubeSat Kit standard PCB
Antenna interface	50 Ω coaxial connector
Data interface towards OBC	LVDS
Off-line mode power consumption	0 W
Transmitter control	Integrated into the transmitter
COTS components	Space heritage
RF output power level	Has to be adjusted according to the throughput requirement
Data rate	Has to be adjusted according to the throughput requirement

The space heritage of the COTS (commercial of the shelf) components used in the design was taken as one of the most important requirement for the transmitter design. The data throughput requirement is 26.3 MB. Therefore, depending on the data rate the transmitter offers, one has to adjust the RF output power: the bit error levels of the transmissions depend both on the RF output power and data rate. The transmitting antenna on the Aalto-1 satellite is a patch antenna having a 50 Ω coaxial connector interface. Thus, similar connector is needed on the transmitter board in order to connect the transmitter and the antenna. The data interface for the transmitter was the requirement set by the Aalto-1 satellite bus. There exists 3.3, 5.0 V and 12 V supply voltages on the satellite bus available for the transmitter. The circuit board dimensions are based on the CubeSat Kit standard PCB shown in Fig. 11 and the transmitter should share the board with the GPS subsystem. The mission of Aalto-1 requires the S-band transmitter to have the control unit of its own.

The radio wave propagation channel will change in time depending on the different conditions existing in the ionosphere and troposphere. The satellite's flight path with respect to the ground station also changes: the satellite might fly directly over the ground station or it can travel just above the horizon. As the elevation angle of the ground station receiving antenna affects the attenuation conditions, the attenuation will change during one fly over and will differ between individual fly overs. Therefore, to make the transmitter operation more efficient in terms of the Aalto-1 mission, the transmitter should have adaptable RF output power levels and data rates. Thus, in good propagation conditions the transmitter would not use the maximum RF output power, therefore saving power. In worse propagation

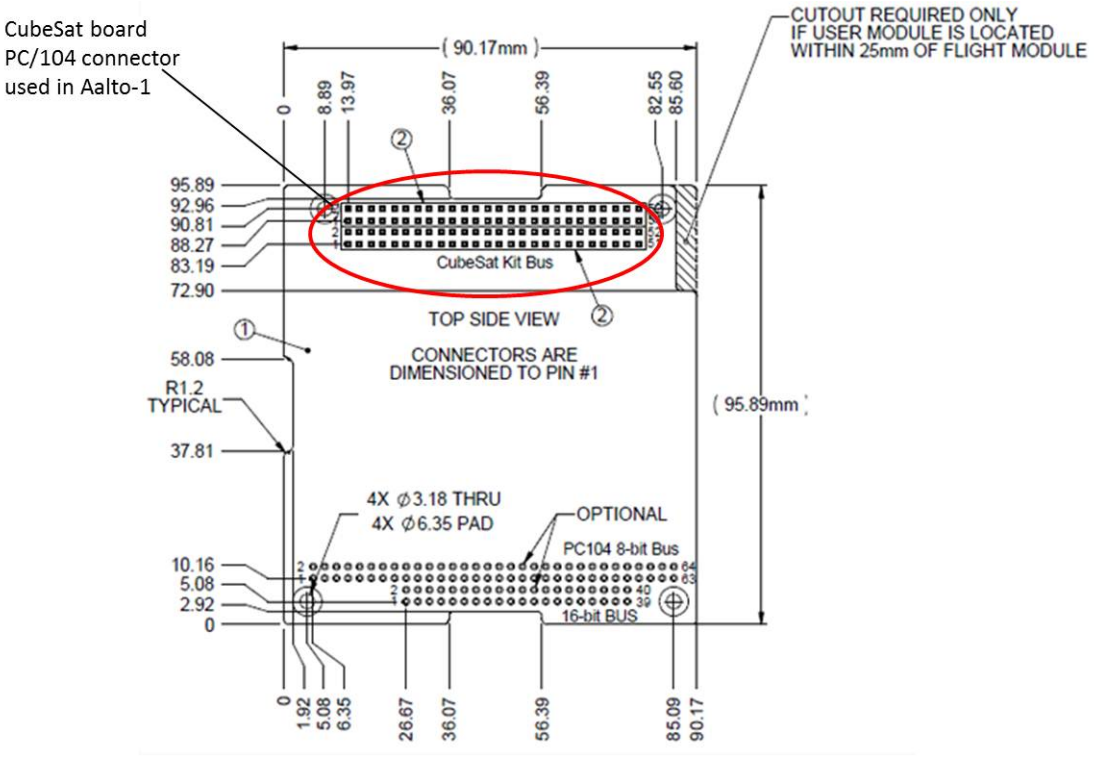

Figure 11: Typical dimensions for a CubeSat Kit standard board [14].

conditions, the transmitter would use more RF output power and decrease the data rate and add FEC to the transmissions in order to ensure a reliable communication link.

3 Implementation

This chapter introduces the design and implementation of the Aalto-1 S-band transmitter. The individual building blocks of the transmitter are described in detail and special attention is given on the RF transmission line design. The first prototype of the transmitter will be introduced including software for controlling the transmitter.

3.1 Architecture of the Aalto-1 S-band transmitter

A custom built solution was chosen for the Aalto-1 S-band transmitter due to the more educational value it offers and also due to the fact that the transmitter can then be optimized for the Aalto-1 mission purposes. When the development costs and duration of the transmitter design process are considered, the use of COTS components is only an advantage. Especially in the case of ISM band frequencies, many commercial transmitters and transceivers are available. Today's mobile technology has accelerated the development of low power RF systems. Due to the low power and high efficiency features of the systems targeted for mobile devices, they are also ideal solutions for CubeSat missions. Space industry has recently had projects that aim to launch a mobile phone to space inside a small satellite [43]. As mentioned in Chapter 2.2, some of the CubeSat satellite mission have used COTS RFIC (radio frequency integrated circuits) components in the communication subsystems. Thus, the usability of the RFIC technology in CubeSat missions has been proven.

Based on a survey on different COTS components, it was decided that the transmitter design should be based on a transceiver circuit that takes in the data to be transmitted, generates baseband signal from the data, modulates the baseband signal to the RF carrier and amplifies the modulated signal. It should also be possible to change the data rate and the RF output power of the transceiver. If the highest output power of the transceiver circuit is not high enough, an additional power amplifier (PA) circuit will be added to the transmitter. Both of the transceiver and PA circuits should be controlled via a microcontroller interface. The microcontroller should provide an interface to the OBC and transmit the data to the transceiver. Fig. 12 shows the basic building blocks for the initial design of the transmitter. As these commercially available off-the-shelf blocks are used, custom design is needed on the highlighted points shown in Fig. 12.

3.2 Transceiver circuit

Based on a survey on COTS transceiver circuits, couple of transceivers were evaluated as possible candidates for the Aalto-1 transmitter circuit, Analog Devices AFD7242 and Texas Intruments CC2500. These two circuits were the only ISM band COTS components having low enough power consumption and providing high enough data rates. The devices are compared in Table 8 [44],[45].

As can be seen from Table 8, ADF7242 offers higher data rate of 2 Mbit/s. CC2500 offers 500 kBaud data rate with shaped MSK modulation, identical to differential offset QPSK. If the modulator/demodulator used in the MSK signal

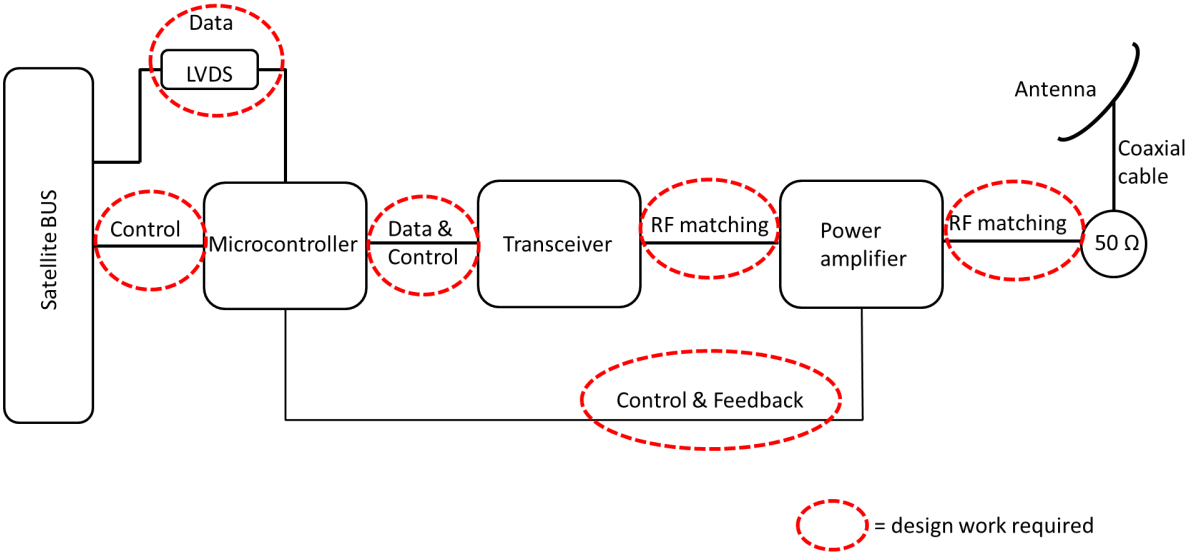

Figure 12: Building blocks of the initial architecture for the S-band transmitter.

generation/detection is an offset QPSK modulator/demodulator instead of a FSK modulator/demodulator, the signal can be regarded as offset QPSK with half-sine shaped pulses, as shown in [46]. Therefore, the actual bit rate is 1 Mbit/s, since the offset QPSK uses two bits per symbol. Both of the transceiver circuits have too low RF output power levels for the Aalto-1 S-band transmitter therefore requiring an additional power amplifier. If the current consumption with respect to the achieved output power level is considered, AD7242 is slightly more efficient than CC2500. When the space legacy of the products is taken into consideration, CC2500 has better specifications. The Texas Instruments Chipcon family (CCxxxx) has been used in several space missions and CC2500 is planned to be used in couple of space missions in the future [47],[48], as summarized in Table 9.

As ADF7242 has no space legacy, one cannot ensure the circuit operation in space. Texas Instruments offers a great amount of material for designing circuit boards for CC2500 [49], software tools for communicating with CC2500 and also guidelines on how to connect MSP430 family microcontroller with CC2500 [50]. Availability of such material speeds up, facilitates and secures the development process around CC2500. Analog Devices offers also some guide lines how to connect the transceiver to an ARM microcontroller and also the driver software for the transceiver [51],[52]. However, the connection schematics for the transceiver are more complicated as compared to the designs for CC2500, thus increasing the complexity of the whole transmitter design. There exits software support for ARM7 microcontroller containing some examples. However, TI MSP430 microcontroller

Table 8: Comparison between TI CC2500 and AD ADF7242.

Feature	**CC2500**	**ADF7242**
Data rate	50 Kbit/s - 2 Mbit/s	2.4 Kbit/s - 1 Mbit/s
Current consumption	21.5 mA @ +3 dBm	21.5 mA @ +1 dBm
Output power	-20 dBm to +4.8 dBm	-30 dBm to +1 dBm
Modulation	GFSK, FSK, GMSK, MSK	OOK, 2-FSK, GFSK, MSK
Programmable RF features	yes	yes
External power amplifier required	yes	yes
Space legacy	yes (the chip family)	no
Development material	good availability	limited
Space legacy of supported controller	yes	no

Table 9: Space heritage of TI Chipcon products.

Mission	**Device**
CP3	CC1000
CP4	CC1000
CAPE1	CC1020
OpenCube	CC1120, CC2500
PilsenCube	CC2500

family has an advantage compared to the ADuC7020 (used in the example code of ADF7242): MSP430 family has had heavy use in CubeSat missions by Pumpkin Inc.'s on board computer modules, as shown later on in chapter 3.4.

In order to check the achievable data throughput with CC2500, a data throughput simulation was run by using the specifications of CC2500. The simulations indicate, that a RF output power level of +27 dBm would result into a 26.3 MB data throughput per one fly over with MSK modulated signal of 1 Mbit/s data rate. Therefore, it was concluded, that TI CC2500 would fulfill the mission requirements if a power amplifier providing 26 dB of gain was used. As the CC2500 has the space heritage, it was chosen as the transceiver for the Aalto-1 S-band transmitter.

3.2.1 TI CC2500 transceiver

TI CC2500 is a complete transceiver circuit based on zero-IF RFIC technology. It is available as QFN (quad-flat no-leads) 20 pin package and the pin layout is shown in Fig. 13. The functional block diagram is shown in Fig. 14. As can be seen from Fig. 14, the microcontroller interface is implemented with a Serial-Peripheral-Interface (SPI) and two digital input/output pins for general use. SPI uses four signal lines, clock (SCLK), Master-In-Slave-Out (MISO), Master-Out-Slave-In (MOSI) and Chip-Select (CSn). GDO0 and GDO2 are the two digital input/output pins that can be used for requesting internal status of the transceiver or they can be used as transmit and receive pins in the synchronous and asynchronous serial modes.

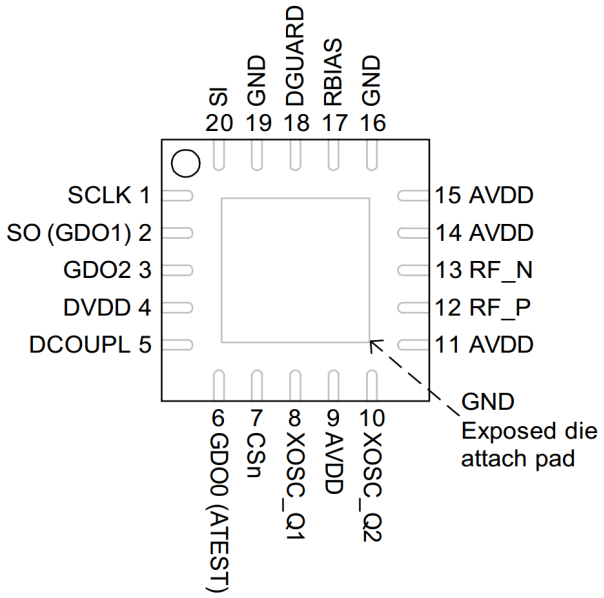

Figure 13: Pin layout for CC2500 [45].

On the SPI, the transceiver is the slave and the microcontroller is the master. The transceiver is programmed and controlled via the SPI and the interface is also used for the data transfer. Programming of the transceiver is achieved by modifying different internal register values on the transceiver. These register values correspond to different functionalities on the transceiver. Manufacturer of the transceiver provides a register configuration tool (TI SmartRF Studio) that can be used to get the correct values for each register(see Fig. 15). The software tool is available for free from Texas Instruments [53].

The operation of the transceiver is based on a built-in state machine. Therefore, the controlling software should be designed to follow the state machine characteristics in order to get full benefits of the low power features. A simplified state machine example is shown in Fig. 16. The transceiver changes state when it receives the corresponding command from the SPI (i.e. STX and SRX) or by pulling the CSn pin low. The transceiver has built-in voltage regulators that provide the supply voltages for the subsystems inside the chip. As is shown in the state machine example in Fig.

16, the Sleep state has the lowest power consumption. At that state, the voltage regulators are off, so the digital electronics is powered off. The ability to switch of the digital electronics is important: as mentioned in Chapter 2.6, the single event latch-ups require a system reset. The SPI register access is shown in Figs. 17 and 18.

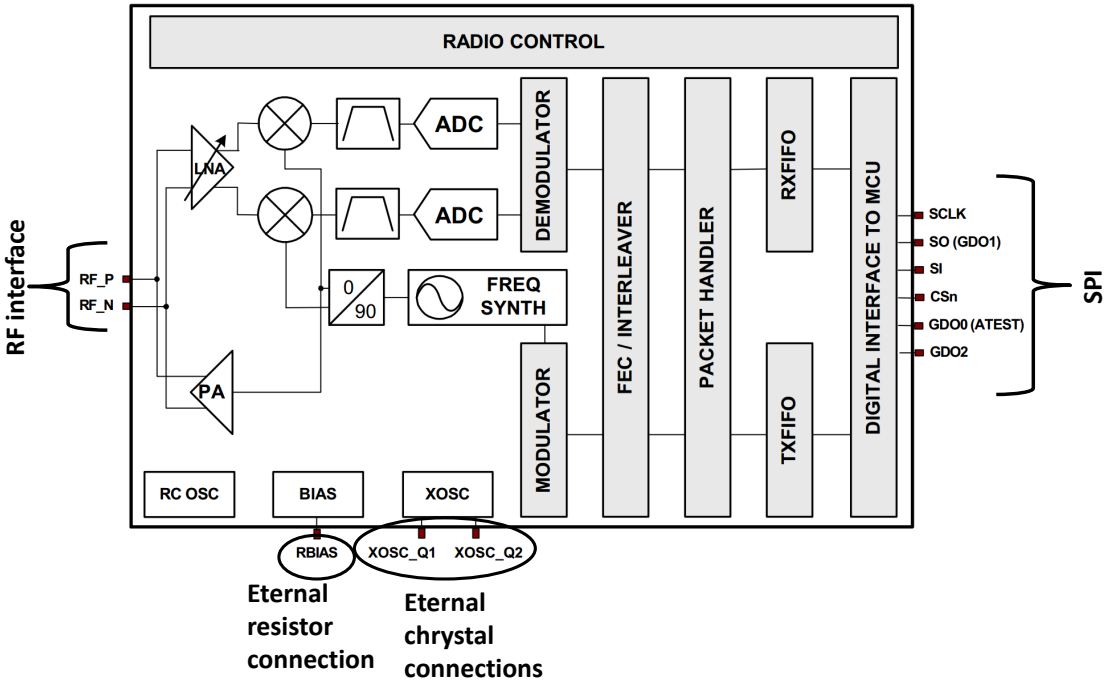

Figure 14: The functional diagram of CC2500 [45].

The transceiver has packet handling capabilities. The use of packet transmissions is evident in the Aalto-1 S-band system due to the following facts:

1. One spectral image can be as large as 10 MB, which necessitates the image to be divided into smaller packages for transmissions.

2. The different data packages of one image are sent individually by the transmitter.

3. After the receiver has received the packages, the image has to be rebuilt from the individual packages. Therefore, the individual packages have to be identified so that the image can be rebuild from them.

The packet format produced by the packet handler is shown in Fig. 17. The size of $TXFIFO$, which contains the actual data to be transmitted, is 64 bytes. Different parts of the packet are programmable, such as the length of the preamble,

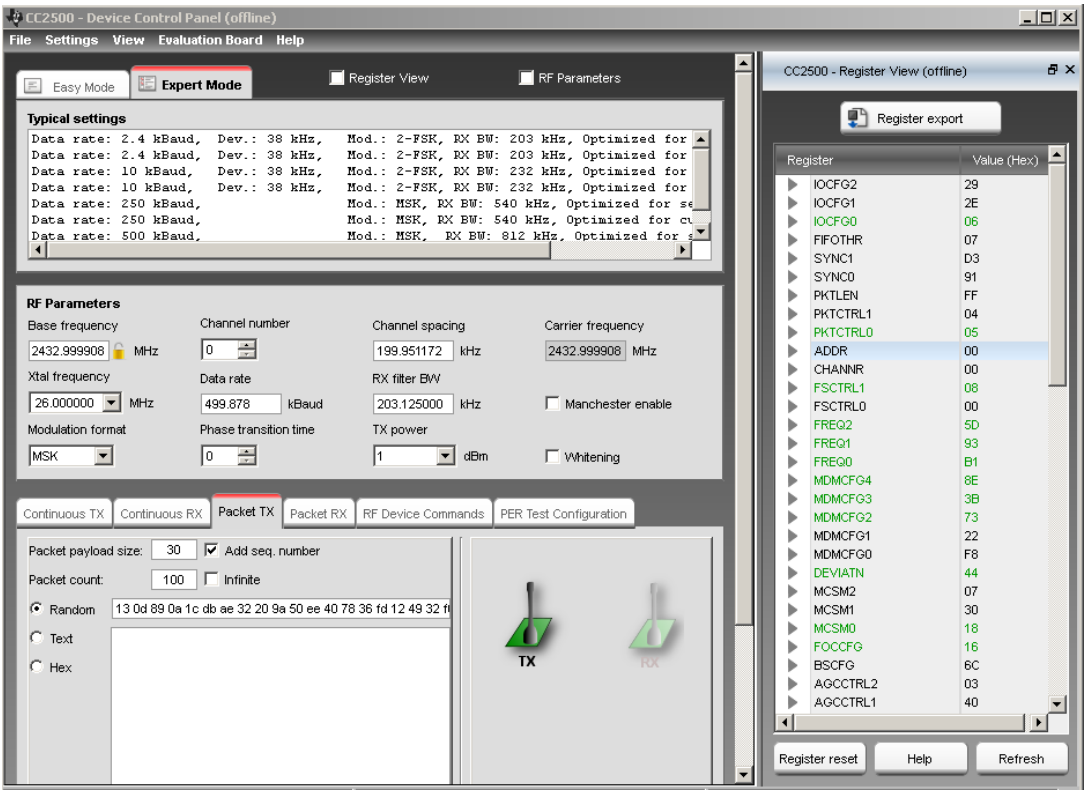

Figure 15: Screenshot of the TI Smart RF Studio register configuration for CC2500 [53].

synchronization word and data packet. On the data packet to be transmitted, the length field, address field and CRC-16 fields are optional. The CRC field is the checksum of the packet to be transmitted. When the Aalto-1 S-band system is considered, CRC would be useful in order to check whether the checksum is the same for the received and transmitted packets. The transceiver supports also forward error correction with interleaving, as shown in Fig. 17. The FEC coder inside the transceiver is a convolutional coder with a rate of 0.5. The errors in real digital communication channels have usually a bursty character and the error correction codes are usually designed for independent errors. By interleaving, the bits in the original sequence are reordered and the errors become quasi-statically independent [54]. The transceiver supports also data whitening. When the data whitening is enabled, the long data sets of zeros and ones are removed by the whitening process. Such an operation will make the data to be transmitted more random and the power distribution is then smoother over the bandwidth [55].

RF transmissions of the transceiver are organized as follows:

1. The transceiver operation state is changed to transmitter.

2. The modulator sends the programmed pre-ample bits.

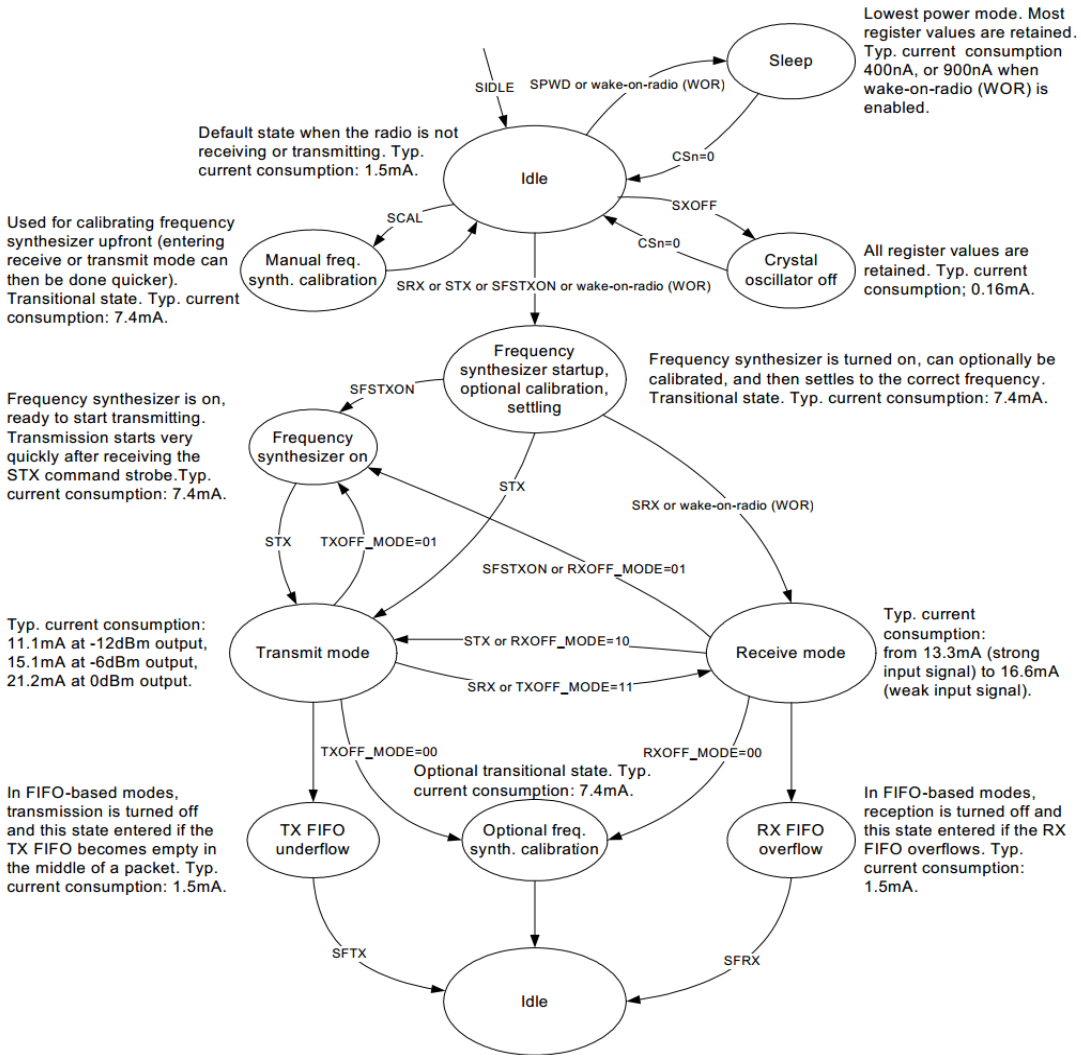

Figure 16: State machine example of CC2500 [45].

3. The first byte is written into $TXFIFO$ register.

4. The modulator sends the synchronization word.

5. The modulator sends the data in the $TXFIFO$ register.

The transmission operation will stay in step 5 until the $TXFIFO$ runs empty. Then, the chip will enter $TXFIFO\_UNDERFLOW$ state. If there was still data to be transmitted, the command $SFTX$ has to be issued in order to transmit rest of the packet, as shown in Fig. 16.

The packet handling in the transceiver can be implemented in two ways, either as interrupt driven solution or by SPI polling. In the interrupt driven solution, the transceiver will send an interrupt via one of the GDIO (general digital input/output) lines to the microcontroller, for example in the case of one data packet transmitted. If the SPI-polling is used, the microcontroller requests the transceiver for different

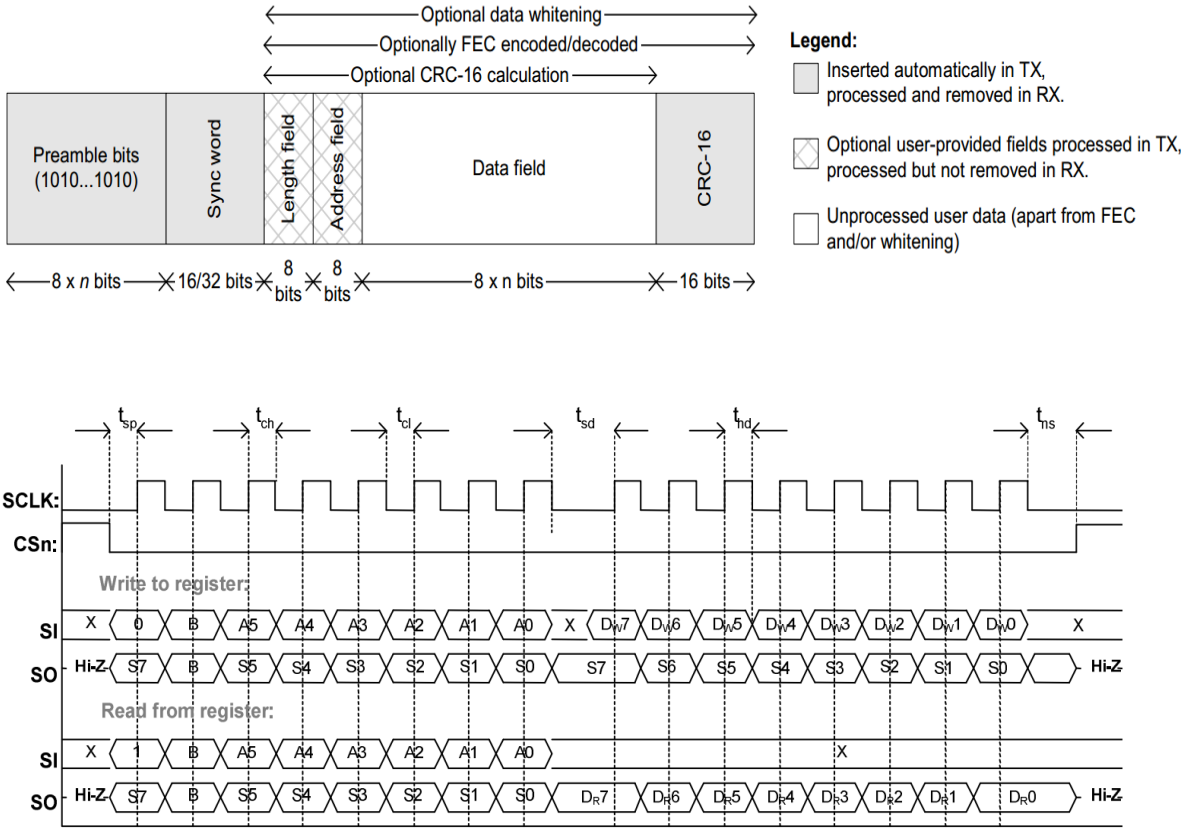

Figure 17: Packet format of the transceiver (top) and the SPI register access timing (bottom) [45].

values of interest, for example the number of bytes remaining in TX FIFO. The interrupt driven solution can be seen as more efficient solution due to the fact that the transceiver invokes immediately the microcontroller without any contribution required from the microcontroller. The data transmission between the microcontroller and the transceiver is optimized, since the microcontroller does not have to request information about the state of the $TXFIFO$ register.

Parameter	Description		Min	Max	Units
f_{SCLK}	SCLK frequency 100 ns delay inserted between address byte and data byte (single access), or between address and data, and between each data byte (burst access).		-	10	MHz
	SCLK frequency, single access No delay between address and data byte			9	MHz
	SCLK frequency, burst access No delay between address and data byte, or between data bytes			6.5	MHz
$t_{sp,pd}$	CSn low to positive edge on SCLK, in power-down mode		150		µs
t_{sp}	CSn low to positive edge on SCLK, in active mode		20	-	ns
t_{ch}	Clock high		50	-	ns
t_{cl}	Clock low		50	-	ns
t_{rise}	Clock rise time		-	5	ns
t_{fall}	Clock fall time		-	5	ns
t_{sd}	Setup data (negative SCLK edge) to positive edge on SCLK (t_{sd} applies between address and data bytes, and between data bytes)	Single access	55	-	ns
		Burst access	76	-	ns
t_{hd}	Hold data after positive edge on SCLK		20	-	ns
t_{ns}	Negative edge on SCLK to CSn high		20	-	ns

Figure 18: CC2500 SPI timing requirements [45].

3.3 Power amplifier module

As stated in Chapter 3.2, the maximum RF output power of the transceiver is +1 dBm. Due to the high losses in the satellite communication link, the signal needs to be amplified. Therefore, an additional power amplifier (PA) module is needed for the Aalto-1 S-band transmitter. Throughput simulations indicated that an RF output power of +27 dBm would be required with the transceiver chip chosen for Aalto-1. As in the case of the transceiver circuit, the PA was chosen from COTS RFIC chips available on the market. As different PAs on the market were evaluated, the RF5602 ISM band PA from RFMD was chosen due to the specifications of the product and previous space mission experience of RFMD devices. The RFMD RF5602 is a RFIC final stage power amplifier with the specifications [56] summarized in Table 11.

RF5602 is a class AB type amplifier, which is a compromise between the highly linear class A amplifiers and the highly efficient class B amplifiers [57]. The maximum RF output power of the RF5602 is +33 dBm. Therefore, the custom build Aalto-1 S-band transmitter could provide 6 dB more RF power compared to the commercial radio. Of course, when driving the RF5602 almost in the compression, the linearity characteristics of the amplifier are suffering: the matching circuit topology recommended by the RFMD is optimized for the linearity at +27 dBm RF output

Table 10: Requirements for the power amplifier module.

Parameter	Requirement
RF output power	+27 dBm
Gain	26 dB (min)
Power consumption	below 5 W
COTS components	Space heritage

Table 11: RF5602 specifications.

Parameter	Value
Supply voltage	3.3 to 5.0 V
Gain	32 to 34 dB
Package	16-pin leadless QFN
1 dB compression point	+33 dBm
Linearity	2.5 % @ +26 dBm
RF output port	Unbalanced, requires an external matching circuit
RF input port	Unbalanced, 50 Ω
Current consumption	450 mA @ +26 dBm, 690 mA @+30 dBm
Power amplifier class	AB

power. However, since the transceiver circuit used in the Aalto-1 S-band transmitter uses MSK modulation scheme, the linearity requirements are not so strict due to the fact that the envelope curve of MSK modulated signals is constant in amplitude.

The RFMD's products have space legacy. RFMD 2117 power amplifier has been used as a part for CP2 communications system design [58] and the actual space experience was introduced with CP4 satellite, the backup satellite of CP2 due to the launch failure of the CP2 [59]. RF2117 has flown also on CAPE1 satellite [9].

3.3.1 RFMD RF5602 power amplifier

RF5602 is available as 3mm x 3mm x 0.45 mm, 16 pin, leadless chip carrier. The pin layout and the internal functional block diagram of the amplifier module are shown in Fig. 19. As can be seen, the power amplifier has a three-stage amplifying chain. The RF input ports are internally matched to 50 Ω. The RF output ports need an external matching circuit. The supply voltages should be provided for each stage individually (VCC1, VCC2 and VCC3) and the last stage should have the supply provided to the RF output ports. The supply lines need DC filtering capacitors. The bias voltages for the amplifying stages are provided by VREG1, VREG2, VREG3 and BIAS VCC pins. The register voltages VREG1, VREG2 and VREG3 control the amount of bias voltage used for the three amplifying stages. BIAS VCC is the

operation voltage for the internal biasing circuitry of the amplifier. The bias voltages need external resistors. RF5602 has also an internal power detector available that provides a voltage signal with the level corresponding to a certain power level. Such a signal could be connected to an I/O port on the microcontroller having analog-to-digital conversion available. RF5602 has also PDOWN pin which can be used to power on/off the three amplifier stages.

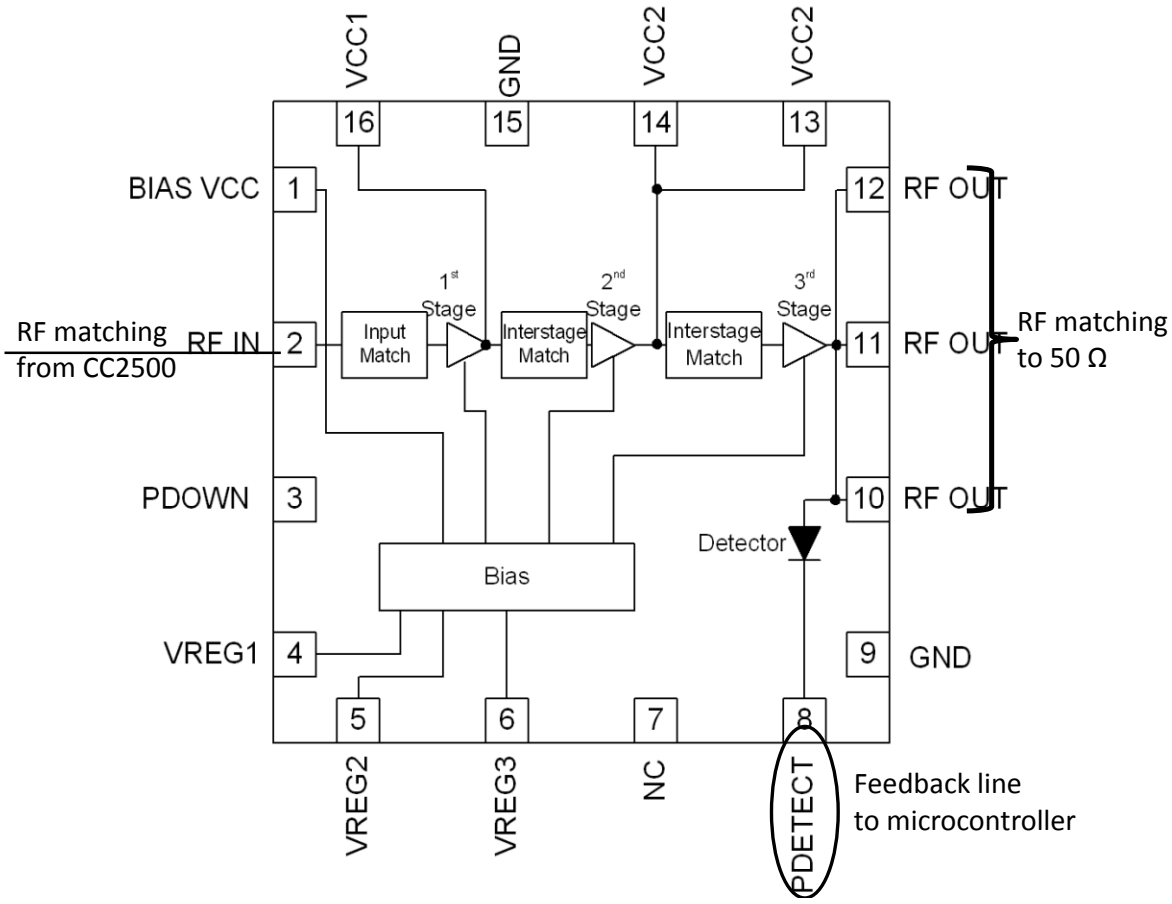

Figure 19: Pin layout and the functional bloc diagram of RF5602 power amplifier module [56].

3.4 Microcontroller unit

At first, the transmitter design process was based on the AVR microcontroller technology and the first tests with the transceiver prototype boards were executed with Arduino which is based on the AVR architecture. However, when the previous space usage was considered, the Texas Intruments MSP430 family was also taken under evaluation. The MSP430 family is used by Pumpkin Inc. as one of the processor possibilities in their CubeSat Kit motherboards [60]. The MSP430 family has been used for example in the recent nanosatellite missions such as GOLIAT [61] and e-st@r [62]. An advantage with the MSP430 family is the fact that the manufacturer has

design guidelines how to connect MSP430F2274 microcontroller to the transceiver circuit. Therefore, MSP430 was chosen as the microcontroller for the transmitter.

3.4.1 TI MSP430F2274 microcontroller

MSP430F2274 is a mixed signal microcontroller with the specifications [63] summarized in Table 12. MSP430F2274 has 40 pins layout, available as DA and RHA packages. RHA package was chosen for the Aalto-1 S-band transmitter design due to the smaller footprint. The RHA package pin layout is shown in Fig. 20. The functional block diagram for the MSP430F2274 is shown in Fig. 21.

The Aalto-1 S-band transmitter should provide LVDS (low voltage differential signalling) interface towards the OBC and the transceiver requires SPI for data transmission and two interrupt pins. MSP430F2274 microcontroller has two serial interfaces USCIA0 and ASCIB0. These two interfaces can be used as UART (universal asynchronous receiver/transmitter), SPI and I2C (two wire interface). The LVDS can be formed from the SPI with a specific driver chip as shown in Chapter 3.7. As can be seen from Fig. 20, clock line UCA0CLK and chip select line UCB0STE share the same pin and clock line UCB0CLK and chip select line UCA0STE share the same pin. Therefore, the two serial interfaces, USCIA0 and USCIB0, cannot be used at the same time, if the clock lines and chip select lines of both interfaces are used at the same time. Thus, the solution used in Aalto-1 S-band transmitter was to use some GPIO pins for the chip select lines due to the fact that the chip select lines are simple enable/disable lines.

The software development for the TI MSP430F2274 microcontroller can be achieved with the TI MSP430 Launchpad development board [64]. The Lauchpad development board has a JTAG interface that can be used to program TI MSP430 family microcontrollers. The wireless development set EZ430-RF2500 has software examples available which can be used to provide the software code for controlling the transceiver. TI Smart RF Studio can be used to get the right register settings for the transceiver.

Table 12: MSP430F2274 microcontroller specifications.

Parameter	**Value**
Supply voltage	1.8 to 3.6 V
Current consumption	270 μA at 1 MHz
Architecture	16-bit RISC
CPU frequency	16 MHz
Flash memory	23 KB + 256 KB
RAM	512 KB
Serial interfaces	2 x SPI/I2C

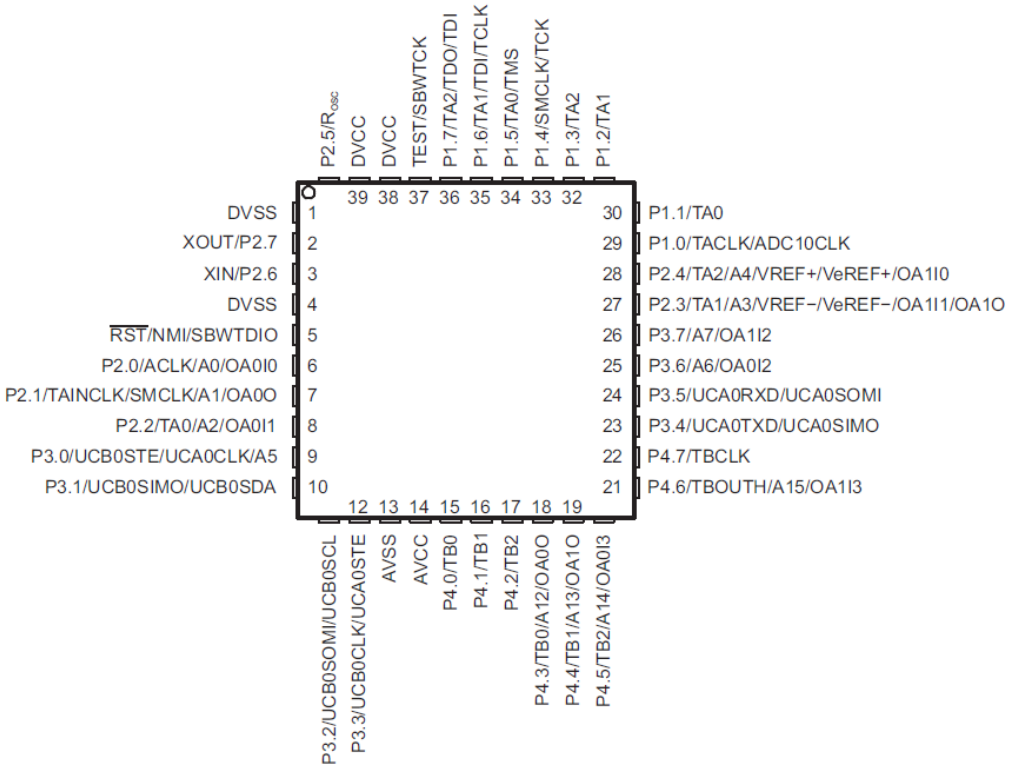

Figure 20: Pin layout for the RHA package of the microcontroller [63].

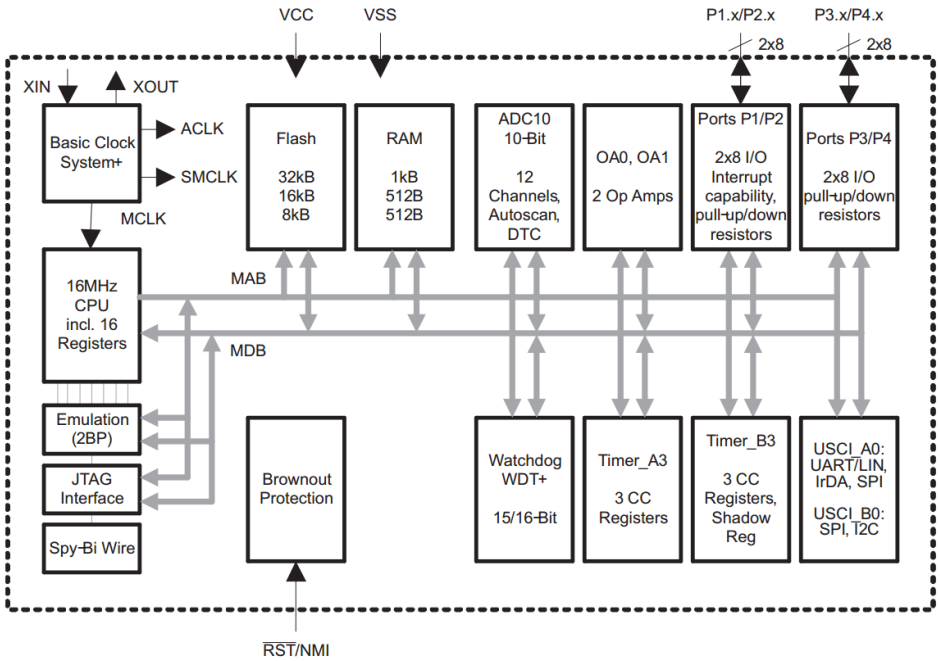

Figure 21: Functional block diagram of the microcontroller [63].

3.5 Conclusions on the transmitter architecture

The chosen architecture for the Aalto-1 S-band transmitter consists of TI CC2500 transceiver, RFMD RF5602 power amplifier and TI MSP430F2274 microcontroller family. The architecture has the specifications as summarized in Table 13. The architecture provides an RF output power level up to +33 dBm. The transceiver module offers MSK modulated transmissions with data rates up to 1 Mbit/s. Data throughput simulations with such values indicate that 41.6 MB of throughput is achievable. The architecture has a maximum power consumption of 4.2 W which is well within the power budget of Aalto-1. The transceiver has also packet handling capabilities and can add FEC to the transmissions. The data rate, RF output power level, modulation scheme, FEC and packet format are programmable. The chosen architecture is therefore adaptable according to the attenuation conditions. Based on these facts, the designed architecture was concluded to fulfill the requirements set by the Aalto-1 mission.

Table 13: The estimated specifications of Aalto-1 S-band transmitter.

Parameter	**Value**
RF output power	up to +33 dBm
Data rate	1 Mbit/s
Power consumption	max 4.2 W
Data throughput	41.6 MB

3.6 Impedance matching for the transmitter

The last stage on the transceiver transmitter chain is a power amplifier. From the RF theory, the power amplifier has to have a certain load impedance in order to deliver the maximum power to the load [65]. The power amplifier at the transceiver has differential output and the manufacturer states that the optimal differential load impedance is 80 + 74j Ω. The final stage power amplifier chosen for the Aalto-1 S-band transmitter has an unbalanced 50 Ω RF input port. Thus, the balanced RF output of the transceiver has to be transformed to the 50 Ω unbalanced RF input. Also, the RF matching circuit has to provide the optimal load impedance for the transceiver. The manufacturer of the transceiver provides a reference RF matching circuit. The reference design uses a balun and π-network of discrete inductors and capacitors (see Fig. 22). The RF signals at the positive and negative RF output ports of the transceiver are 180 degrees out of phase as compared to each other. Therefore, the balun should even the phases of the two signals in order to sum up the amplitudes of the two signal lines and thus maximizing the power delivered to the output. The purpose of the π-network is to match the balun output impedance to 50 Ω and also to filter out harmonics caused by the transceiver's power amplifier nonlinear features. There are two DC-block capacitors located at the input of the balun.

Since the RF interface of the transmitter is a 50 Ω coaxial connector, the output of the RF5602 power amplifier has to be matched to 50 Ω. The matching circuit has to also provide the optimal load impedance for the power amplifier, that is 2 - 4.75j Ω at 2.425 GHz. The manufacturer of the power amplifier RF5602 provides a reference design optimized for the linearity purposes at +27 dBm RF output power. The reference design has also been tested to provide 1 dB compression point at +33 dBm. The reference design is shown in Fig. 24. As can be seen, the design uses discrete capacitors and short microstrip stubs. The RF-block for the supply line is implemented with a network of discrete inductor and capacitor. The required matching circuits for the transmitter architecture are summarized in Fig. 23.

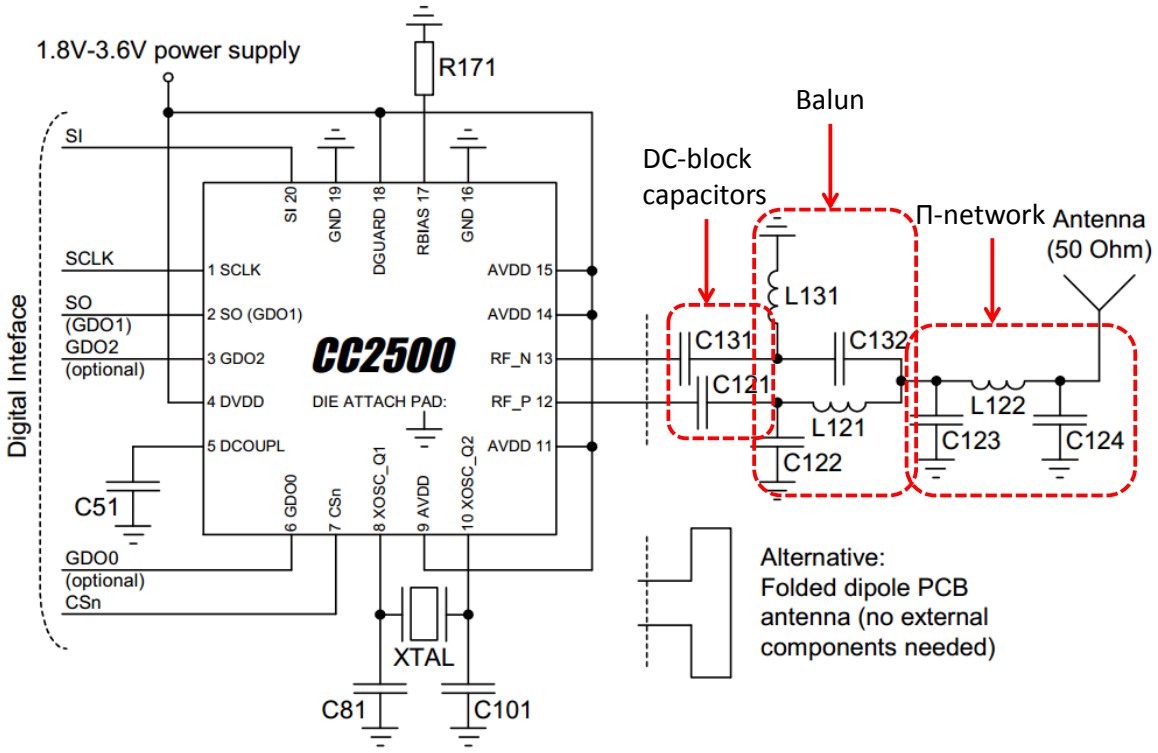

Figure 22: Reference design for the transceiver RF output matching circuit [45].

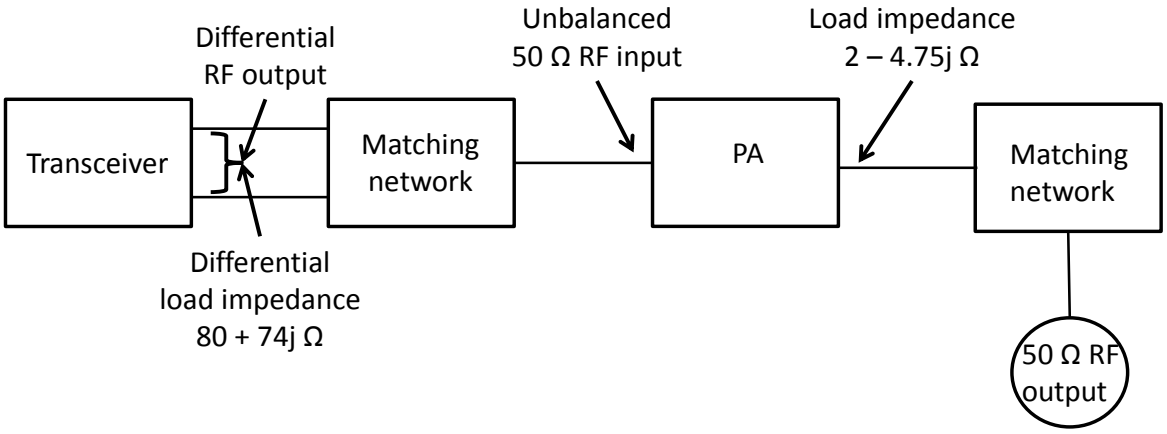

Figure 23: Required RF matching circuits for the transmitter architecture [56].

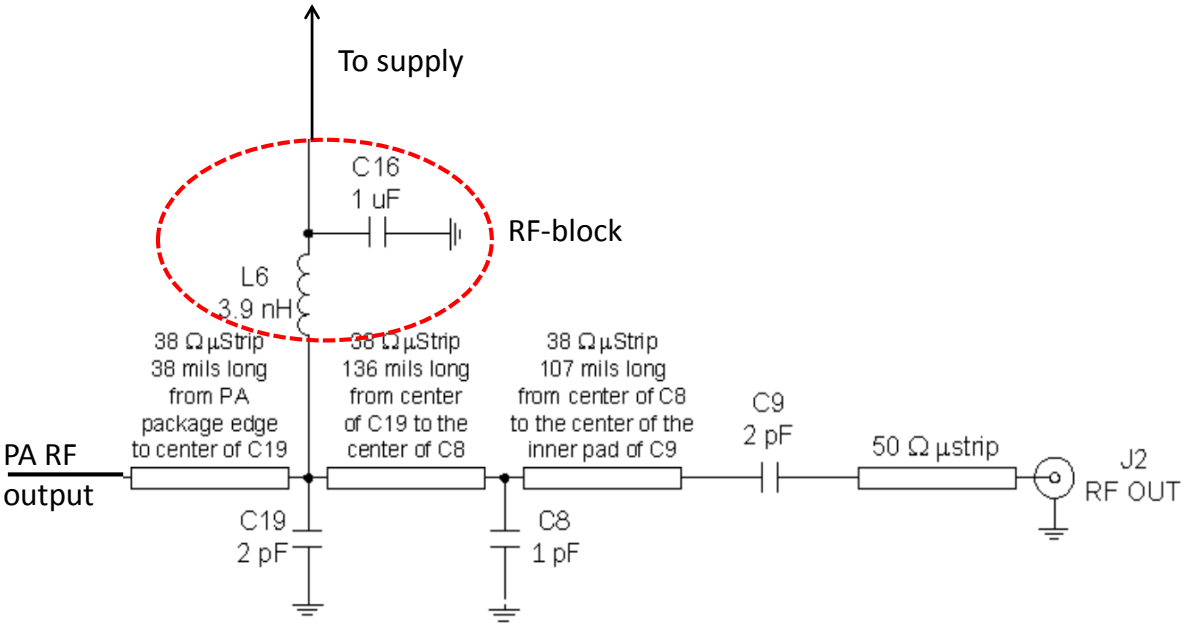

Figure 24: Reference design for the power amplifier RF output matching [56].

3.6.1 Theory on microstrip elements

The reference designs of the transceiver's and power amplifier's RF output matching circuits are based on the use of discrete components. As compared to a microstrip stub matching, such an approach saves space on the board when minimum sized components, such as 0402, are used. However, the use of discrete components will increase the amount of soldering required on the RF matching circuit. Soldering of

the components for a space application has to be done in a specific way in order to avoid for example air bubbles inside the soldering material. A break down of a discrete component or loss of the connection to the signal line, will result as loss of connection or short circuit for the signal. Such an event may cause a complete loss of the transmitter operation. Therefore, to decrease the number of soldered discrete components on the RF signal paths, a microstrip implementation was chosen for Aalto-1 S-band transmitter design. The topology of the matching circuits were decided to be the same as in the reference designs: the discrete components are replaced with interdigital and gap capacitors, via holes and microstrip stubs.

Fig. 25 shows the structure of a typical interdigital capacitor [66]. Based on the dimensions shown in Fig. 25, the total capacitance in pF of such an interdigital capacitor can be approximated with the following equation:

$$C_{tot} = (\epsilon_r + 1)l[(N-3)A_1 + A_2] \text{ (pF)}, \tag{19}$$

where A_1 and A_2 are defined as:

$$A_1 = 4.409 \tanh[0.55(\frac{h}{W})^{0.45}] \cdot 10^{-6} \text{ (pF}/\mu\text{m)}, \tag{20}$$

$$A_2 = 9.92 \tanh[0.52(\frac{h}{W})^{0.45}] \cdot 10^{-6} (\text{ pF}/\mu\text{m}). \tag{21}$$

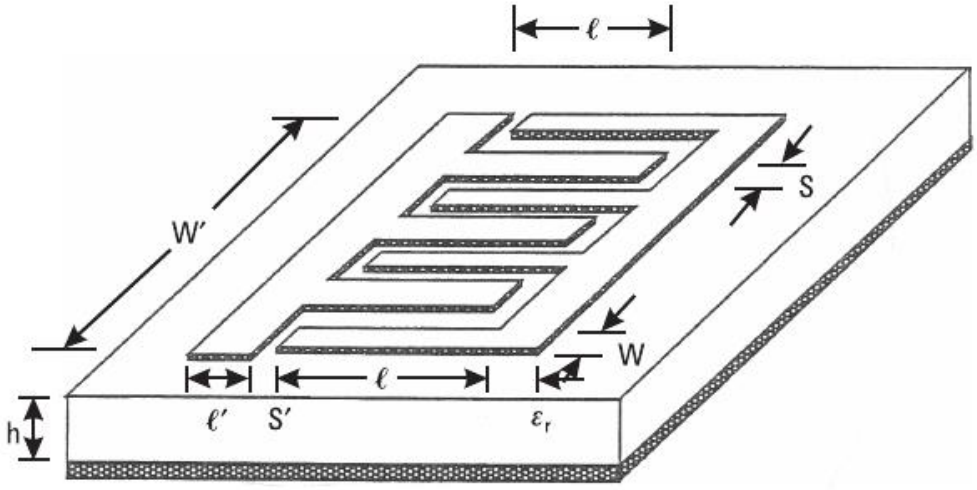

Figure 25: Typical structure of an interdigital capacitor [66].

(19), (20) and (21) are valid only if the l', S', W and S are of the same size and the length of the structure is $l < \lambda\ /\ 4$. The correspondence of parameters l', S', W, S, l, ϵ_r and h to the interdigital capacitor structure is shown in Fig. 25.

A gap capacitance is formed when a microstrip stub has a cut-off for some distance. The structure for such capacitor is shown in Fig. 26. The capacitance value for the gap can be approximated with the following equation [57]:

$$C = (C_{o2} - C_{e2}/2)/2, \tag{22}$$

where C_{o2} and C_{e2} are odd and even mode capacitances defined as:

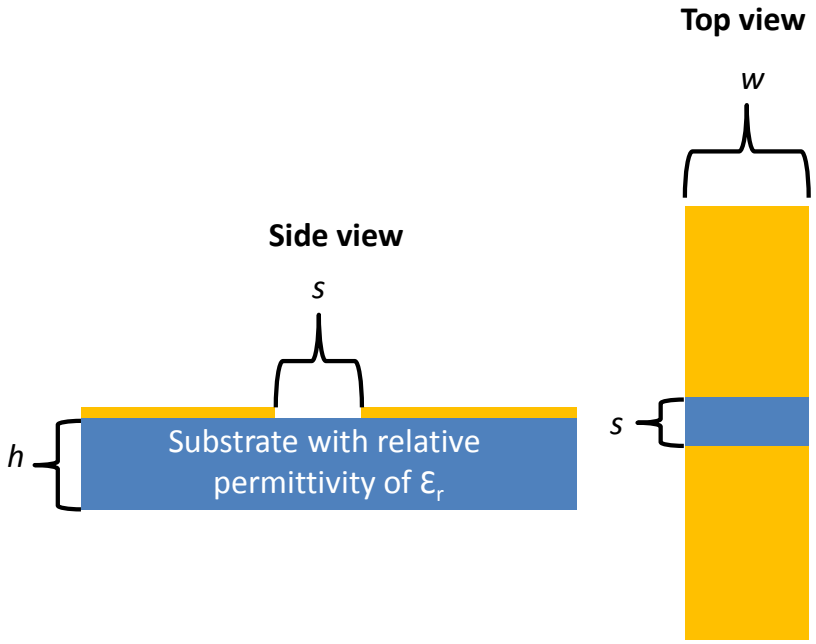

Figure 26: Typical structure of gap capacitor.

$$C_{o2} = C_{o1}(\epsilon_r/9.6)^{0.8}, \tag{23}$$

$$C_{e2} = C_{e1}(\epsilon_r/9.6)^{0.9}, \tag{24}$$

where C_{o1} and C_{e1} are again odd and even mode capacitances defined as:

$$C_{o1} = w(s/w)^{m_o}e^{k_o}, \tag{25}$$

$$C_{e1} = w(s/w)^{m_e}e^{k_e}, \tag{26}$$

where m_o, m_e, k_o and k_e are odd and even mode parameters and defined as:

$$m_o = (w/h)(0.267\ \log(w/h) - 0.3853), \tag{27}$$

$$m_e = 0.8675, \tag{28}$$

$$k_o = 4.26 - 0.631 \log(w/h), \tag{29}$$

$$k_e = 2.043(w/h)^{0.12}. \tag{30}$$

When the microsrtip line has to be connected to ground plane, it is usually implemented with a via hole. Such a configuration introduces a small inductance and has to be taken into account in the circuit design. The following equation is given for the inductance introduced by the via hole [66]:

$$L_{via} = 0.2[h - \ln(\frac{h + \sqrt{r^2 + h^2}}{r}) + 1.5(r - \sqrt{r^2 + h^2})] \text{ (pH)}, \tag{31}$$

where h is the height and r is the radius of the via hole. Short individual microstrip lines can be seen as capacitances and inductances. If the length of the line is $l < \lambda$ / 4 and the line has high characteristic impedance, the line can be modeled as a series inductance. Length of a line having a series inductance of L is (with the characteristic impedance of Z_{oh}):

$$l = \frac{\lambda}{2\pi}\arcsin(\omega L/Z_{oh}). \tag{32}$$

If the length of the line is $l < \lambda$ / 4 and the line has low characteristic impedance, the line can be modeled as a shunt capacitance. Length of a line having a shunt capacitance of C is (with the characteristic impedance of Z_{ol}):

$$l = \frac{\lambda}{2\pi}\arcsin(\omega C Z_{ol}). \tag{33}$$

3.6.2 Impedance matching for the transceiver and the power amplifier

The impedance matching circuits for the transceiver and the power amplifier were implemented with microstrip elements. The topologies of the reference designs given by the manufacturers were used as the design basis. The discrete inductors were replaced with short lines and via holes and capacitors with gap and interdigital capacitors. The microstrip elements were first designed with (22), (25), (34) and (35). Then, Agilent's Advanced Design System (ADS) 2011 circuit simulator was used to optimize the microstrip elements. The circuits were designed on an FR4 substrate having thickness of 1.6 mm. The permittivity was estimated to be about 4.4 for the transceiver simulator model and for the power amplifier 4.1, since different manufacturers were planned to be used for providing the circuit boards. The simulation setups for the transceiver and the power amplifier are shown in Fig. 27. A vector network analyzer (VNA) model with ungrounded ports was used with the transceiver to simulate the balanced impedance. VNA with grounded ports was used with the power amplifier. The second port on both of the VNAs was set to have an impedance of the complex conjugate of the optimal load impedance. The port was then connected to the input of the matching circuits. The first port on both of the VNAs was set have an impedance of 50 Ω and was connected to the output of the matching circuits.

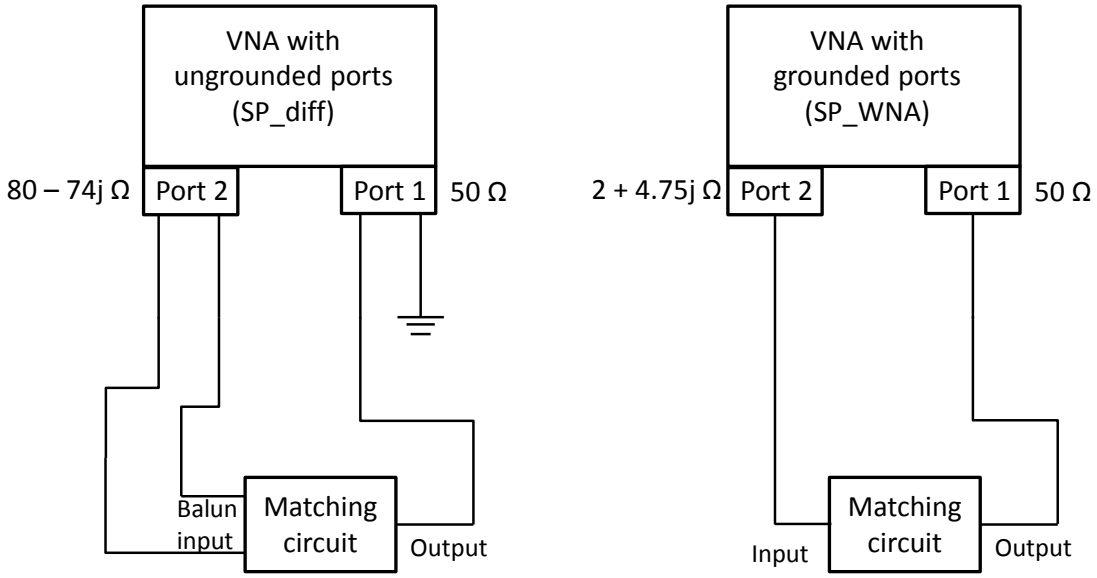

Figure 27: ADS 2011 simulation setup for the transceiver matching circuit on the left and for the power amplifier on the right.

The optimized layout of the microstrip matching circuit for the transceiver is shown in Fig. 28. The DC-block capacitors located before the balun input in the reference design were not replaced with microstrip elements due their large capacitance value, since a large capacitance is difficult to obtain with microstrip elements.

The optimized matching circuit for the power amplifier is shown in Fig. 29. As can be seen, the biasing of the RF output stage was implemented with a radial stub and λ / 4 length stub.

In order to ensure a fluent development process of the Aalto-1 S-band transmitter, the transceiver and power amplifier circuits were decided to be tested first individually. The transceiver chip requires some number of external components. A 26 MHz crystal is required to provide an external clock reference. Also one bias resistor, a few supply filtering capacitors and one inductor are needed. The required components are shown in Fig. 30. The manufactured prototype of the transceiver is shown in Fig. 31. The RF5602 power amplifier requires also some external components to operate. The required external components are shown in Fig. 33. The manufactured prototype of the power amplifier is shown in Fig. 32. The simulation and measurement results of matching circuits are shown and analyzed in Chapter 4.1.

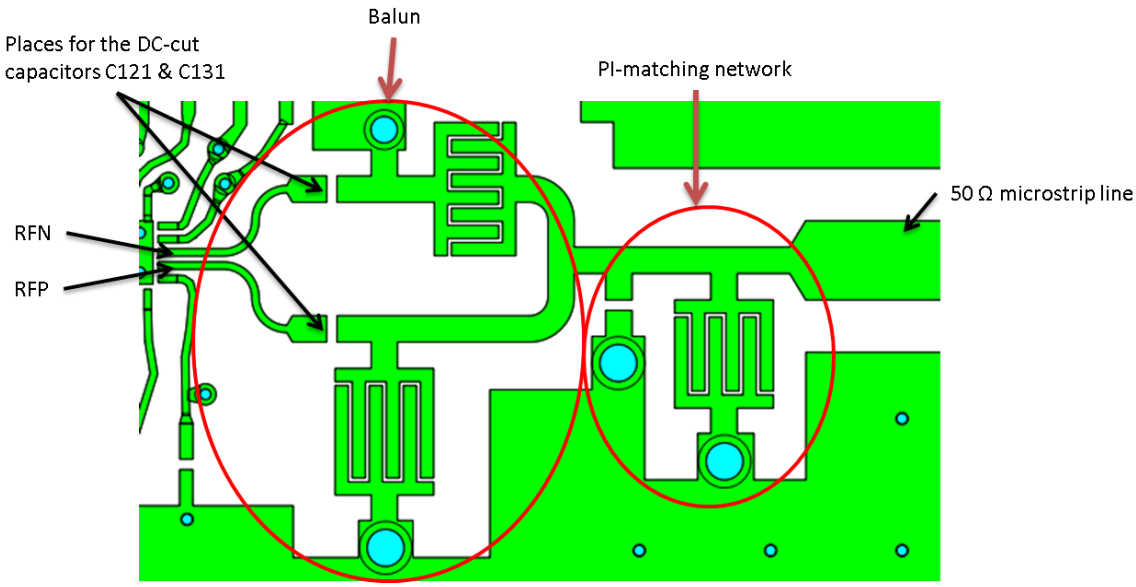

Figure 28: Layout of the microstrip matching circuit for the transceiver.

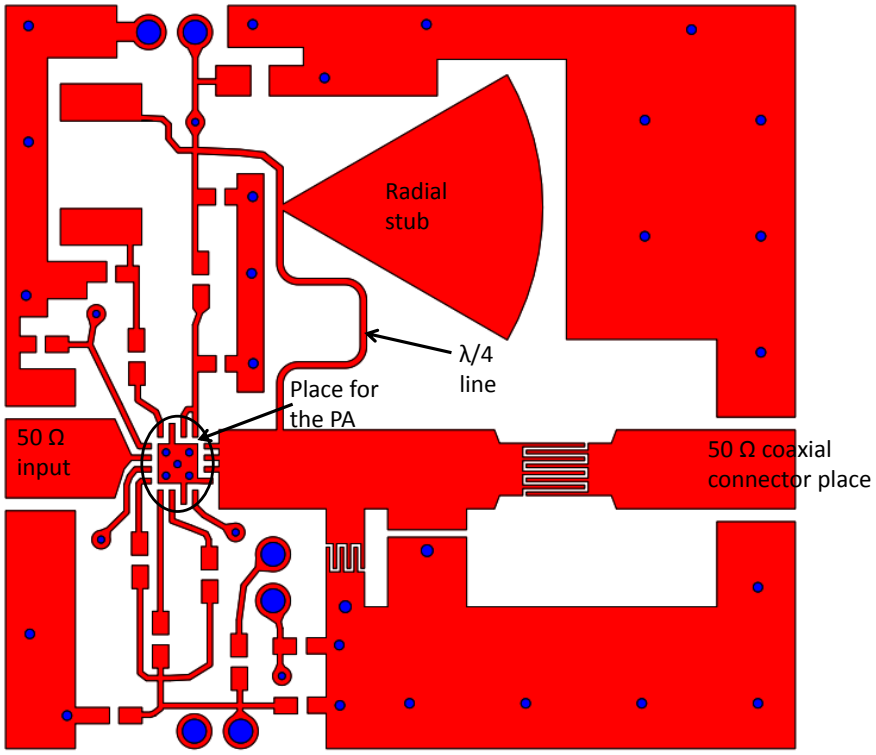

Figure 29: The output matching circuit designed for the PA.

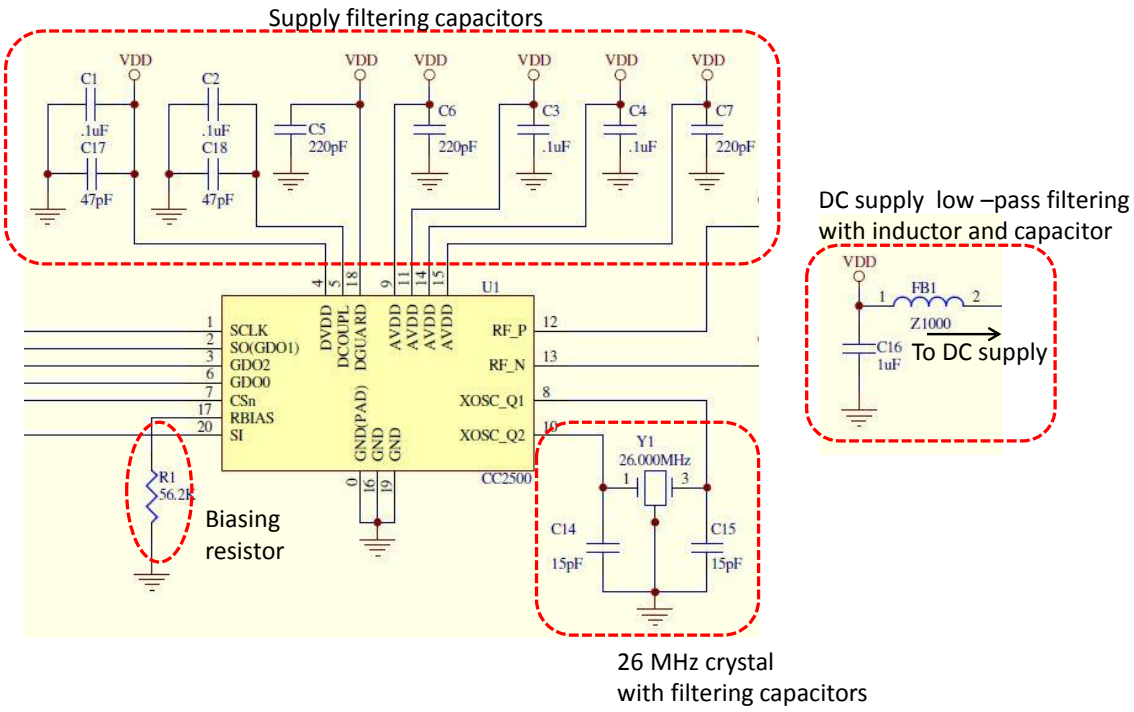

Figure 30: External components needed for the transceiver chip [67].

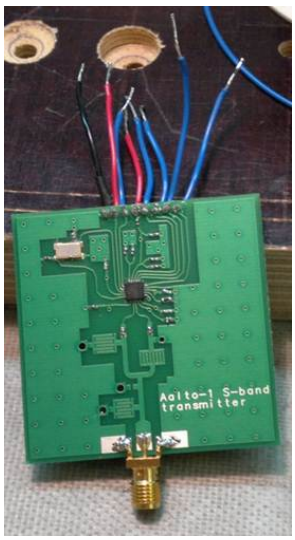

Figure 31: Photograph of the first manufactured prototype of the transceiver.

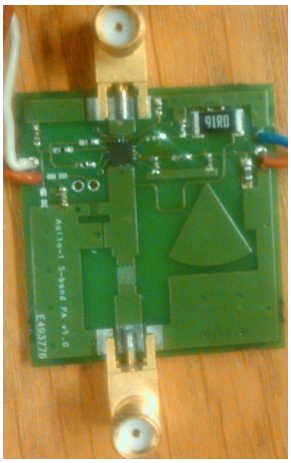

Figure 32: Photograph of the first manufactured prototype of the power amplifier.

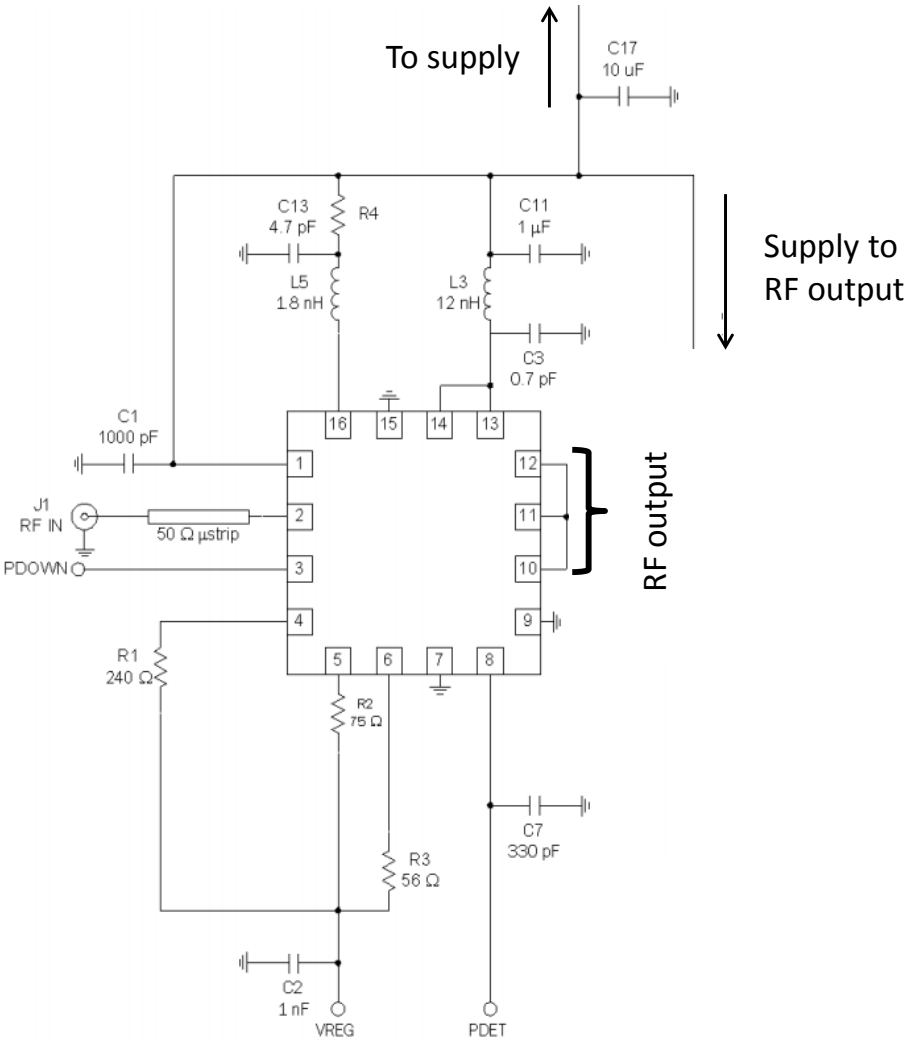

Figure 33: Required external components for the power amplifier [56].

3.7 Aalto-1 S-band transmitter first prototype

In order to test the operation of the whole transmitter circuit, a prototype board layout was designed with EAGLE containing the MSP430F2274 microcontroller, the CC2500 transceiver and the RF5602 power amplifier. Additional external discrete components were added to the microcontroller, transceiver and power amplifier according to the recommendations of the manufacturers.

The power amplifier has a power consumption of 10 mA in the power-down mode that is too high for the Aalto-1 power budget. Therefore, it should be possible to completely turn of the power amplifier when the transmitter is not used. Thus, a power switch was added to the supply line of the power amplifier. The power switch chosen for the transmitter first prototype circuit was TI TPS2556. It is a current-limited power switch, with the current limit threshold from 500 mA to 5.0 A which is set with an external resistor. The functional block diagram of the power switch with the additional external components needed is shown in Fig. 35 [68]. In order to adjust the current limit to a certain maximum, the following equation given by the manufacturer can be used:

$$R_{ILIM}(\mathrm{k\Omega}) = (\frac{99038V}{I_{lim,max}\mathrm{mA}})^{1/0.947}. \tag{34}$$

As the maximum tolerable supply current for the power amplifier is 800 mA, a good maximum current could be 750 mA. The formula gives for the resistor value about 174 kΩ.

The microcontroller has SPI support but does not provide ports for LVDS. Therefore, a special LVDS transceiver circuit was added for the SPI - LVDS conversion. The LVDS transceiver chosen was TI SN65LVDS049, a dual-flow-through differential line driver-receiver. The functional diagram and pin configuration of SN65LVDS049 are shown in Fig. 34 [69].

The basic connections of the first prototype board are shown in Fig. 36. The connection schematics for the transceiver, power amplifier, microcontroller, power switch, LVDS transceiver and satellite bus are shown in Appendices A, B and C. The Aalto-1 satellite bus pin layout is shown in Appendix D [14]. The layout design is shown in Appendix E. The manufactured board is shown in Fig. 37. As can be seen, the GPS system is located on the same board.

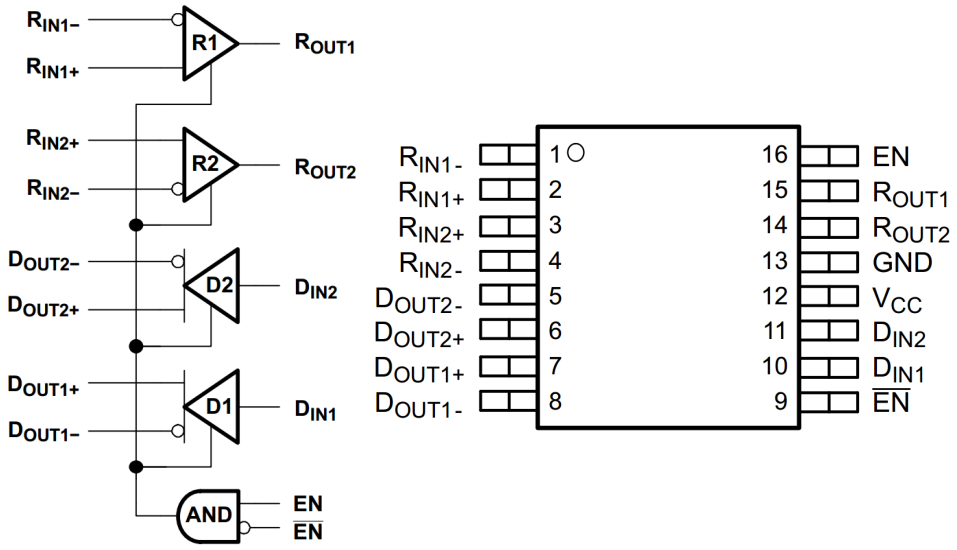

Figure 34: Functional block diagram (left) and pin configuration (right) of SN65lvds049 [69].

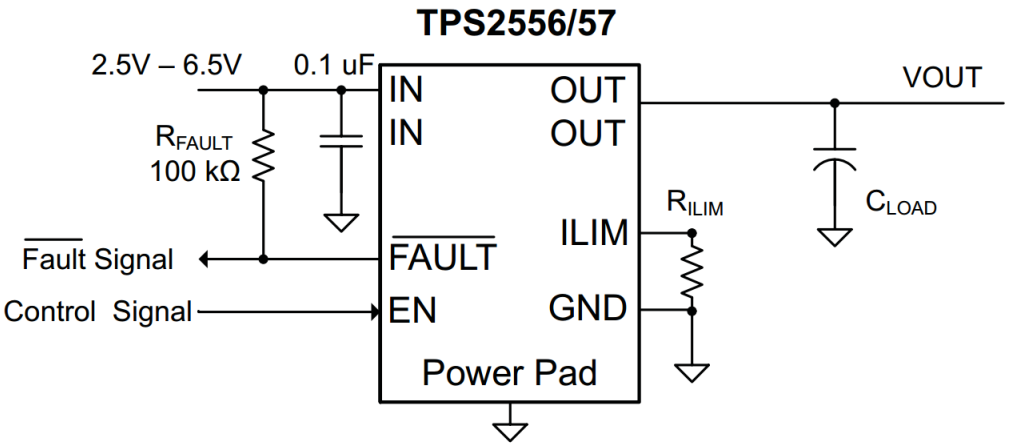

Figure 35: Functional block diagram of TPS2556 power switch [68].

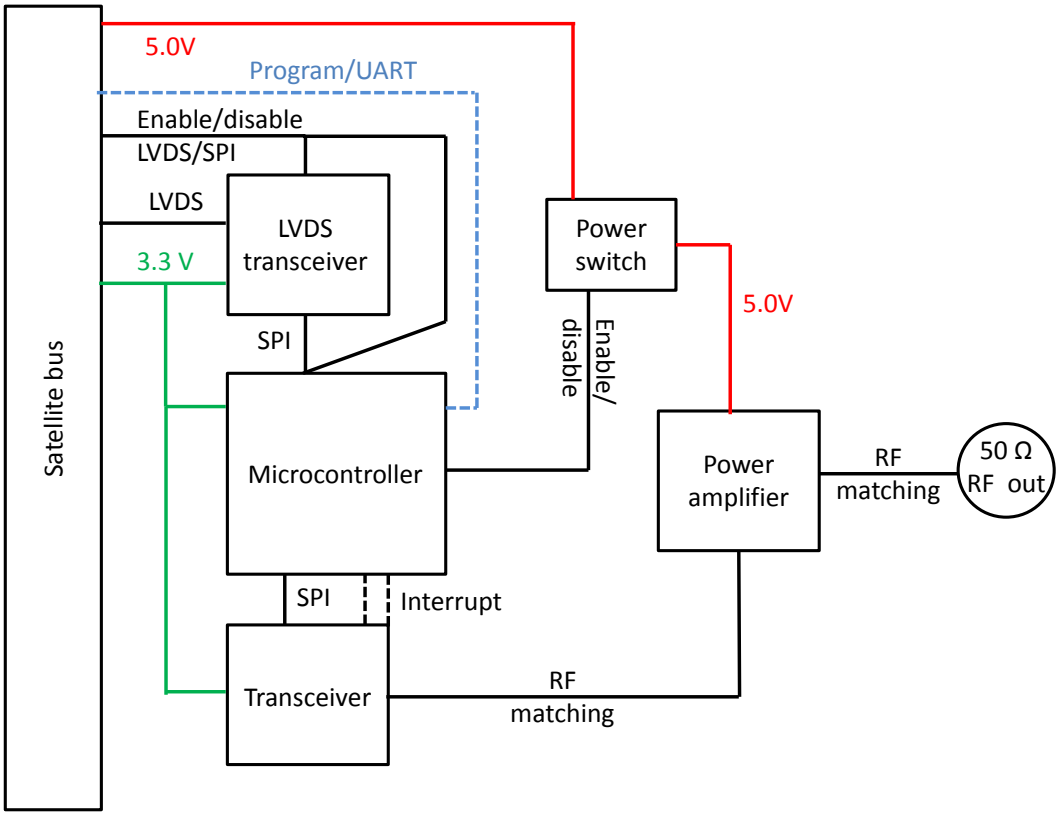

Figure 36: Basic connections on the prototype board.

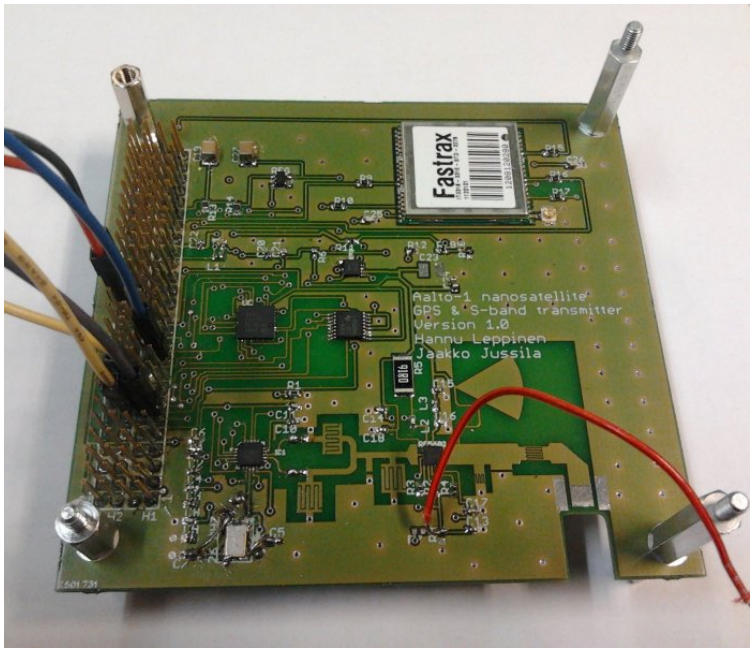

Figure 37: Photograph of the Aalto-1 S-band transmitter and GPS first prototype board.

The first version of the Aalto-1 S-band transmitter software is based on the sample library available from the manufacturer of the microcontroller [70]. The stack diagram of the library files is shown in Fig. 38. As can be seen, the library contains the hardware level definitions for the microcontrollers and transceivers. The SPI layer contains the functions for accessing the SPI. Application layer contains the configuration files for the transceivers, transmit and receive functions and also the main program routine. The source files listed in Fig. 38 are described in Table 14.

In order to test the whole transmitter, a main program routine was implemented by using the sample library. The main SW routine is shown in Appendix F. The main routine supports both packet transmission and continuous transmission. It is also possible to test the microcontroller UART interface. The transmission part of the software is illustrated in Fig. 39. As can be seen, when the user interacts via the UART interface to start the RF transmission, the registers and microcontroller pins are configured according to the interface and register definition files of the library. The definition files have to be modified before executing the main program. The transceiver enters then idle state. When the user issues the transmit command, the transmitter starts to transmit either an unmoludated carrier wave or a predefined packet. When the user issues the idle-state command, the transmitter will stop transmitting. The tests executed with the first prototype board and software are introduced and analyzed in Chapter 4.2.

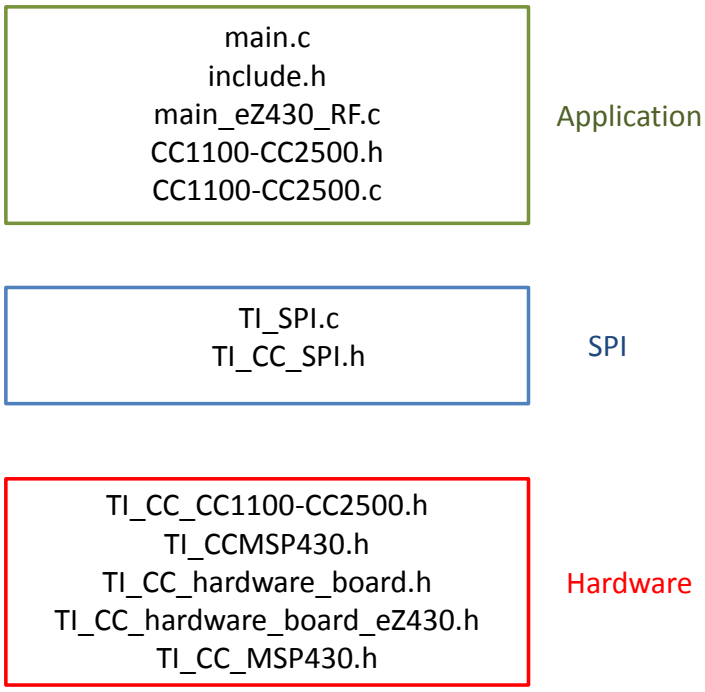

Figure 38: Structure of the sample library [71].

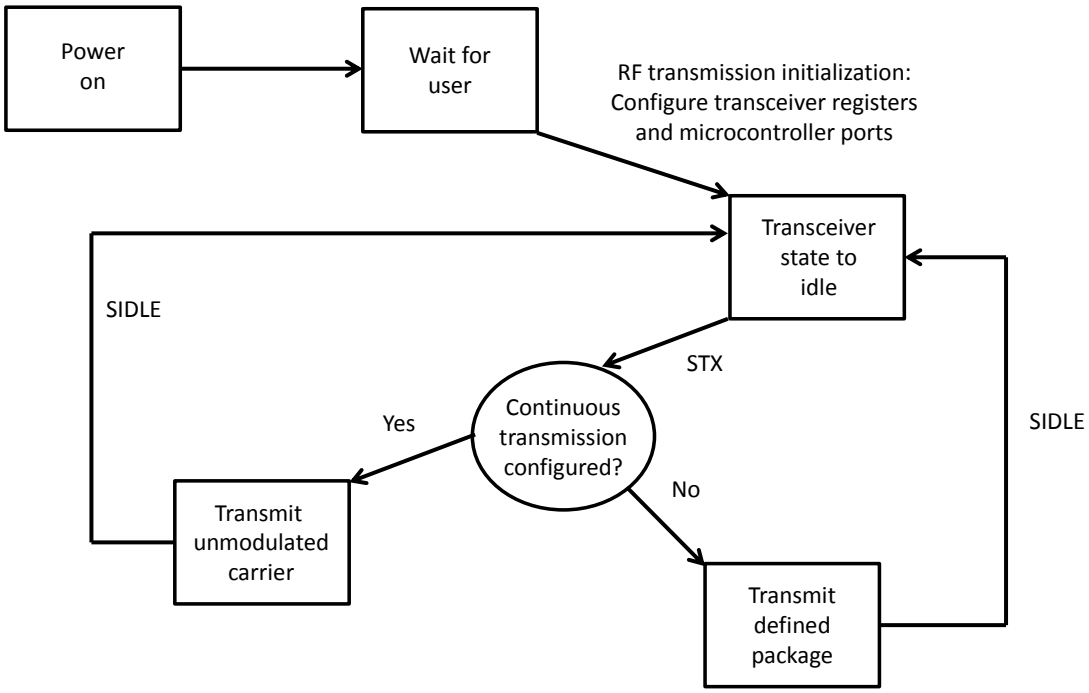

Figure 39: Transmission flow chart of the transmitter's control software main routine.

Table 14: Example library for MSP430 and CC2500.

Filename	Description
TI_CC_CC1100-CC2500.h	Definitions specific to the CC1100/2500 devices, including register locations and commonly-used masks for use with these registers.
TI_CC_MSP430.h	Definitions specific to the MSP430 device; primarily, the pins used in the SPI interface. Definitions for USART0/1, USCI_A0/1/2/3, USCI_B0/1/2/3, USI, and bit-banging are included. Also, labels are defined for use with the system variable RF_SER_INTF. This selects the modules to be used for the CCxxxx SPI interface
TI_CC_hardware_board.h	Definitions specific to the board being used; that is, the connections between the MSP430 and CC1100/2500, such as the GDO pins. SPI connections are not defined here because they are defined inherently within TI_CC_MSP430.h. This file defines connections to a generic board.
TI_CC_hardware_board_eZ430.h	Definitions similar to TI_CC_hardware_board.h except the ports are configured specifically for the eZ430-RF2500 kit.
TI_CC_spi.c	Functions for accessing CC1100/CC2500 registers via SPI from MSP430.
TI_CC_spi.h	Function declarations for TI_CC_spi.c.
CC1100-CC2500.c	Functions for programming the CC1100/CC2500, including calls for initialization, send, packet, and receive packet.
CC1100-CC2500.h	Function declarations for CC1100-CC2500.c
include.h	High-level include file that lists all other include files.
main.c	Function declarations for CC1100-CC2500.c
main_eZ430_RF.c	Application code file written specifically for the eZ430-RF2500 kit

4 Results

This chapter introduces the results achieved with the transmitter design. The simulation and measurement results of the RF matching circuits are introduced and analyzed. The tests executed with the first prototype board are also introduced. Based on the results, design optimization ideas are introduced for the future versions of the S-band transmitter.

4.1 Simulation and measurement results of the RF matching circuits

The matching circuit designed for the transceiver's RF output was tested individually with the board containing only the transceiver, introduced in chapter 3.6. For the tests, the microcontroller platform chosen was Arduino Uno. The registers settings for the transceiver were configured with TI Smart RF Studio software and the Arduino microcontrol then programmed the transceiver. In order to measure the matching level of the RF matching circuit, the transceiver had to be put into receiver mode. The manufacturer of the chip also uses the S_{11} measurement to test the matching circuit [72]. S_{11} was measured by connecting VNA 50 Ω port to the coaxial output connector of the transceiver prototype board, as shown in Fig. 40.

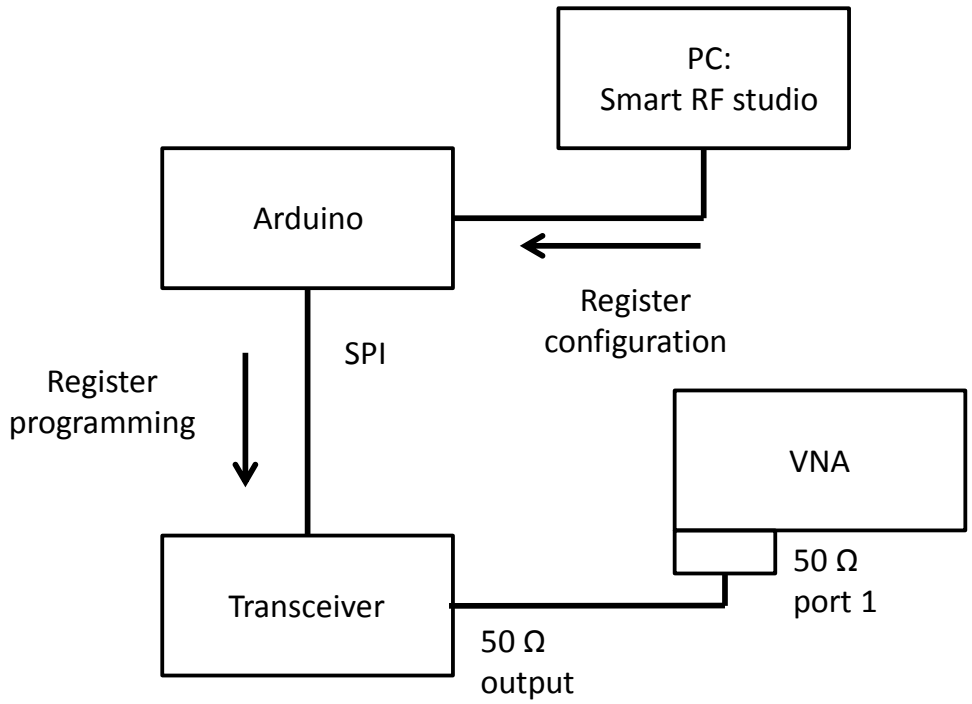

Figure 40: Measurement configuration of S_{11} for the transceiver.

S_{11} simulation and measurement results of the transceiver's matching circuit are shown in Fig. 41. As can be seen, the best matching levels have shifted from the

simulation: the design frequency has shifted up to about 3.1 GHz. The reason for having different result for the measurement is the fact that the relative permittivity of the real substrate material is differs from that used in the simulations. Therefore, the microstrip stubs have different characteristics - the relative permittivity affects the design of microstrip components. As can be seen from Fig. 31, solder resist was used with the prototype board. The solder resist has some relative permittivity value different from vacuum and air, thus affecting to the relative permittivity value of the design [73]. As the design is not optimal at the desired frequencies, the power amplifier of the transceiver is not able to produce the maximum available power to the load. Therefore, optimization work is required on the matching circuit. The simulation model has to be more accurate according to the real substrate material and the use of solder resist should be avoided on top of the microstrip stubs.

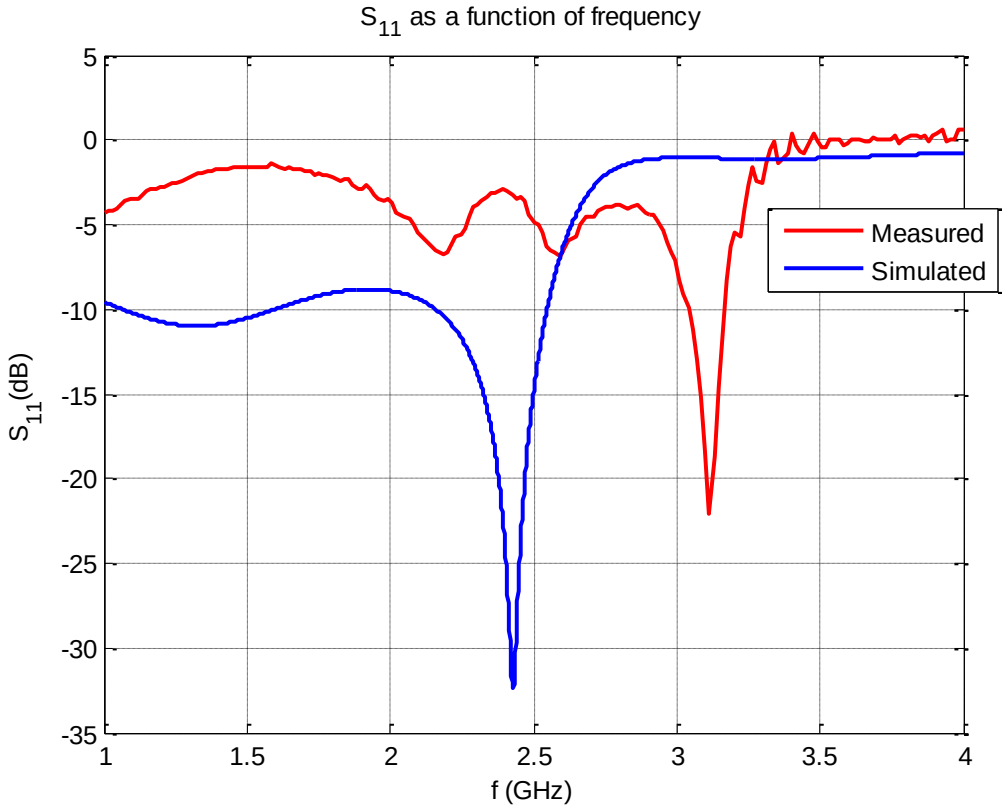

Figure 41: Simulation and measurement results of the S_{11} for the transceiver's matching circuit.

The simulation result of the matching circuit designed for the power amplifier is shown in Fig. 42, where the 50 Ω impedance is located in the center of the Smith's chart. Since the complex conjugate of the desired load impedance was set as the input for the matching circuit and the input impedance is simulated at the output, the matching circuit should provide the desired load impedance according to the simulation results.

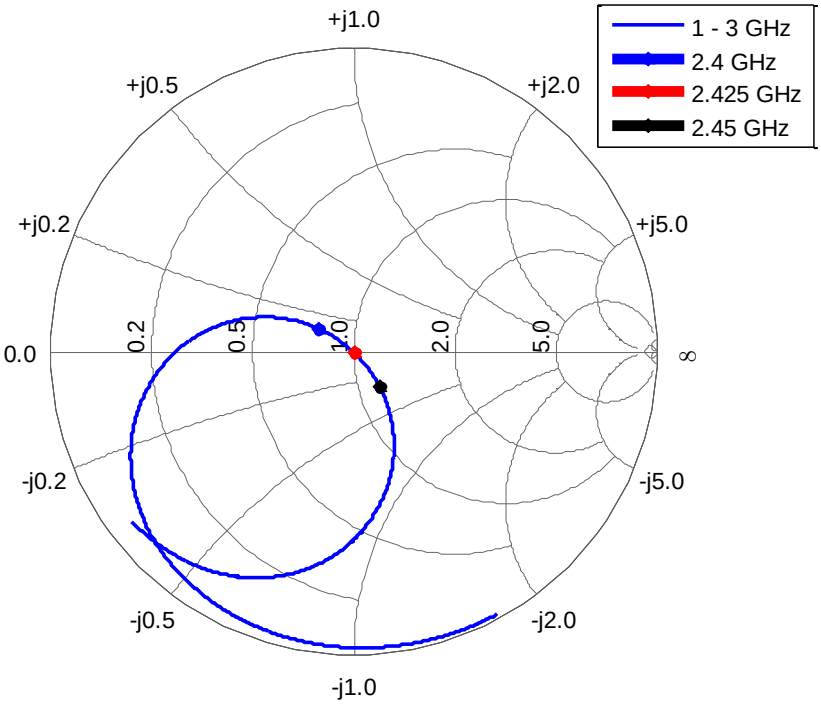

Figure 42: Simulation result of the input impedance of the designed matching circuit for the power amplifier.

The matching circuit for the power amplifier was measured with the board containing only the power amplifier, designed in chapter 3.6. The matching circuit was measured by connecting the RF input of the prototype board to a signal generator and the output to the spectrum analyzer. The measurement setup is shown in Fig. 43. The measurement result with 2.5 V bias level at 2.425 GHz is shown in Fig. 44. As can be seen, the output power saturates too early, at about + 18 dBm. The expected power level with such bias voltage value should be at least +26 dBm. The maximum output power level achieved was about +20 dBm at 2.425 GHz with 2.9 V bias level when the expected power level is about +30 dBm. The amplifier tends also to oscillate at bias voltages higher than 2.5 V.

The load impedance seen by the PA RF output defines the amount of power transfered to the load. Therefore, the load impedance achieved with the manufactured prototype board is not the most optimal one. Thus, as with the transceiver, the simulated model differs from the real substrate material. There exists also a possibility, that the supply lines providing the supply voltages for the two other amplifier stages to pins VCC1 and VCC2, include components having incorrect capacitance, inductance or resistance values due to the uncertainties in the component tolerances. Due to the incorrect component values the RF signal might be leaking to the supply pins or the supply voltage values for the two amplifier stages are incorrect. Therefore, the last stage may not have the required RF signal power level at the input in order to produce the required RF output power. However, since the

discrete components used have component tolerances maximum of about 10%, the relative change in the component value is low and therefore should not affect too much to the supply conditions of the two amplifier stages.

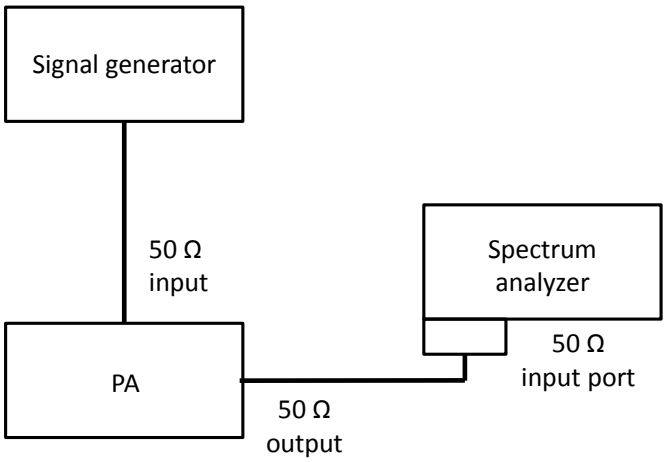

Figure 43: Measurement setup for the power amplifier.

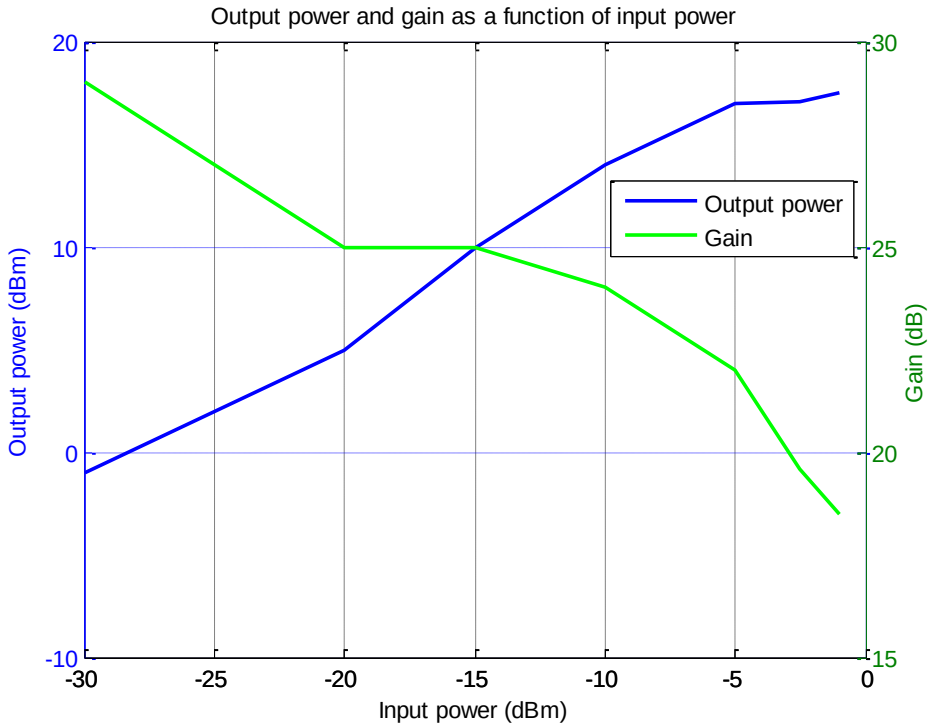

Figure 44: Measured output power and gain vs. input power.

As the RF5602 is the final part of the RF amplifying chain in the transmitter, the gain produced by it is critical when the whole radio link is considered. Therefore, the

matching circuit needs optimization in order to provide the optimal load impedance for the PA. The simulation model has to be accurate according to the real substrate material and the use of solder resist should be avoided. Also, a load-pull analysis [57] should be performed with the PA hardware. The radial stub and the DC-cut interdigital capacitor can be left in their places. Then, the two shunt microstrip capacitors should be removed and replaced with discrete capacitors. From the output of RF5602 to the beginning of the DC-cut interdigital capacitor should be placed a 38 Ω microstrip line, as in the reference design. Then, the place of these two discrete capacitors should be varied and the corresponding output power measured. The values of these discrete capacitors could also be modified. Such an iterative process would continue until the 1 dB compression point of the amplifier is close to the +33 dBm value given by the manufacturer. When the optimal places of the discrete capacitors and their optimal values are found, they could be replaced with interdigital capacitors and new microstrip implementation could be achieved. Fig. 45 illustrates the idea. Also the components located on the supply lines providing the supply voltages for the first two amplifier stages should have as low component tolerances as possible.

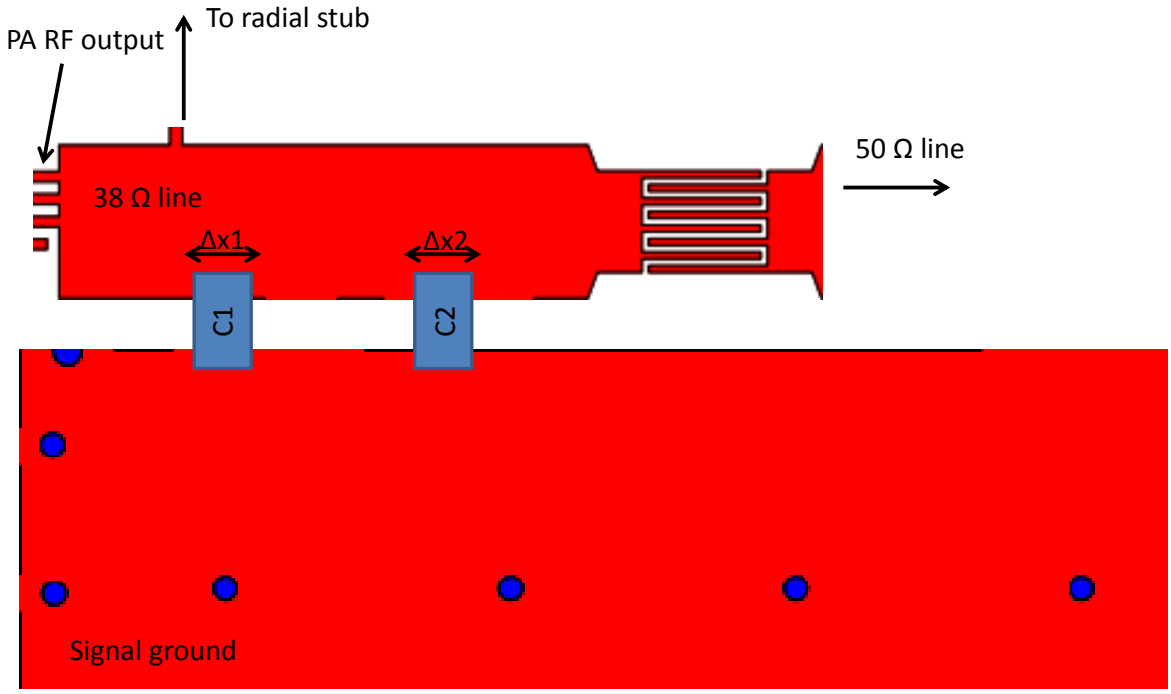

Figure 45: Load-pull analysis implementation principle for the PA.

Instead of using discrete capacitors to tune the load impedance, an impedance

transformer could be used. Then, a 38 Ω microstrip stub would be connected between the output of the power amplifier and the DC-cut capacitor. The transformer would be connected to the coaxial connector of the board. Then, the impedance transformer would be tuned to find the optimal load impedance. After the correct setting has been found, the load impedance of the transformer would be measured. Then, the effects caused by the 38 Ω stub and DC-cut capacitor would be added to the load impedance. Thus, the optimal load impedance for the power amplifier could be determined. Then, the simulator would be used to design the matching circuit according to the measured load impedance.

4.2 S-band transmitter first prototype board tests

The operation of the first prototype board of the Aalto-1 S-band transmitter was tested with the developed control software. The test cases included the UART interface tests and continuous unmodulated carrier wave tests. The test setup is shown in Fig. 46. The UART test was completed successfully, the microcontroller received and transmitted characters via the interface. The RF transmission was tested by connecting the transmitter to a spectrum analyzer. Continuous wave transmissions were registered at the desired frequencies on the spectrum analyzer. Thus, it was concluded that the developed prototype board is a suitable platform for operating the chosen architecture. However, as the matching circuits are not optimized for the design frequencies, the current prototype board is not able to provide high enough output power. As stated before, the power amplifier output power saturates at +20 dBm when the required output power is +27 dBm.

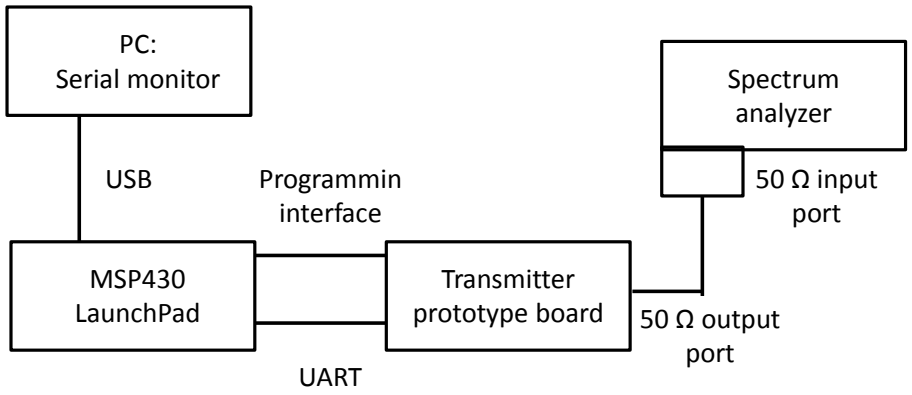

Figure 46: Testing setup for the prototype board [71].

4.3 Failure modes, effects and criticality analysis (FMECA) of the first prototype board

FMECA analysis is required with space applications. It is a bottom-up analysis considering each single elementary failure mode and assessing its effects up to the

boundary of the product or process under analysis [74]. The FMECA analysis for the first prototype board of Aalto-1 S-band transmitter is shown in Appendix E. The analysis was executed based on different signals available from the transmitter's internal modules. The individual discrete capacitors, inductors and resistors were also taken into account in the analysis. The criticality number (CN) column gives an estimation of the seriousness of each individual failure for the whole satellite mission. The CN is formed by multiplying the severity number (SN) and probability number (PN) having scales 1 to 5.

When the S-band transmitter subsystem is considered as part of the Aalto-1 mission, the loss of S-band transmitter would mean major degradation for the whole mission, since the S-band transmitter is the only communication module on the satellite capable of transmitting the images of the spectral imager with high enough data throughput. Also, any degradation in the S-band RF transmission would result as degradation of the received image quality. Therefore, the scale used for the severity number of different failure scenarios is from 1 to 2. The probability number was estimated as 1 or 2 in each individual failure case. As a result of the FMECA analysis, serious attention should be given to the failure scenarios having the highest CN values. Such places are the supply lines for the transmitter and the data interfaces. High quality discrete components should of course be used on the whole transmitter circuit.

4.4 Design improvement ideas

During the manufacturing process of the first prototype board of Aalto-1 S-band transmitter some minor PCB design errors appeared. The capacitors C7 and C5 were mistakenly connected between the ground pins of the external oscillator and PCB ground, while they should be connected between the oscillator signal lines and ground to reduce noise. On the power switch, the first ground pin was not connected to ground. These design mistakes are to be corrected for the future versions of the transmitter board.

The power amplifier power-on sequence requires the supply voltage to be connected prior to the bias voltages. Therefore, one additional power switch should be introduced for the bias voltages in order to switch them individually. The power switch would then require one additional disable/enable pin from the microcontroller and a software delay between the supply and bias voltages enable/disable. Instead of a power switch, a voltage regulator could be more suitable due to the fact that the 5.0 V supply voltage has to be transformed to 2.9 V. The disable/enable pin should be allocated and the software delay added on the microcontroller for the next versions of the transmitter board and suitable voltage regulator should be selected.

Already during the individual tests of the power amplifier module and during the transmission tests of the first prototype board of the whole transmitter, the power amplifier chip was heating up relatively fast. Therefore, additional thermal vias should be introduced in order to boost the heat transfer from the power amplifier to the ground plane.

The RF matching circuits need to be optimized, since the power amplifier power

saturates too early and the transmitter is not able to produce the required RF output power. The transceiver's matching circuit needs to be optimized in order to ensure maximum input power delivered for the power amplifier. The power amplifier tends also to oscillate at bias voltage values higher than 2.5 V. The load-pull analysis introduced in Chapter 4.1 should be performed.

The microstrip matching circuits occupy relatively large area on the PCB. Thus, it is hard to implement a redundant system for the transmitter, since the PCB is also shared with the GPS subsystem. Thus, if the matching circuits were implemented with discrete components, more space would be available for a redundant system. One possibility would be to use an integrated balun from Johanson Technology at the transceiver RF output [75]. The PA RF output circuit has to be implemented with some length of microstrip stubs introducing the series inductances. The shunt capacitances and the DC-cut capacitances can be provided with discrete capacitors. However, as the FMECA analysis indicated in Chapter 4.3, using discrete components at critical parts of the transmitter introduces possibility for the loss of the whole subsystem. On the other hand, designing microstrip matching circuits requires more optimization work due to the strong dependence on the PCB substrate permittivity value. Therefore, the decision whether to use discrete components or microstrip approach is a trade-off between the space required, reliability and time. The problems with the uncertainties of the substrate's relative permittivity could be also avoided by using a PCB material having a stable relative permittivity as a function of frequency. Such materials are available from Rogers Corporation [76].

In order to receive diagnostic information from the transmitter, OBC requires the transmitter to have a transmitting interface towards the OBC. At the moment, there exists a secondary UART interface with transmit and receive capabilities. However, the UART interface cannot be used at the same time with the LVDS. Therefore, there should be introduced also MISO line for the OBC S-band transmitter SPI/LVDS connection: the MISO line is easier to use than another UART; the MISO line does not require the LVDS since only the status is provided. Thus, high speed is not required.

The first version of the transmitter control software was tested and proven functional. However, the software has to optimized to get full benefits of the low power features of the microcontroller. Also the SPI - LVDS interface communication between the OBC and the transmitter should be implemented. As mentioned above, an additional software delay should be added for the power amplifier power on sequence. All the design improvement ideas are summarized in Table 15 from which the optimization of the matching circuits are the most critical.

Table 15: Design improvement ideas for the transmitter.

Improvement	**Purpose**
Additional power switch for the PA	Optimize the PA's power on sequence
More thermal vias for the PA	Boost the heat transfer of the PA to ground plane
Transceiver output matching circuit optimization	Transceiver can deliver maximum power to PA
PA output matching circuit optimization	More RF output power for the transmissions
Microstrip implementation to discrete components	Space saving
Change of substrate material	More accurate matching with microstrip elements
Control SW optimization	Full benefits of the microcontroller low power features
SPI - LVDS SW interface for the microcontroller	Data interface towards the OBC
Additional SW delay for the microcontroller	PA power on sequence
MISO line for OBC	Diagnostic information available for OBC

5 Summary

This thesis designed the first prototype for the Aalto-1 S-band transmitter. The design is based on a custom combination of discrete RF components. The architecture of the transmitter is based on Texas Instruments CC2500 transceiver, RFMD RF5602 power amplifier and Texas Instruments MSP430 microcontroller family. Simulations with sun-synchronous orbit of 900 km indicate that data throughputs up to 42 MB are achievable with the chosen architecture during one fly-over in average. Such a value is twice the amount of achievable throughput with the commercial option chosen for the transmitter. The maximum power consumption of about 4.2 W is within the CubeSat power constraints. The transmitter has been designed with component families having space legacy, thus improving the space worthiness of the system. The transmitter has the control unit integrated, thus enabling the transmitter to operate with minimum outside contribution. The transceiver has adaptive RF features: the data rate, RF output power and modulation scheme are programmable. Thus, the operation of the transmitter can be optimized according to the attenuation conditions. The transceiver has packet handling capabilities, offers forward-error-correction with interleaving and data whitening. The achievable data rate is 500 kBaud with MSK modulated signal, the perfect modulation scheme in terms of linearity requirements since the envelope of the carrier wave is constant in amplitude. The power amplifier is able to produce RF output power up to +33 dBm in compression. The microcontroller offers SPI/LVDS, UART and programming interfaces towards the satellite bus. The RF output of the transmitter is a 50 Ω coaxial connector.

The first prototype board was implemented based on the chosen architecture. The controlling software was developed and tested successfully. The matching networks were implemented with microstrip elements, proven as more reliable solution for space applications. The simulation results indicated that good levels of matching are achievable with the chosen implementation. However, the measurement results showed that optimization work is required in order to achieve the desired matching levels. The reason for the non-optimal matching levels was identified as the uncertainty related to the relative permittivity of the substrate material. The simulation models have to be more accurate according to the real substrate material in order to ensure the desired capacitance and inductance values for the microstrip elements. The load-pull analysis should be performed with the power amplifier hardware in order to find the optimal load impedance.

This thesis started the design process of the Aalto-1 S-band transmitter. All the important design parameters were concluded and a suitable architecture developed. The chosen transmitter topology was proven to be functional within the CubeSat framework and fulfill the requirements set by the Aalto-1 mission. The design of the transmitter will continue by optimizing the matching circuits and the control software for the transmitter.

References

[1] Missions, *NASA*, [Online] 2013, Available: http://www.nasa.gov/missions/index.html (Accessed Apr. 29, 2013).

[2] Aqua: Project Science, *NASA*, [Online] 2013, Available http://aqua.nasa.gov/about/instruments.php (Accessed Apr. 29, 2013).

[3] R. Munakata, "CubeSat Design Specification, Rev. 12," (Developers), [Online] 2013, Available: http://www.cubesat.org/images/developers/cds_rev12.pdf (Accessed Apr. 22, 2013).

[4] A. Kestilä, T. Tikka, P. Peitso, J. Rantanen, A. Näsilä, K. Nordling, H. Saari, R. Vainio, P. Janhunen, J. Praks, and M. Hallikainen, "Aalto-1 nanosatellite - technical description and mission objectives," *Geoscientific Instrumentation, Methods and Data Systems Discussions*, Vol. 2, No. 1, pp. 121 - 130, 2013.

[5] R. Nugent, R. Munakata, A. Chin, R. Coelho, and Dr. Jordi Puig-Suari, "The CubeSat: The Picosatellite Standard for Research and Education," in *AIAA SPACE 2008 Conf.& Expo.*,San Diego, Calif., 2008.

[6] CubeSat Kit, *Pumpkin Inc.*, [Online] 2013, Available http://www.cubesatkit.com/index.html (Accessed Apr. 29, 2013).

[7] CubeSatShop.com, *ISIS*, [Online] 2013, Available: http://www.cubesatshop.com (Accessed Apr. 29, 2013).

[8] Frequencies and Modulation schemes, *GENSO*, [Online] 2013, Available: http://www.genso.org/index.php/frequencies-and-modulation-schemes (Accessed Jan. 23, 2013).

[9] B. Klofas and J. Anderson, "A Survey of CubeSat Communication Subsystem," in *5th Annual CubeSat Workshop*, Cal Poly 2008.

[10] TI CC1000 datasheet, *Texas Instruments*, [Online] 2013, Available: http://www.ti.com/lit/ds/symlink/cc1000.pdf (Accessed Apr. 29, 2013).

[11] TI CC1020 datasheet, *Texas Instruments*, [Online] 2013, Available: http://www.ti.com/lit/ds/symlink/cc1020.pdf (Accessed Apr. 29, 2013).

[12] STX, *Clyde Space*, [Online] 2013, Available: www.clyde-space.com/documents/2398 (Accessed Apr. 29, 2013).

[13] HISPICO - Highly Integrated S-Band Link for PICO and NANO satellite, *IQ wireless*, [Online] 2013, Available: http://www.iq-wireless.com/en/radio-technology/hispicobroadband-s-band-link-from-pico-and-nano-satellites (Accessed Apr. 29, 2013).

[14] A1-SYS-EID-01-v6, "Experiment Interface Document," Aalto-1 satellite design documentation, 2012.

[15] A1-MEC-DW-07-v1, "Long stack assembly," Aalto-1 satellite design documentation, 2012.

[16] A1-MEC-DW-06-v1. "Short stack assembly," Aalto-1 satellite design documentation, 2012.

[17] Frequency allocations, *Ficora*, [Online] 2013, Available: `https://www.viestintavirasto.fi/taajuudet/radiotaajuuksienkaytto/taajuusjakotaulukko.html` (Accessed Apr. 29, 2013)

[18] G. Maral, M. Bousquet and S. Zhili, *Satellite Communications Systems - Systems, Techniques and Technology*, 5th ed., John Wiley and Sons, 2009.

[19] Rec. ITU-R P618: Propagation data and prediction methods required for the design of Earth-space telecommunication systems, Aug., 2007.

[20] Rec. ITU-R P.676: Attenuation by atmospheric gases, Feb., 2012.

[21] SG3 database: rsg3-p676-gaseous-absorption, *ITU-R*, [Online] 2009, Available: `http://www.itu.int/oth/R0A0400001B/en` (Accessed Apr. 25, 2013).

[22] Rec. ITU-R P840: Attenuation due to clouds and fog, Feb., 2012.

[23] SG3 database: rsg3-p840-Attenuation due to clouds and fog, *ITU-R*, [Online], Available: `http://www.itu.int/oth/R0A04000064/en` (Accessed Par. 29, 2013).

[24] Rec. ITU-R P838: Specific attenuation model for rain for use in prediction methods, March, 2013.

[25] SG3 database: rsg3-p839-rain-height, *ITU-R*, [Online] 2013, Available: `http://www.itu.int/oth/R0A04000028/en` (Accessed Apr. 29, 2013).

[26] SG3 database: rsg3-p453-refractivity-wet-term, *ITU-R*, [Online] 2013, Available: `http://www.itu.int/oth/R0A04000016/en` (Accessed Apr. 29, 2013).

[27] Rec. ITU-R P531: Ionospheric propagation data and prediction methods required for the design of satellite services and systems, Feb., 2012.

[28] GISM web interface, *IEEA*, [Online] 2013, Available: `http://www.ieea.fr/en/gism-web-interface.html` (Accessed Apr. 29, 2013).

[29] A. Lehto and A. Räisänen, *Radiotekniikan perusteet*, 13th ed., Helsinki, Finland: Otatieto, 2011.

[30] Rec. ITU-R P372: Radio noise, Oct., 2009.

[31] D. Juyong, D.M. Akos and P.K. Enge, "L and S bands spectrum survey in the San Francisco bay area," *Proceedings of the Position Location and Navigation Symposium,* 2004, PLANS 2004 , Vol., No., pp.566 - 572, Apr., 2004.

[32] L. Wilfried et al., *Handbook of space technology*, Chichester, U.K. : Wiley, 2009, pp. 33 - 51.

[33] A.S. Keys and J.T. Howell, Technology Developments in Radiation-Hardened Electronics for Space Environments, *The Radiation Hardened Electronics for Space Environments (RHESE)*, [Online] 2013, Available: `http://ntrs.nasa.gov/archive/nasa/casi.ntrs.nasa.gov/20080032798_2008033428.pdf` (Accessed Nov. 17, 2012).

[34] J. Rhea, BAE Systems moves into third generation rad-hard processors *Military and Aerospace*, [Online] 2002, Available: `http://www.militaryaerospace.com/articles/print/volume-13/issue-5/news/bae-systems-moves-into-third-generation-rad-hard-processors.html` (Accessed Nov. 17, 2012).

[35] Learn About me: Curiosity, *JPL*, [Online] 2013, Available: `http://mars.jpl.nasa.gov/msl/multimedia/interactives/learncuriosity/l` (Accessed Apr. 29, 2013).

[36] Avionics Innovations for the Mars Exploration Rover Mission: Increasing Brain Power, *JPL*, [Online] 2013, Available: `http://marsrover.nasa.gov/technology/bb_avionics.html` (Accessed Apr. 29, 2013).

[37] Introduction to Radiation Shielding, *NASA*, [Online] 2012, Available: `http://spacemath.gsfc.nasa.gov/weekly/3Page25.pdf` (Accessed Apr. 29, 2013).

[38] Intelligent systems Division, *NASA*, [Online] 2012, Available: `http://ti.arc.nasa.gov/m/pub-archive/1075h/1075\%20(Mehlitz).pdf` (Accessed Nov. 18, 2012).

[39] Material outgassing database, *ESA*, [Online] 2012, Available: `http://esmat.esa.int/Services/outgassing_data/outgassing_data.html` (Accessed Nov. 18, 2012).

[40] NASA-STD-8739.3 w/Change 2, Soldered electrical connections, NASA technical standard, *NASA*, [Online] 2012, Available: `http://nepp.nasa.gov/docuploads/06AA01BA-FC7E-4094-AE829CE371A7B05D/NASA-STD-8739.3.pdf` (Accessed Nov. 11, 2012).

[41] C. Berrou, A. Glavieux, and P. Thitimajshima, "Near Shannon limit error correcting coding and decoding: Turbo codes," *Proceedings of the IEEE International Conference on Communications*, Geneva, Switzerland, May 2003, pp. 1064 - 1070.

[42] Rack-mount rdms telemetry receiver, *Quasonix*, [Online] 2013, Available: http://www.quasonix.com/uploads/qsx_rackmount_rdms_datasheet.pdf (Accessed Apr. 29, 2013).

[43] Smartphone Nanosatellite, *Surray Space Technology LTD*, [Online] 2012, Available: http://www.sstl.co.uk/Divisions/Earth-Observation-Science/Science-Missions/STRaND-nanosatellite (Accessed Oct. 28, 2012).

[44] ADF7242 transceiver, *Analog Devices*, [Online] 2012, Available: http://www.analog.com/en/rfif-components/rfif-transceivers/adf7242/products/product.html (Accessed Nov. 11, 2012).

[45] TI CC2500 transceiver datasheet, *Texas Instruments*, Available: http://www.ti.com/lit/ds/symlink/cc2500.pdf (Accessed Nov. 12, 2012).

[46] A. Burr, *Modulation and Coding: For wireless communications*, Pearson Education Limited, 2001.

[47] M. Pokorny, "S-band Conventional Radio Connection of the PilsenCUBE Satellite," *Proceedings of the 4th European CubeSat Symposium*, Jan. 30 - Feb. 1, 2012, Ecole Royale Militaire, Brussels.

[48] OpenCube project communication system, *OpenCube*, [Online] 2012, Available: http://opencubeproject.org/projects/comm (Accessed Nov. 12, 2012).

[49] TI CC2500, *Texas Instruments*, [Online] 2012, Available: http://www.ti.com/product/cc2500 (Accessed Nov. 12, 2012).

[50] eZ430-RF2500 Development Tool User's Guide, *Texas Instruments*, Available: http://www.farnell.com/datasheets/86226.pdf (Accessed Nov. 12, 2012).

[51] ADF7242 evaluation board design, *Analog Devices*, [Online] 2013, Available: http://www.analog.com/en/evaluation/eval-adf7242/eb.html#DOCUMENTATION (Accessed Apr. 29, 2013).

[52] AD7242 driver SW for ARM7-based ADuC7020 microcontroller, *Analog Devices*, [Online] 2013, Available: http://www.analog.com/en/evaluation/eval-adf7242/CU_ADF70XX_Device_Drivers_evaluation_tools/fca.html (Accessed Apr. 29, 2013).

[53] TI Smart RF Studio, *Texas Instruments*, [Online] 2013, Available: http://www.ti.com/tool/smartrftm-studio&DCMP=hpa_rf_general&HQS=Other+OT+smartrfstudio (Accessed Apr. 29, 2013).

[54] K. Wesolowski, *Introduction to Digital Communication Systems*, Hoboken, NJ, USA: Wiley, 2009.

[55] Design Note DN509, Data whitening, *Texas Instruments*, [Online] 2013, Available: http://www.ti.com/lit/an/swra322/swra322.pdf (Accessed Apr. 29, 2013).

[56] RFMD RF5602 datasheet, *RFMD*, [Online] 2012, Available: http://www.rfmd.com/CS/Documents/5602DS.pdf (Accessed Dec. 3, 2012).

[57] A. Lehto and A. Räisänen, *RF- ja mikroaaltotekniikka*, 7th ed., Otatieto, 2002, pp. 37 - 156.

[58] C. Noe, "Design and Implementation of the Communications Subsystem for the Cal Poly CP2 Cubesat Project", *Computer Engineering Department, California Polytechnic State University, San Luis Obispo*, [Online] 2012, Available: http://polysat.calpoly.edu/PublishedPapers/ChrisNoe_srproj.pdf (Accessed Dec. 3, 2012).

[59] Cal Poly CP4 satellite mission, *Cal Poly*, [Online] 2012, Available: http://polysat.calpoly.edu/CP4.php (Accessed Dec. 3, 2012).

[60] In Space, *Pumpkin Inc.*, [Online] 2013, Available: http://www.cubesatkit.com/content/space.htmll (Accessed Apr. 29, 2013).

[61] Goliat nanosatellite, *Golliat*, [Online] 2013, Available: http://www.goliat.ro/index.php/satellite/on-board-computer (Accessed Apr. 29, 2013).

[62] e-st@r nanosatellite, *E-ST@R*, [Online] 2013, Available: http://areeweb.polito.it/ricerca/E-STAR/# (Accessed Apr. 29, 2013).

[63] MSP430F2274 datasheet, *Texas Instruments*, [Online] 2012 Available: http://www.ti.com/lit/ds/symlink/msp430f2274.pdf (Accessed Dec. 3, 2012).

[64] TI MSP430 Launchpad, *Texas Instruments*, [Online] 2012, Available: http://www.ti.com/ww/en/launchpad/msp430_head.html (Accessed Dec. 3, 2012).

[65] S.C. Cripps, *RF Power Amplifiers for Wireless Communications, Second Edition*, Norwood, MA, USA: Artech House, 2006.

[66] I. J. Bahl, *Lumped Elements for Rf and Microwave Circuits*, Artech House, 2003.

[67] 62 mils reference design for TI CC2500, *Texas Instruments*, [Online] 2013, Available: http://www.ti.com/tool/CC2500_REFDES_062 (Accessed Apr. 29, 2013).

[68] TPS2556 datasheet, *Texas Instruments*, [Online] 2013, Available: http://www.ti.com/lit/ds/symlink/tps2556.pdf (Accessed Apr. 29, 2013).

[69] SN65LVDS049 datasheet, *Texas Instruments*, [Online] 2013, Available: http://www.ti.com/lit/ds/symlink/sn65lvds049.pdf (Accessed Apr. 29, 2013).

[70] Example SW library for TI CC2500 transceiver and MSP430 microcontroller family, *Texas Instruments*, [Online] 2013, Available: http://www.ti.com/general/docs/litabsmultiplefilelist.tsp?literatureNumber=slaa325a (Accessed Apr. 29, 2013).

[71] MSP430 and transceiver sample interface library, *Texas Instruments*, [Online] 2013, Available: `http://www.ti.com/lit/an/slaa325a/slaa325a.pdf` (Accessed Apr. 29, 2013).

[72] TI Application Note AN068, *Texas Instruments*, [Online] 2013, Available: `http://www.ti.com/lit/an/swra236a/swra236a.pdf` (Accessed Apr. 29, 2013).

[73] M. Cauwe and J. De Baets, "Broadband Material Parameter Characterization for Practical High-Speed Interconnects on Printed Circuit Board," *IEEE Transactions on Advanced Packaging*, Vol. 31, No. 3, pp. 649 - 656, Aug., 2008.

[74] Space Product Assurance: Failure modes, effects (and criticality) analysis (FMEA/FMECA), ECSS-Q-ST-30-02C, ECSS, March 6^{th} 2009.

[75] Johanson Technology integrated balun for CC2500, *Johanson Technology*, [Online] 2013, Available: `http://www.johansontechnology.com/integrated-passives/rohs-compliant-baluns.html` (Accessed Apr. 29, 2013).

[76] Rogers Corporation advanced substrate materials, *Rogers*, [Online] 2013, Available: `http://www.rogerscorp.com/acm/producttypes/2/Rogers-High-Frequency-Laminates.aspx` (Accessed Apr. 29, 2013).

A Connection schematics for transceiver.

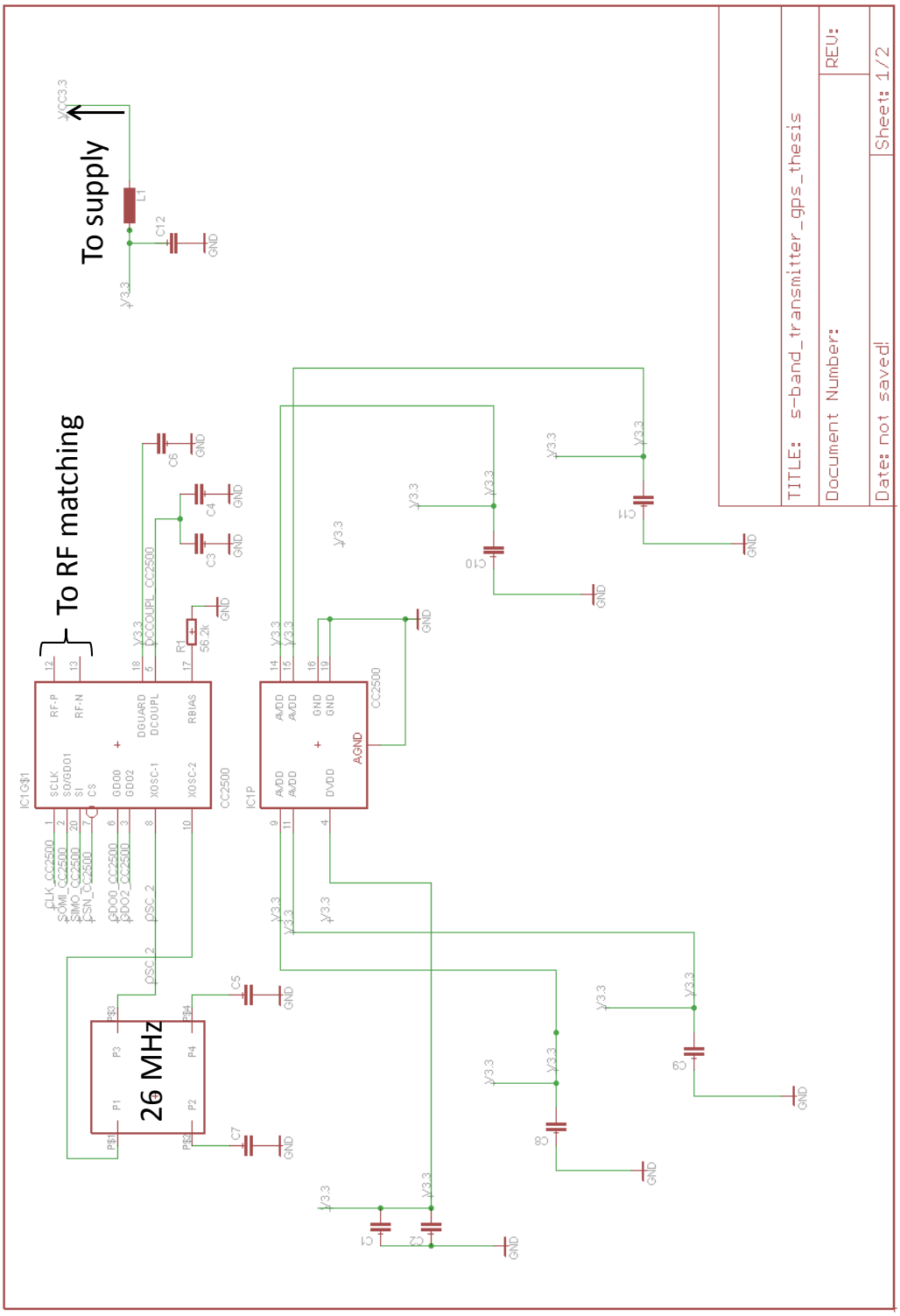

Figure 1: Transceiver connections.

B Connection schematics for microcontroller, LVDS transceiver and satellite bus.

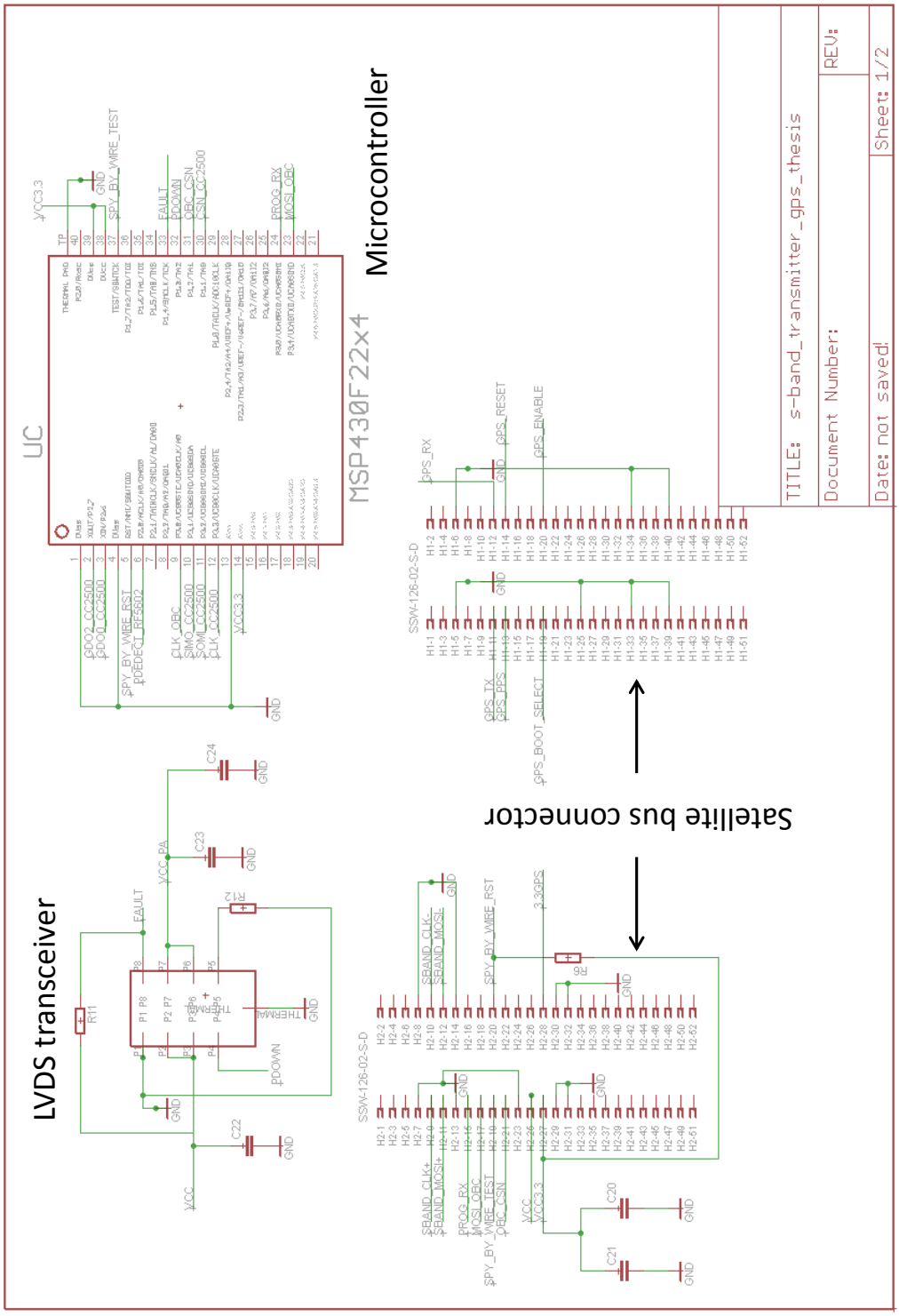

Figure 2: Microcontroller, LVDS transceiver and satellite bus connections.

C Connection schematics for power amplifier and power switch.

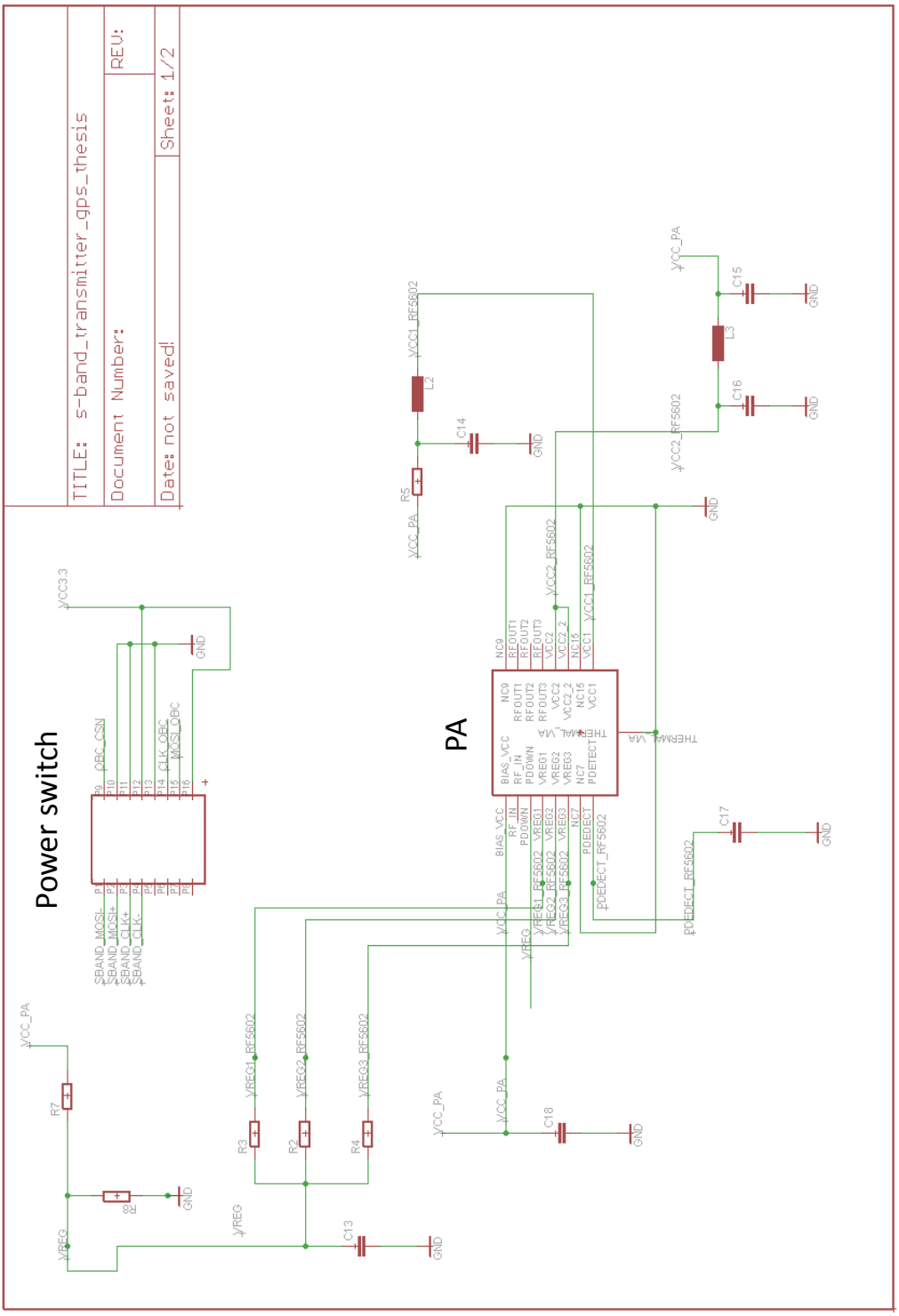

Figure 3: Power amplifier and power switch connections.

D Satellite bus pin configuration on the Aalto-1 nanosatellite.

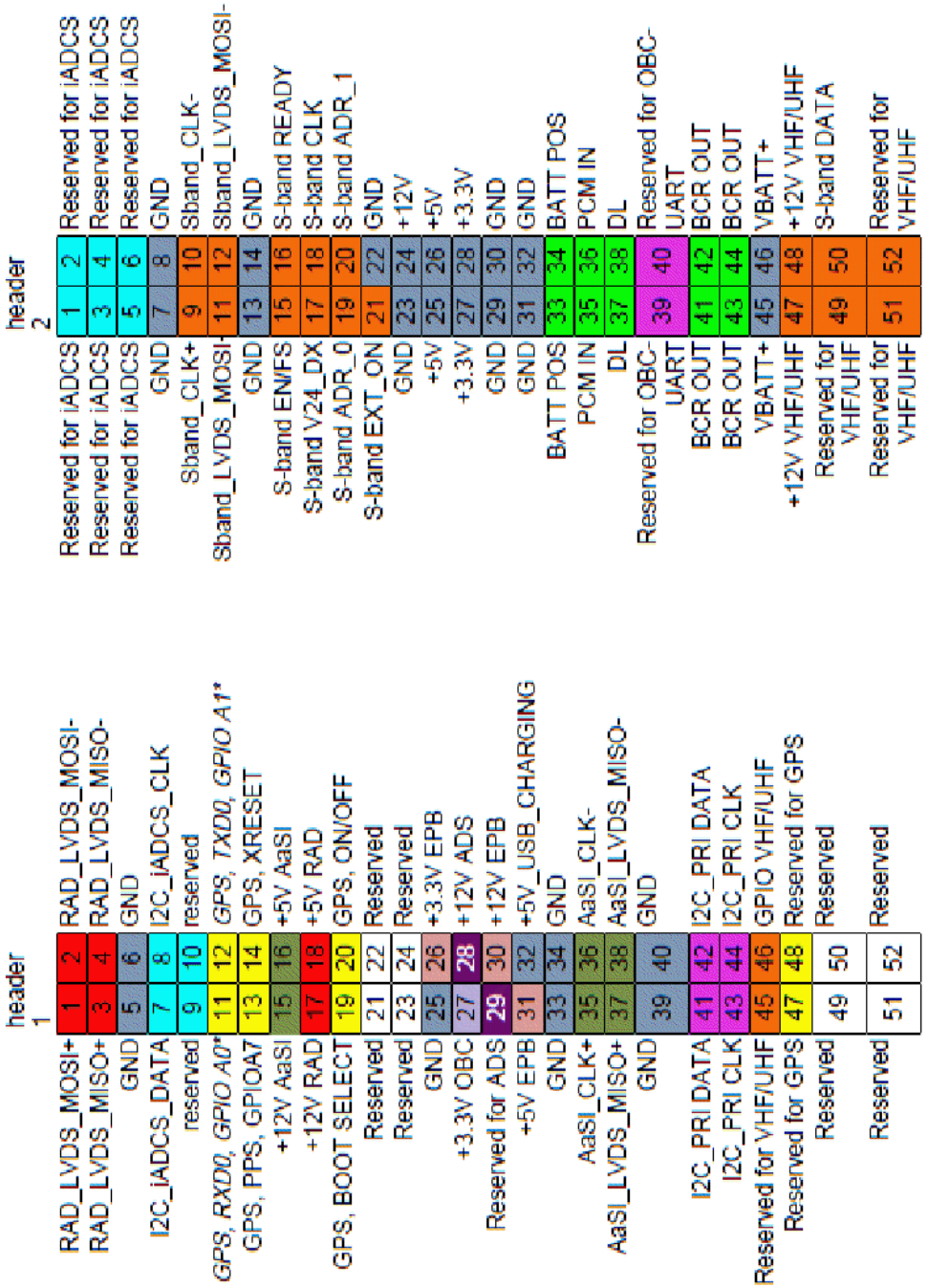

Figure 4: Pin configuration on the Aalto-1 satellite bus.

E Aalto-1 S-band transmitter prototype board layout design.

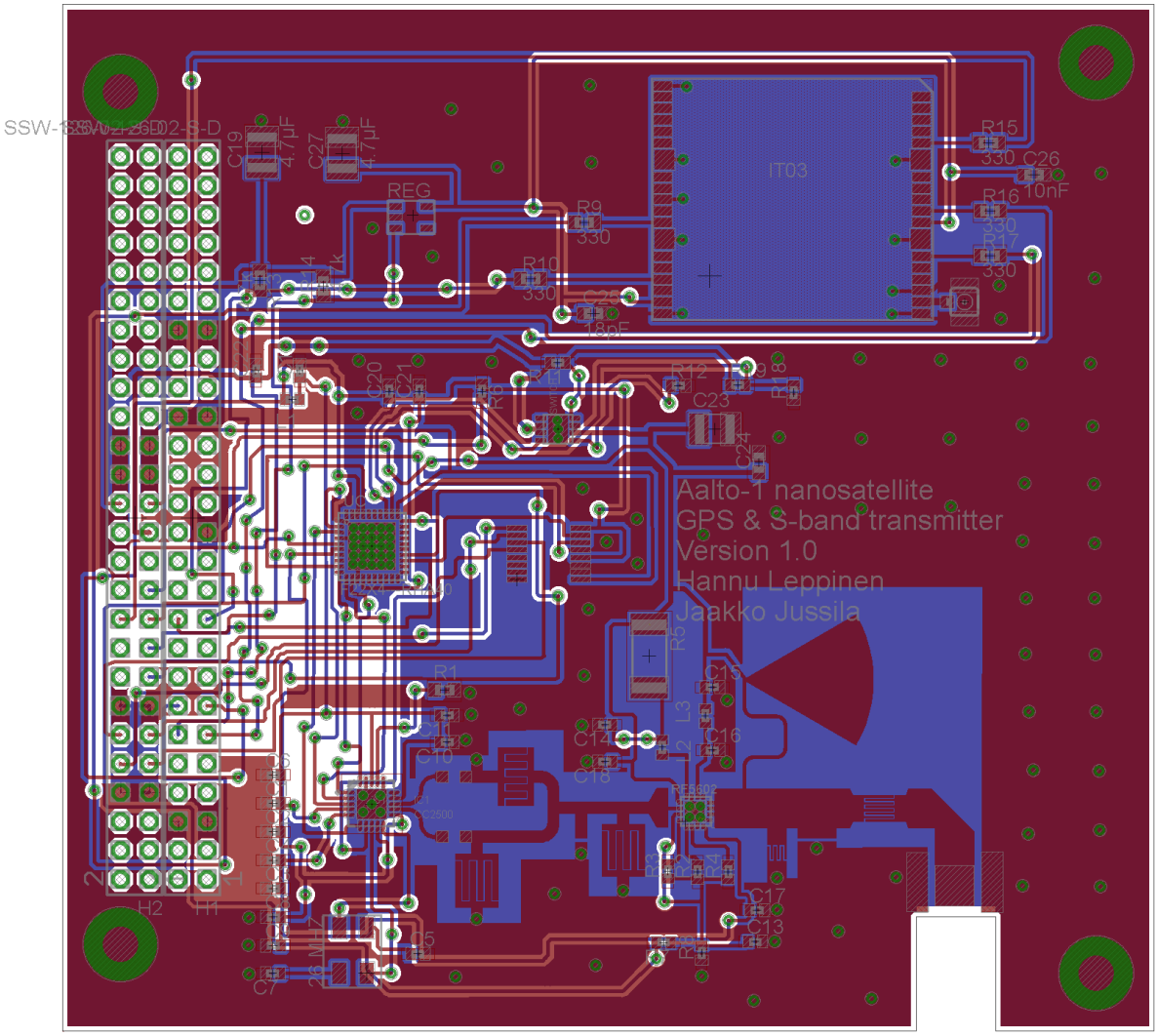

Figure 5: Aalto-1 S-band transmitter and GPS first prototype layout design with EAGLE.

F FMECA analysis results

Table 1: FMECA analysis of first prototype board of Aalto-1 S-band transmitter, part 1.

No	Item	Function	Failure mode	Failure cause
1	**MSP430F2274 microcontroller**	Digital ground pin 1	Ground connection fail	SC/OC (Short Circuit / open circuit)
No	**Failure effects**	**Detection**	**Prevention**	**Migitation**
1	Loss of transmitter	Microcontroller does not work	High quality solders	-
No	**Severity no**	**Probability no**	**Criticality no**	**Notes**
1	2	2	4	-
No	**Item**	**Function**	**Failure mode**	**Failure cause**
2	**MSP430F2274 microcontroller**	Digital ground pin 4	Ground connection fail	SC/OC
No	**Failure effects**	**Detection**	**Prevention**	**Migitation**
2	Loss of transmitter	Microcontroller does not work	High quality solders	-
No	**Severity no**	**Probability no**	**Criticality no**	**Notes**
2	2	2	4	-
No	**Item**	**Function**	**Failure mode**	**Failure cause**
3	**MSP430F2274 microcontroller**	Analog ground pin 13	Ground connection fail	SC/OC
No	**Failure effects**	**Detection**	**Prevention**	**Migitation**
3	Loss of transmitter	Microcontroller does not work	High quality solders	-
No	**Severity no**	**Probability no**	**Criticality no**	**Notes**
3	2	2	4	-
No	**Item**	**Function**	**Failure mode**	**Failure cause**
4	**MSP430F2274 microcontroller**	Analog supply voltage pin 14	Supply voltage failure	SC/OC
No	**Failure effects**	**Detection**	**Prevention**	**Migitation**
4	Loss of transmitter	Microcontroller does not work	High quality solders	-
No	**Severity no**	**Probability no**	**Criticality no**	**Notes**
4	2	2	4	-

Table 2: FMECA analysis for the first prototype board of Aalto-1 S-band transmitter, part 2.

No	Item	Function	Failure mode	Failure cause
4	**MSP430F2274 microcontroller**	Digital supply voltage pins 38 & 39	Supply voltage failure	SC/OC
No	**Failure effects**	**Detection**	**Prevention**	**Migitation**
4	Loss of transmitter	Microcontroller does not work	High quality solders	-
No	**Severity no**	**Probability no**	**Criticality no**	**Notes**
5	2	2	4	-
No	**Item**	**Function**	**Failure mode**	**Failure cause**
5	**MSP430F2274 microcontroller**	I/O failure on GDIO pins 2 & 3	Microcontroller I/O failure	SC/OC
No	**Failure effects**	**Detection**	**Prevention**	**Migitation**
5	Some transmission methods do not work	Possibly no RF transmission	High quality solders	-
No	**Severity no**	**Probability no**	**Criticality no**	**Notes**
5	1	2	2	-
No	**Item**	**Function**	**Failure mode**	**Failure cause**
6	**MSP430F2274 microcontroller**	I/O failure on programming interface pins 5 & 6	Microcontroller I/O failure	SC/OC
No	**Failure effects**	**Detection**	**Prevention**	**Migitation**
6	Microcontroller programming not possible	Programming interface does not respond	High quality solders	-
No	**Severity no**	**Probability no**	**Criticality no**	**Notes**
6	1	2	2	-
No	**Item**	**Function**	**Failure mode**	**Failure cause**
7	**MSP430F2274 microcontroller**	I/O failure on power detection pin 6	Microcontroller I/O failure	SC/OC
No	**Failure effects**	**Detection**	**Prevention**	**Migitation**
7	No RF power information from PA available	No power information included in the transmission	High quality solders	-
No	**Severity no**	**Probability no**	**Criticality no**	**Notes**
7	1	2	2	-

Table 3: FMECA analysis for the first prototype board of Aalto-1 S-band transmitter, part 3.

No	Item	Function	Failure mode	Failure cause
8	**MSP430F2274 microcontroller**	I/O failure on power switch fault detection pin 6	Microcontroller I/O failure	SC/OC
No	**Failure effects**	**Detection**	**Prevention**	**Migitation**
8	No fault information from power switch available	No fault information included in the transmission	High quality solders	-
No	**Severity no**	**Probability no**	**Criticality no**	**Notes**
8	1	2	2	-
No	**Item**	**Function**	**Failure mode**	**Failure cause**
9	**MSP430F2274 microcontroller**	I/O failure on power switch fault detection pin 6	Microcontroller I/O failure	SC/OC
No	**Failure effects**	**Detection**	**Prevention**	**Migitation**
9	No fault information from power switch available	No fault information included in the transmission	High quality solders	-
No	**Severity no**	**Probability no**	**Criticality no**	**Notes**
9	1	2	2	-
No	**Item**	**Function**	**Failure mode**	**Failure cause**
10	**MSP430F2274 microcontroller**	I/O failure on PA control pin 32	Microcontroller I/O failure	SC/OC
No	**Failure effects**	**Detection**	**Prevention**	**Migitation**
10	PA control not possible	No RF transmission	High quality solders	-
No	**Severity no**	**Probability no**	**Criticality no**	**Notes**
10	2	2	4	-
No	**Item**	**Function**	**Failure mode**	**Failure cause**
11	**MSP430F2274 microcontroller**	I/O failure on OBC SPI enable pin 31	Microcontroller I/O failure	SC/OC
No	**Failure effects**	**Detection**	**Prevention**	**Migitation**
11	SPI/LVDS to OBC does not work	Transmitter does not respond	High quality solders	-
No	**Severity no**	**Probability no**	**Criticality no**	**Notes**
11	2	2	4	-

Table 4: FMECA analysis for the first prototype board of Aalto-1 S-band transmitter, part 4.

No	Item	Function	Failure mode	Failure cause
12	**MSP430F2274 microcontroller**	I/O failure on SPI to transceiver enable pin 30	Microcontroller I/O failure	SC/OC
No	**Failure effects**	**Detection**	**Prevention**	**Migitation**
12	Transceiver cannot be programmed	No RF transmission	High quality solders	-
No	**Severity no**	**Probability no**	**Criticality no**	**Notes**
12	2	2	4	-
No	**Item**	**Function**	**Failure mode**	**Failure cause**
13	**MSP430F2274 microcontroller**	I/O UART RX pin 24	Microcontroller I/O failure	SC/OC
No	**Failure effects**	**Detection**	**Prevention**	**Migitation**
13	The UART interface does not work	The UART interface does not respond	High quality solders	-
No	**Severity no**	**Probability no**	**Criticality no**	**Notes**
13	1	2	2	-
No	**Item**	**Function**	**Failure mode**	**Failure cause**
14	**MSP430F2274 microcontroller**	I/O failure on OBC SPI MOSI / UART TX pin 23	Microcontroller I/O failure	SC/OC
No	**Failure effects**	**Detection**	**Prevention**	**Migitation**
14	The LVDS/SPI to OBC / UART interface does not work	The transmitter does not respond / UART interface does not work	High quality solders	-
No	**Severity no**	**Probability no**	**Criticality no**	**Notes**
14	2	2	4	-
No	**Item**	**Function**	**Failure mode**	**Failure cause**
15	**MSP430F2274 microcontroller**	I/O failure on OBC LVDS lock pin 9	Microcontroller I/O failure	SC/OC
No	**Failure effects**	**Detection**	**Prevention**	**Migitation**
15	The LVDS interface does not work	Transmitter does not respond	High quality solders	-
No	**Severity no**	**Probability no**	**Criticality no**	**Notes**
15	2	2	4	-

Table 5: FMECA analysis for the first prototype board of Aalto-1 S-band transmitter, part 5.

No	Item	Function	Failure mode	Failure cause
16	**MSP430F2274 microcontroller**	I/O failure on transceiver SPI pins 10, 11 or 12	Microcontroller I/O failure	SC/OC
No	**Failure effects**	**Detection**	**Prevention**	**Migitation**
16	The transceiver cannot be programmed	No RF transmission	High quality solders	-
No	**Severity no**	**Probability no**	**Criticality no**	**Notes**
16	2	2	4	-
No	**Item**	**Function**	**Failure mode**	**Failure cause**
17	**SN65LVDS049 transceiver**	Ground pins 10, 11 or 13	Grounding failure	SC/OC
No	**Failure effects**	**Detection**	**Prevention**	**Migitation**
17	The LVDS transceiver does not work	Transmitter does not respond	High quality solders	-
No	**Severity no**	**Probability no**	**Criticality no**	**Notes**
17	2	2	4	-
No	**Item**	**Function**	**Failure mode**	**Failure cause**
18	**SN65LVDS049**	Supply voltage pins 12 or 16	Supply voltage failure	SC/OC
No	**Failure effects**	**Detection**	**Prevention**	**Migitation**
18	The LVDS transceiver does not work	The transmitter does not respond	High quality solders	-
No	**Severity no**	**Probability no**	**Criticality no**	**Notes**
18	2	2	4	-
No	**Item**	**Function**	**Failure mode**	**Failure cause**
19	**SN65LVDS049 transceiver**	LVDS differential pins 1, 2, 3 or 4	LVDS transceiver I/O failure	SC/OC
No	**Failure effects**	**Detection**	**Prevention**	**Migitation**
19	The LVDS interface does not work	The transmitter does not respond	High quality solders	-
No	**Severity no**	**Probability no**	**Criticality no**	**Notes**
19	2	2	4	-
No	**Item**	**Function**	**Failure mode**	**Failure cause**
20	**SN65LVDS049 transceiver**	SPI enable pin 9	LVDS transceiver I/O failure	SC/OC
No	**Failure effects**	**Detection**	**Prevention**	**Migitation**
20	The LVDS interface does not work	Transmitter does not respond	High quality solders	-
No	**Severity no**	**Probability no**	**Criticality no**	**Notes**
20	2	2	4	-

Table 6: FMECA analysis for the first prototype board of Aalto-1 S-band transmitter, part 6.

No	Item	Function	Failure mode	Failure cause
21	**SN65LVDS049 transceiver**	SPI clock pin 14	LVDS transceiver I/O failure	SC/OC
No	**Failure effects**	**Detection**	**Prevention**	**Migitation**
21	The LVDS interface does not work	The transmitter does not respond	High quality solders	-
No	**Severity no**	**Probability no**	**Criticality no**	**Notes**
21	2	2	4	-
No	**Item**	**Function**	**Failure mode**	**Failure cause**
22	**SN65LVDS049 transceiver**	SPI MOSI pin 15	LVDS transceiver I/O failure	SC/OC
No	**Failure effects**	**Detection**	**Prevention**	**Migitation**
22	The LVDS interface does not work	Transmitter does not respond	High quality solders	-
No	**Severity no**	**Probability no**	**Criticality no**	**Notes**
22	2	2	4	-
No	**Item**	**Function**	**Failure mode**	**Failure cause**
23	**TPS2556 power switch**	Ground pin 1	Ground connection failure	SC/OC
No	**Failure effects**	**Detection**	**Prevention**	**Migitation**
23	The power switch does not work	No RF transmission	High quality solders	-
No	**Severity no**	**Probability no**	**Criticality no**	**Notes**
23	2	2	4	-
No	**Item**	**Function**	**Failure mode**	**Failure cause**
24	**TPS2556 power switch**	Supply voltage pin 2 or 3	Supply failure	SC/OC
No	**Failure effects**	**Detection**	**Prevention**	**Migitation**
24	The power switch does not work	No RF transmission	High quality solders	-
No	**Severity no**	**Probability no**	**Criticality no**	**Notes**
24	2	2	4	-
No	**Item**	**Function**	**Failure mode**	**Failure cause**
24	**TPS2556 power switch**	Power switch fault pin 8	Power switch I/O failure	SC/OC
No	**Failure effects**	**Detection**	**Prevention**	**Migitation**
25	No fault information from power switch available	No fault information included in the transmission	High quality solders	-
No	**Severity no**	**Probability no**	**Criticality no**	**Notes**
25	1	2	2	-

Table 7: FMECA analysis for the first prototype board of Aalto-1 S-band transmitter, part 7.

26	**TPS2556 power switch**	Power switch PDOWN pin 4	Power switch I/O failure	SC/OC
No	**Failure effects**	**Detection**	**Prevention**	**Migitation**
26	The power amplifier cannot be turned on/off	No RF transmission / transmitter draws too much current in off-mode	High quality solders	-
No	**Severity no**	**Probability no**	**Criticality no**	**Notes**
26	2	2	4	-
27	**TPS2556 power switch**	Power switch current limit pin 5	Power switch I/O failure	SC/OC
No	**Failure effects**	**Detection**	**Prevention**	**Migitation**
27	The power switch does not work	No RF transmission	High quality solders	-
No	**Severity no**	**Probability no**	**Criticality no**	**Notes**
27	2	2	4	-
28	**TPS2556 power switch**	PA supply pins 7 or 8	Power switch I/O failure	SC/OC
No	**Failure effects**	**Detection**	**Prevention**	**Migitation**
28	No supply voltage for power amplifier	No RF transmission	High quality solders	-
No	**Severity no**	**Probability no**	**Criticality no**	**Notes**
28	2	2	4	-
29	**Capacitor C22**	DC-filter capacitor on 5.0 V supply line	Capacitor short circuit	SC
No	**Failure effects**	**Detection**	**Prevention**	**Migitation**
29	No supply voltage for power switch	No RF transmission	High quality discrete capacitor	-
No	**Severity no**	**Probability no**	**Criticality no**	**Notes**
29	2	2	4	-
30	**Resistor R11**	FAULT line pull-up resistor	Resistor short circuit	SC
No	**Failure effects**	**Detection**	**Prevention**	**Migitation**
30	No supply voltage for power switch	No RF transmission	High quality discrete resistor	-
No	**Severity no**	**Probability no**	**Criticality no**	**Notes**
30	2	2	4	-

Table 8: FMECA analysis for the first prototype board of Aalto-1 S-band transmitter, part 8.

31	**Capacitors C23 or C24**	PA supply DC-filtering capacitors	Capacitor short circuit	SC
No	**Failure effects**	**Detection**	**Prevention**	**Migitation**
31	No supply voltage for PA	No RF transmission	High quality discrete capacitors	-
No	**Severity no**	**Probability no**	**Criticality no**	**Notes**
31	2	2	4	-
32	**Resistor R19**	Voltage division resistor on FAULT line	Resistor connection break	OC
No	**Failure effects**	**Detection**	**Prevention**	**Migitation**
32	FAULT signal line connection break	No fault information included in the transmission	High quality discrete resistors	-
No	**Severity no**	**Probability no**	**Criticality no**	**Notes**
32	1	2	2	-
33	**Resistor R18**	Voltage division resistor on FAULT line	Resistor shor circuit	SC
No	**Failure effects**	**Detection**	**Prevention**	**Migitation**
33	Short circuit to ground on FAULT line	No fault information included in the transmission	High quality discrete resistors	-
No	**Severity no**	**Probability no**	**Criticality no**	**Notes**
33	1	2	2	-
34	**RF5602 power amplifier**	BIAS supply pin 1	Power amplifier supply failure	SC/OC
No	**Failure effects**	**Detection**	**Prevention**	**Migitation**
34	No bias voltage available for PA	No RF transmission	High quality solders	-
No	**Severity no**	**Probability no**	**Criticality no**	**Notes**
34	2	2	4	-
35	**RF5602 power amplifier**	RF input pin 2	Power amplifier I/O failure	SC/OC
No	**Failure effects**	**Detection**	**Prevention**	**Migitation**
35	No RF input signal for PA	No RF transmission	High quality solders	-
No	**Severity no**	**Probability no**	**Criticality no**	**Notes**
35	2	2	4	-
36	**RF5602 power amplifier**	PDOWN pin 3	Power amplifier I/O failure	SC/OC
No	**Failure effects**	**Detection**	**Prevention**	**Migitation**
36	No enable signal available for PA	No RF transmission	High quality discrete resistor	-
No	**Severity no**	**Probability no**	**Criticality no**	**Notes**
36	2	2	4	-

Table 9: FMECA analysis for the first prototype board of Aalto-1 S-band transmitter, part 9.

37	**RF5602 power amplifier**	Bias circuit control voltage pins 4,5 or 6	Power amplifier I/o failure	SC/OC
No	**Failure effects**	**Detection**	**Prevention**	**Migitation**
37	Bias circuit of PA does not work	No RF transmission	High quality solders	-
No	**Severity no**	**Probability no**	**Criticality no**	**Notes**
37	2	2	4	-
38	**RF5602 power amplifier**	Thermal ground	Power amplifier ground connection fail	OC
No	**Failure effects**	**Detection**	**Prevention**	**Migitation**
38	PA does not work	No RF transmission	High quality solders	-
No	**Severity no**	**Probability no**	**Criticality no**	**Notes**
38	2	2	4	-
39	**RF5602 power amplifier**	Power detection pin	Power amplifier I/O failure	SC/OC
No	**Failure effects**	**Detection**	**Prevention**	**Migitation**
39	No information of RF output power available	No power information included in the transmission	High quality solders	-
No	**Severity no**	**Probability no**	**Criticality no**	**Notes**
39	1	2	2	-
40	**RF5602 power amplifier**	RF output / VCC1 supply pins	Power amplifier I/O / supply failure	SC/OC
No	**Failure effects**	**Detection**	**Prevention**	**Migitation**
40	Power amplifier does not work	No RF transmission	High quality solders	-
No	**Severity no**	**Probability no**	**Criticality no**	**Notes**
40	2	2	4	-
41	**RF5602 power amplifier**	Supply voltage pins 13 or 14	Power amplifier supply failure	SC/OC
No	**Failure effects**	**Detection**	**Prevention**	**Migitation**
41	PA does not work	No RF transmission	High quality solders	-
No	**Severity no**	**Probability no**	**Criticality no**	**Notes**
41	2	2	4	-
42	**RF5602 power amplifier**	Supply voltage pin 16	Power amplifier supply failure	SC/OC
No	**Failure effects**	**Detection**	**Prevention**	**Migitation**
42	No supply voltage for PA available	No RF transmission	High quality discrete resistor	-
No	**Severity no**	**Probability no**	**Criticality no**	**Notes**
42	2	2	4	-

Table 10: FMECA analysis for the first prototype board of Aalto-1 S-band transmitter, part 10.

43	**Capacitor C17**	Power detection noise reduction capacitor	Capacitor failure	SC
No	**Failure effects**	**Detection**	**Prevention**	**Migitation**
43	No power information available	No power information included in the transmission	High quality discrete capacitors	-
No	**Severity no**	**Probability no**	**Criticality no**	**Notes**
43	1	2	2	-
44	**Capacitor C18**	DC-filtering capacitor on bias voltage line	DC-filtering capacitor failure	SC
No	**Failure effects**	**Detection**	**Prevention**	**Migitation**
44	PA does not work	No RF transmission	High quality solders	-
No	**Severity no**	**Probability no**	**Criticality no**	**Notes**
44	2	2	4	-
45	**Capacitors C16, C15 or C14**	PA supply DC-filtering capacitors	DC-filtering capacitor failure	SC
No	**Failure effects**	**Detection**	**Prevention**	**Migitation**
45	Power amplifier does not work	No RF transmission	High quality solders	-
No	**Severity no**	**Probability no**	**Criticality no**	**Notes**
45	2	2	4	-
46	**Inductors L3 or L2**	PA supply voltage line inductors	Inductor failure	OC
No	**Failure effects**	**Detection**	**Prevention**	**Migitation**
46	Power amplifier does not work	No RF transmission	High quality solders	-
No	**Severity no**	**Probability no**	**Criticality no**	**Notes**
46	2	2	4	-
47	**Capacitor C13**	Bias control voltage DC-filtering capacitors	Capacitor failure	SC
No	**Failure effects**	**Detection**	**Prevention**	**Migitation**
47	PA does not work	No RF transmission	High quality solders	-
No	**Severity no**	**Probability no**	**Criticality no**	**Notes**
47	2	2	4	-
48	**Resistor R5**	Supply line biasing resistor	Resistor failure	OC
No	**Failure effects**	**Detection**	**Prevention**	**Migitation**
48	PA does not work	No RF transmission	High quality discrete resistor	-
No	**Severity no**	**Probability no**	**Criticality no**	**Notes**
48	2	2	4	-

Table 11: FMECA analysis for the first prototype board of Aalto-1 S-band transmitter, part 11.

49	**Resistor R8**	Voltage division resistor	Resistor failure	SC
No	**Failure effects**	**Detection**	**Prevention**	**Migitation**
49	Power amplifier does not work	No RF transmission	High quality discrete resistor	-
No	**Severity no**	**Probability no**	**Criticality no**	**Notes**
49	2	2	4	-
50	**Resistor R7**	Voltage division resistor	Resistor failure	OC
No	**Failure effects**	**Detection**	**Prevention**	**Migitation**
50	PA does not work	No RF transmission	High quality discrete resistor	-
No	**Severity no**	**Probability no**	**Criticality no**	**Notes**
50	2	2	4	-
51	**CC2500 transceiver circuit**	SPI clock pin 1	Transceiver I/O failure	SC/OC
No	**Failure effects**	**Detection**	**Prevention**	**Migitation**
51	SPI does not work	No RF transmission	High quality solders	-
No	**Severity no**	**Probability no**	**Criticality no**	**Notes**
51	2	2	4	-
52	**CC2500 transceiver**	SPI SOMI pin 2	Transceiver I/O failure	SC/OC
No	**Failure effects**	**Detection**	**Prevention**	**Migitation**
52	SPI does not work	No RF transmission	High quality solders	-
No	**Severity no**	**Probability no**	**Criticality no**	**Notes**
52	2	2	4	-
53	**CC2500 transceiver**	SPI SIMO pin 20	Transceiver I/O failure	SC/OC
No	**Failure effects**	**Detection**	**Prevention**	**Migitation**
53	SPI does not work	No RF transmission	High quality solders	-
No	**Severity no**	**Probability no**	**Criticality no**	**Notes**
53	2	2	4	-
54	**CC2500 transceiver**	SPI enable pin 7	Transceiver I/O failure	SC/OC
No	**Failure effects**	**Detection**	**Prevention**	**Migitation**
54	SPI does not work	No RF transmission	High quality solders	-
No	**Severity no**	**Probability no**	**Criticality no**	**Notes**
54	2	2	4	-
55	**CC2500 transceiver**	GIO pins GDO0 (6) or GDO2 (3)	Transceiver I/O failure	SC/OC
No	**Failure effects**	**Detection**	**Prevention**	**Migitation**
55	Some transmission modes do not work	Possibly no RF transmission	High quality solders	-
No	**Severity no**	**Probability no**	**Criticality no**	**Notes**
55	1	2	2	-

Table 12: FMECA analysis for the first prototype board of Aalto-1 S-band transmitter, part 12.

56	**CC2500 transceiver**	External oscillator pins 8 or 10	Transceiver I/O failure	SC/OC
No	**Failure effects**	**Detection**	**Prevention**	**Migitation**
56	Transceiver does not work	No RF transmission	High quality solders	-
No	**Severity no**	**Probability no**	**Criticality no**	**Notes**
56	2	2	4	-
57	**CC2500 transceiver circuit**	Analog supply voltage pins 9, 11, 15 or 14	Transceiver supply failure	SC/OC
No	**Failure effects**	**Detection**	**Prevention**	**Migitation**
57	Transceiver does not work	No RF transmission	High quality solders	-
No	**Severity no**	**Probability no**	**Criticality no**	**Notes**
57	2	2	4	-
58	**CC2500 transceiver**	Digital supply pins 4 or 18	Transceiver supply failure	SC/OC
No	**Failure effects**	**Detection**	**Prevention**	**Migitation**
58	Transceiver does not work	No RF transmission	High quality solders	-
No	**Severity no**	**Probability no**	**Criticality no**	**Notes**
58	2	2	4	-
59	**CC2500 transceiver**	Supply coupling pin 5	Transceiver I/O failure	SC/OC
No	**Failure effects**	**Detection**	**Prevention**	**Migitation**
59	Transceiver operation degraded	RF transmission quality degraded	High quality solders	-
No	**Severity no**	**Probability no**	**Criticality no**	**Notes**
59	2	2	4	-
60	**Resistor R1**	Bias resistor for the transceiver	Resistor failure	SC/OC
No	**Failure effects**	**Detection**	**Prevention**	**Migitation**
60	Transceiver does not work	No RF transmission	High quality solders	-
No	**Severity no**	**Probability no**	**Criticality no**	**Notes**
60	2	2	4	-
61	**CC2500 transceiver**	RF output ports	Transceiver I/O failure	SC/OC
No	**Failure effects**	**Detection**	**Prevention**	**Migitation**
61	Transceiver does not work	No RF transmission	High quality solders	-
No	**Severity no**	**Probability no**	**Criticality no**	**Notes**
61	2	2	4	-
62	**CC2500 transceiver**	Ground pins 16 or 19	Transceiver ground connection failure	SC/OC
No	**Failure effects**	**Detection**	**Prevention**	**Migitation**
62	Transceiver does not work	No RF transmission	High quality solders	-
No	**Severity no**	**Probability no**	**Criticality no**	**Notes**
62	2	2	4	-

Table 13: FMECA analysis for the first prototype board of Aalto-1 S-band transmitter, part 13.

63	**CC2500 transceiver circuit**	Thermal ground	Transceiver ground connection failure	SC/OC
No	**Failure effects**	**Detection**	**Prevention**	**Migitation**
63	Transceiver does not work	No RF transmission	High quality solders	-
No	**Severity no**	**Probability no**	**Criticality no**	**Notes**
63	2	2	4	-
64	**Capacitors C1, C2, C8, C9, C11, C10 or C12**	DC-filtering capacitors on supply line	Capacitor failure	SC
No	**Failure effects**	**Detection**	**Prevention**	**Migitation**
64	Transceiver does not work	No RF transmission	High quality discrete capacitors	-
No	**Severity no**	**Probability no**	**Criticality no**	**Notes**
64	2	2	4	-
65	**Capacitors C3 or C4**	Noise reduction capacitors	Capacitor failure	SC
No	**Failure effects**	**Detection**	**Prevention**	**Migitation**
65	Transceiver does not work	No RF transmission	High quality discrete capacitors	-
No	**Severity no**	**Probability no**	**Criticality no**	**Notes**
65	2	2	4	-
66	**Inductor L1**	Transceiver biasing inductor	Inductor failure	OC
No	**Failure effects**	**Detection**	**Prevention**	**Migitation**
66	Transceiver does not work	No RF transmission	High quality discrete inductor	-
No	**Severity no**	**Probability no**	**Criticality no**	**Notes**
66	2	2	4	-

Table 14: FMECA analysis for the first prototype board of Aalto-1 S-band transmitter, part 14.

67	**Capacitors C7 or C5**	External crystal noise reduction capacitors	Capacitor failure	SC/OC
No	**Failure effects**	**Detection**	**Prevention**	**Migitation**
67	External crystal operation degraded	RF transmission quality degraded	High quality discrete capacitors	-
No	**Severity no**	**Probability no**	**Criticality no**	**Notes**
67	1	2	4	-
68	**Capacitors C21 or C20**	DC-filtering capacitors	Capacitor failure	SC
No	**Failure effects**	**Detection**	**Prevention**	**Migitation**
68	No 3.3 supply voltage available for the transmitter	Transmitter does not respond	High quality discrete capacitors	-
No	**Severity no**	**Probability no**	**Criticality no**	**Notes**
68	2	2	4	-
69	**Resistor R6**	Pull-up resistor for uC programming interface	Resistor failure	SC
No	**Failure effects**	**Detection**	**Prevention**	**Migitation**
69	uC programming interface does not work	uC programming interface does not respond	High quality discrete resistor	-
No	**Severity no**	**Probability no**	**Criticality no**	**Notes**
69	2	2	4	-

G SW main routine for testing the transmission

```
#include "include.h"

extern char paTable[];
extern char paTableLen;

char txBuffer[64];
char rxBuffer[4];
unsigned int i = 0;
unsigned int transmitter = 0;

#define LED BIT0
#define RXD BIT5
#define TXD BIT4
char test_string[8];

volatile unsigned int rx_flag;
volatile unsigned int tx_flag;
volatile unsigned char tx_char;
char res, res2;

volatile unsigned int rx_flag;
volatile unsigned char rx_char;


void uart_init(void)
{
        P3SEL = RXD + TXD;
        //P3SEL2 = RXD + TXD;

    //P1DIR |= LED;
    //P1OUT |= LED;

        UCA0CTL1 |= UCSSEL_2;

        UCA0BR0 = 52;
        UCA0BR1 = 0;
        UCA0MCTL = 0x10|UCOS16;
        UCA0CTL1 &= ~UCSWRST;
        IE2 |= UCA0RXIE;

        rx_flag = 0;
        tx_flag = 0;

        return;
}
```

```
unsigned char uart_getc()
{
        while (rx_flag == 0);
        rx_flag = 0;
    return rx_char;
}


void uart_gets(char* Array, int length)
{
        unsigned int i = 0;

        while((i < length))
        {
                Array[i] = uart_getc();
                if(Array[i] == '\r')
                {
                        for( ; i < length ; i++)
                        {
                                Array[i] = '\0';
                        }
                        break;
                }
                i++;
        }

    return;
}


void uart_putc(unsigned char c)
{
        tx_char = c;
        IE2 |= UCA0TXIE;
        while(tx_flag == 1);
        tx_flag = 1;
        return;
}


void uart_puts(char *str)
{
     while(*str) uart_putc(*str++);
     return;
}
```

```
void main (void)
{
        char* Array2;
        unsigned int j = 0;
  WDTCTL = WDTPW + WDTHOLD;                     // Stop WDT
  BCSCTL1 = CALBC1_8MHZ;
  DCOCTL = CALDCO_8MHZ;

  // 5ms delay to compensate for time to startup between MSP430
  and CC1100/2500
  __delay_cycles(5000);

  uart_init();

  __enable_interrupt();


  uart_puts((char *)"Hello Jaakko\n\r");

  uart_puts((char *)"PRESS a key  ... ");

  unsigned char c = uart_getc();

      uart_putc(c);

      uart_puts((char *)"\n\rTest OK!\n\r");
      uart_puts((char *)"\n\rEnter a String of 8 Chars or press
      ENTER...\n\r");

      while(1)
      {
        uart_gets(test_string, 1);
        uart_puts(test_string);
        uart_puts((char *)"\n\r");
        if(transmitter == 1)
        {
                uart_puts((char *)"Putting CC2500 into packet
                     transmit mode\n\r");
                uart_puts((char *)"Selecting P2.6 and P2.7 as
                     GPIO\n\r");
                P2SEL = 0;              // Sets P2.6 & P2.7 as GPIO
                uart_puts((char *)"Resetting CC2500\n\r");
                TI_CC_PowerupResetCCxxxx();
                     // Reset CCxxxx
                uart_puts((char *)"Writing the RF registers in
                     CC2500\n\r");
                writeRFSettings();                      // Write RF
                     settings to config reg
```

```
            uart_puts((char *)"Programming the RF
                 output power\n\r");
            TI_CC_SPIWriteBurstReg(TI_CCxxx0_
                 PATABLE, paTable, paTableLen);//Write PATABLE
            // Configure ports -- switch inputs, LEDs,
                 GDO0 to RX packet info from CCxxxx
            TI_CC_SW_PxREN = TI_CC_SW1;  // Enable
                 Pull up resistor
            TI_CC_SW_PxOUT = TI_CC_SW1;   // Enable
                 pull up resistor
            TI_CC_SW_PxIES = TI_CC_SW1;   // Int
                 on falling edge
            TI_CC_SW_PxIFG &= ~(TI_CC_SW1);  // Clr
                 flags
            TI_CC_SW_PxIE = TI_CC_SW1;   // Activate
                 interrupt enables
            TI_CC_GDO0_PxIES |= TI_CC_GDO0_PIN;  // Int on
                 falling edge (end of pkt)
            TI_CC_GDO0_PxIFG &= ~TI_CC_GDO0_PIN;  // Clear flag
            TI_CC_GDO0_PxIE |= TI_CC_GDO0_PIN; // Enable int
                 on end of packet
            TI_CC_SPIStrobe(TI_CCxxx0_STX);   // Initialize
                 CCxxxx in RX mode.
            uart_puts((char *)"\n\rTransmitting data\n\r");
            // Build packet
            txBuffer[0] = 2;       // Packet length
            txBuffer[1] = 0x01;     // Packet address
            txBuffer[2] = (~TI_CC_SW_PxIFG << 1) & 0x02; // Load
                 switch inputs
            for(j = 3; j < 64; j++)
                    txBuffer[j] = j;
            RFSendPacket(txBuffer, 63);    // Send value over RF
            __delay_cycles(5000);   // Switch debounce
            uart_puts((char *)"\n\rData transmitted\n\r");
            transmitter = 0;
    }
    if(transmitter == 2)
    {
            uart_puts((char *)"Initializing SPI interface
            of CC2500\n\r");
            TI_CC_SPISetup();   // Initialize SPI port
        transmitter = 0;
    }
    if(transmitter == 3)
    {
            uart_puts((char *)"Getting register value from
            CC2500\n\r");
            res = TI_CC_SPIReadReg(TI_CCxxx0_FREQ2);
```

```
            uart_putc(res);
            res = TI_CC_SPIReadReg(TI_CCxxx0_FREQ1);
            uart_putc(res);
            res = TI_CC_SPIReadReg(TI_CCxxx0_FREQ0);
            uart_putc(res);
            //res = res&0xF;
            //if(res < 0xA)
            //        res2 = res+'0';
            //else
                    //res2 = (res-0xA)+'A';
            uart_putc(res);
            transmitter = 0;
    }
    if(transmitter == 4)
    {
            uart_puts((char *)"Packet received\n\r");
            transmitter = 0;
    }
    if(transmitter == 5)
    {
        uart_puts((char *)"Turning CC2500 to idle\n\r");
      TI_CC_SPIStrobe(TI_CCxxx0_SRES);
        transmitter = 0;
    }
    if(transmitter == 6)
    {
            uart_puts((char *)"Configuring continuous
            transmission\n\r");
            TI_CC_PowerupResetCCxxxx();  // Reset CCxxxx
            //__delay_cycles(10000);
            writeRFSettings(); // Write RF settings to config reg
            //__delay_cycles(10000);
            TI_CC_SPIWriteBurstReg(TI_CCxxx0_PATABLE,
            paTable, paTableLen);//Write PATABLE
            //__delay_cycles(10000);
            //SYNC1     = 0xAA;
            //SYNC0     = 0xAA;
            uart_puts((char *)"Radio into transmission
            mode\n\r");
            TI_CC_SPIStrobe(TI_CCxxx0_STX);  // Initialize
            CCxxxx in RX mode.
            //__delay_cycles(10000);
            //TI_CC_SPIStrobe(TI_CCxxx0_STX);   // Initialize
            CCxxxx in TX mode
            /* Wait for radio to enter TX. */
            uart_puts((char *)"Waiting for radio to go
            transmission mode\n\r");
            //while (TI_CC_SPIReadStatus(TI_CCxxx0_IOCFG2)
```

```
                & MARCSTATE_MARC_STATE) != MARC_STATE_TX);
                //__delay_cycles(10000);
                uart_puts((char *)"Radio now in
                transmission mode\n\r");
                /* Radio is now in TX. Infinite loop. */
                while (1);
            transmitter = 0;
        }
      }
}


// The ISR assumes the interrupt came from a pressed button
#pragma vector=PORT1_VECTOR
__interrupt void Port1_ISR (void)
{
  // If Switch was pressed
  if(TI_CC_SW_PxIFG & TI_CC_SW1)
  {
    // Build packet
    txBuffer[0] = 2;        // Packet length
    txBuffer[1] = 0x01;     // Packet address
    txBuffer[2] = (~TI_CC_SW_PxIFG << 1)
    & 0x02; // Load switch inputs
    RFSendPacket(txBuffer, 3); // Send value over RF
    __delay_cycles(5000);     // Switch debounce
  }
  TI_CC_SW_PxIFG &= ~(TI_CC_SW1);  // Clr flag that caused int
}

#pragma vector = USCIAB0TX_VECTOR
__interrupt void USCI0TX_ISR(void)
{
        UCA0TXBUF = tx_char;
        tx_flag = 0;
        IE2 &= ~UCA0TXIE;
}

#pragma vector = USCIAB0RX_VECTOR
__interrupt void USCI0RX_ISR(void)
{
        rx_char = UCA0RXBUF;
        rx_flag = 1;
        if(rx_char == 't')
                transmitter = 1;
        if(rx_char == 'i')
                        transmitter = 2;
        if(rx_char == 'g')
```

```
                    transmitter = 3;
        if(rx_char == 'd')
                            transmitter = 5;
        if(rx_char == 'c')
                    transmitter = 6;
        //P1OUT ^= LED;
}
```